Some Tribological Aspects of the Hard Disk Drive Head-Disk Interface for Quasi Contact Conditions: Contact Detection, Lubricant Modulation and Wear

by

Yung-Kan Chen

A dissertation submitted in partial satisfaction of the

requirements for the degree of

Doctor of Philosophy

in

Engineering – Mechanical Engineering

in the

Graduate Division

of the

University of California, Berkeley

Committee in charge:

Professor David B. Bogy, Chair
Professor David J. Steigmann
Professor John A. Strain

Summer 2015

Some Tribological Aspects of the Hard Disk Drive Head-Disk Interface for Quasi Contact Conditions: Contact Detection, Lubricant Modulation and Wear

Abstract

Some Tribological Aspects of the Hard Disk Drive Head-Disk Interface for Quasi Contact Conditions: Contact Detection, Lubricant Modulation and Wear
by

Yung-Kan Chen

Doctor of Philosophy in Engineering-Mechanical Engineering
University of California, Berkeley
Professor David B. Bogy, Chair

The magnetic recording hard disk drive has been one of the most important storage strategies since 1956. Among all storage solutions, hard disk drives possess the unrivaled advantageous combination of storage capacity, speed, reliability and cost over optical strategies and flash memory. Unlike other storage solutions, hard disk drives utilize a mechanical interface to perform the magnetic read/write process, and therefore its success relies heavily on the stability of the head-disk interface (HDI) which is composed of a magnetic transducer carried by an air bearing slider, an air gap of a few nanometers thick, and a disk surface coated with multiple layers of molecularly-thin films. This dissertation addresses the physics of the interface in terms of contact detection, lubricant modulation and wear.

Contact detection serves as one of the core requirements in HDI reliability. The writing process demands a strict spacing control, and its accuracy is based on a proper choice of a contact reference from slider dynamics and therefore the heads' signal. While functioning in a real drive the only feedback signal comes from sensors neighboring the read-write transducer, and a high speed head-disk contact is associated with complex structural responses inherent in an air-bearing/suspension/lubricant system that may not be well explained solely by magnetic signals. Other than studying the slider-disk interaction at a strong interplay stage, this dissertation tackles the contact detection by performing component-level experimental and simulation studies focusing on the dynamics of air-bearing sliders at disk proximity. The slider dynamics detected using laser Doppler vibrometry indicates that a typical head-disk contact can be defined early as in-plane motions of the slider, which is followed by vertical motions at a more engaged contact. This finding confirms and is in parallel with one of the detection schemes used in commercial drives by magnetic signals.

Lubricated disk surfaces play an important role in contact characteristics. As the nature of contact involves two mating surfaces, the modulation of disk lubricant films should be investigated to further understand the head-disk contact in addition to the slider dynamics. In this dissertation, the lubricant modulation is studied under various contact conditions with reference to slider dynamics. It is found that lubricant modulation can be directly associated with the slider's dynamics in a location specific way, and its evolution is likely to affect the slider's stable back-off fly-height as the contact is retracted. In addition to

modulations at contact proximities, the lubricant response to passive flying and continuous contacting conditions are also addressed for different lubricant types and thicknesses. By integrating the observations from slider dynamics and lubricant modulations, we can establish an insightful understanding towards the transition from flying to the onset of contact.

Head wear is also a concern when an erroneous contact detection occurs or imperfections from disk surface exists. Typically a protective diamond-like carbon (DLC) layer of thickness 1-2 nm is coated over the area of the reader/writer shields, and this film loss poses a threat to long term reliability. In this dissertation, in-situ methods of monitoring head wear is proposed in two ways. One method is to evaluate the touchdown power variations as a measure of spacing increase by DLC wear, which was verified by using Auger Electron Spectroscopy, and the other method studies the temperature contact sensor response to gauge mechanical wear. The later possesses the advantage of detecting wear without going into actual contact, but it may be affected by the location difference between the touchdown sensor and wear area.

To my wife, Yu-Chu, and my daughter, Athena

TABLE OF CONTENTS

List of Figures ..... **v**

List of Abbreviations ..... **xi**

Acknowledgments ..... **xii**

Chapter 1 *Introduction* 1

1.1 The basics of a hard disk drive and its evolution 1
1.2 A tribological challenge in HDDs: the head-disk interface 3
1.3 The thermal flying-height control technology 4
1.4 Objective of this work 7
1.5 Organization of the dissertation 7

Chapter 2 *Preliminary study of the head-disk interface with TFC slider* 8

2.1 Introduction 8
2.2 Experimental Setup 9
2.2.1 Laser Doppler Vibrometer 9
2.2.2 Acoustic emission sensors 10
2.2.3 Optical Surface Analyzers (OSA) 11
2.2.4 Load cell and strain gauge 11
2.2.5 Data acquisition and flying-height control 11
2.3 Calibration Procedures for the Optical Surface Analyzer 12
2.3.1 Sample Preparation 12
2.3.2 Calibration Procedure 12
2.3.3 Calibration Results 13
2.4 Methodology 14
2.4.1 Experimental schemes 14
2.4.2 Numerical simulation 15
2.4.3 Data processing 16
2.5 Results and Discussion 16
2.5.1 Slider dynamics and acoustic emission sensor 16
2.5.2 Lubricant response 20
2.5.3 Numerical simulations 21
2.5.4 Interfacial friction force: comments on the feasibility of surfing 22
2.6 Summary and Conclusion 23

Chapter 3 *Thermal protrusion-induced slider's flying height modulation at contact proximity* 26

3.1 Introduction 26
3.2 Experiments 27

3.2.1 LDV measurement system update 28
3.2.2 Visualization of the laser spot 29
3.2.3 Data acquisition update 30
3.3 Methodology 31
3.3.1 Rationale 31
3.3.2 Samples and Experimental Schemes 31
3.4 Simulations 32
3.4.1 Finite Element Modeling 33
3.4.2 Estimation of the effect of air-bearing stiffness 33
3.4.3 Transient and harmonic analysis 33
3.5 Results and Discussions 33
3.5.1 Experiment 34
3.5.2 Simulation 43
3.6 Summary and Conclusions 49

Chapter 4 *Characterization of slider-disk contacts* 50

4.1 Introduction 50
4.2 Experiments 51
4.3 Modulation Regime 52
4.3.1 Physical meaning of modulation regime 52
4.3.2 Lubricant effects on the Modulation Regime 54
4.4 Post-verification of the MR using TFC overdrives 56
4.4.1 Introduction to TFC overdrive 57
4.4.2 Modulation regime and overdrive regime 58
4.5 Summary and Conclusions 60

Chapter 5 *Lubricant modulation under air bearing sliders* 61

5.1 Introduction 61
5.2 Lubricant modulation under passive flying 62
5.3 Lubricant modulation under thermal protrusion-induced slider-disk contacts 64
5.3.1 Experiments 64
5.3.2 Lubricant modulation under touchdown and overdrive 66
5.3.3 Lubricant modulation under continuous contacts 69
5.3.4 Data Processing 70
5.3.5 Lubricant modulation, TDP and modulation regime 71
5.4 Causality of slider modulation and lubricant modulation 74
5.5 Conclusions 77

Chapter 6 *Wear in the head-disk interface* 82

6.1 Introduction 82
6.2 Wear development and estimation using TDP 83

6.2.1 Experiments....84
6.2.2 Wear development and estimations....85
6.2.3 Comparative study at CML....90
6.3 Wear estimations using Temperature Response....91
6.3.1 Experiments....92
6.3.2 Wear estimation using the touchdown sensor....93
6.4 Limiations on the use of TR and dTDP for wear estimation....96

Chapter 7 *Conclusions and Future Research Directions*....98

7.1 Summary....98
7.2 Future Research Directions....99
7.2.1 Heat transfer modeling in the HDI with TDS support....100
7.2.2 Wear resistant HDI....100
7.2.3 Contact-stable HDI design....101

Bibliography....102

LIST OF FIGURES

Figure 1.1.1 An early Winchester drive around 1975. It works on 14" disks and holds a storage capacity of 20 Mega-bytes. The "brown-orange" material on the disk is the hue of iron oxide particles. Its size is considerably huge compared to a more modern Western Digital 3.5" drive manufactured in 2008 with 40 Giga-bytes capacity on the top-right of the figure. 2

Figure 1.3.1. Zoomed section of the read-write portion on the ABS. Left part of the metal stripes are reader shields, and the writer return poles are on the right 4

Figure 1.3.2 (a) Photograph of one of the ABS designs used in this dissertation, (b) simulated ABS pressure and (c) the representative heater protrusion profile at a maximum height of 11 nm. 6

Figure 2.2.1 The experiment setup contains (a) LDV, (b) AE sensor and (c) OSA for in-situ measurements. 10

Figure 2.3.3.1 Representative diagram showing the Pre/Post Lube calibration procedure 12

Figure 2.3.3.2 The calibration result using the Prelube/Postlube methods. The slope of the linear fitting line is -0.0217% with R^2=0.9739 13

Figure 2.4.1.1 Step-up power history with 30 ms dwell time 14

Figure 2.4.1.2 (left) Part of the suspension from the ABS side's view (in the background) (right) Top view of the suspension in part. TEC is marked using a red circle, where the LDV takes the measurement. 15

Figure 2.5.1.1 (a) Dynamic signals in time domain and (b) the 3σ of time domain signals with corresponding powers (c) the frequency spectrum at different powers 17

Figure 2.5.1.2 Comparison of dynamical behaviors in both time domain (left) and frequency domain (right) at different heater powers (a) P1, (b) P2 and (c) P3, respectively. Dominant peaks are indicated by arrows. 19

Figure 2.5.2.1 OSA raw data showing lubricant depletion under Phase III at 3 minutes, 7 minutes and 12 minutes separately. 20

Figure 2.5.2.2 Lubricant modulation profile along the radial direction ranging from 4 minutes to 12 minutes in phase III. 21

Figure 2.5.3.1 Simulation results on (a) frequency response and (b) corresponding nodal lines of dominant frequencies plotted on the ABS. The solid line located between 0.8 and 1 indicates the slider's trailing edge (TE).....22

Figure 2.5.4.1 Data with friction force measured. 23

Figure. 3.2.1.1. Experimental setup for *in-situ* measurements on (a) vertical dynamics, and (b) down-track dynamics. 28

Figure. 3.2.1.2. Laser spots focused on (a) TEC, (b) LEC, and (c) DTD. The brightest red dots are the focused laser spots, which are surrounded by scattered lights.....29

Figure. 3.2.3.1. Representative data acquisition diagram used in this chapter. On PCI-6110, AI 0-3 are synchronized analog input channels. 30

Figure. 3.4.1.1 Suspension design of HGA#1 (a) and HGA#2 (b). TEC is circled in white and LEC is circled in red for both figures. 32

Figure. 3.5.1.1 A typical AE-based contact detection scheme. (a) Five consecutive TD tests at the same contact power with dashed AE threshold line. (b) The corresponding time domain traces with post-processed LEC modulations. 35

Figure. 3.5.1.2 AE dynamic patterns transitions from (a) 1 mW back-off to (b) TD to (c) over-push using the same HGA in five consecutive power-up cycles. Over-pushes are applied four times after TDs. Repeatable patterns could be observed from cycle to cycle, but the location specific patterns vanish at (c).....36

Figure. 3.5.1.3 Typical synchronized measurement results on (a) LEC and (b) TEC. TFC pulses are synchronized to spindle indexes. Closed-up figures from 0.0109 s to 0.0115 s are presented to show the differences between LEC and TEC velocity modulations in time domain.....37

Figure. 3.5.1.4 Comparison of displacement modulations on (a) TEC, (b) LEC, and (c) DTD with AE signals as references.....38

Figure. 3.5.1.5 Frequency spectra on (a) TEC, (b) LEC, (c) DTD, and (d) AE signals at a typical slider-disk contact event.....40

Figure. 3.5.1.6 Representative evolutions of (a) maximum 3-sigma displacement modulations on LEC, TEC, and DTD; (b) corresponding AE modulations. Solid marks are the averaged value and the error bar indicates plus/minus one standard deviation from 10 TD tests. 41

Figure. 3.5.1.7 Modulation growth rate with respect to the decrease in flying-height of LEC, TEC and DTD. 42

Figure. 3.5.2.1 Frequency response of harmonic analysis for HGA#1. 43

Figure. 3.5.2.2 Nodal lines on the slider ABS extracted from harmonic analysis of HGA#1 showing DTD and roll modes (a), typical pitch modes (b), and suspension-coupled modes (c). 44

Figure. 3.5.2.3 Frequency response of HGA#2 from harmonic analysis (a) and the corresponding nodal lines on slider ABS (b). 45

Figure. 3.5.2.4 Frequency spectra from transient analysis with vertical excitation (a), off-track excitation (b) and down-track excitation (c). R1 in (b) denotes the location on the slider that represent roll modes. 46

Figure. 3.5.2.5 Comparison between the simulated spectrum (a), and experimental spectra at DTD (b) and LEC (c) for HGA#1 subjected to DTD excitation. 47

Figure. 3.5.2.6 Comparison between the simulated spectrum (a), and experimental spectra at DTD (b) and LEC (c) for HGA#2 subjected to DTD excitation. 48

Figure. 4.2.1 Representative heater protrusion at around 10 nm for (a) HGA#1 and (b) HGA#2 when viewed from the ABS surface and from sides (c)-(d) respectively. It is noted that HGA#1 is much sharper and therefore possesses smaller contact area. The sharper profile also increases the thermal actuation efficiency. The scale of the color bar is in nm. 51

Figure. 4.2.2 Experimental setup: (a) OFV-130-5 microscopic lens, (b) fiber optics and (c) Navitar lens with filter. 52

Figure. 4.3.1.2 (left) Summarized modulation regime observed on design #1 and #2. The error bar indicates the +1/-1 standard deviation among the 7 samples for each design. (right) Normalized MR shows a similar value between designs. 53

Figure. 4.3.1.1 Representative modulation regimes for different HGA designs over ZTMD disks. The 15th TFC power steps indicates touchdown here. 53

Figure. 4.3.2.1 Representative modulation regimes for design #1 on Z-Dol 12 Å and ZTMD media. Z-Dol 12 Å results in a much larger modulation regime. TFC power step #15 is the defined touchdown power. 55

Figure. 4.3.2.2 Summarized modulation regime on ZTMD and Z-Dol media for design#1. 55

Figure. 4.3.2.3 Summarized modulation regime on ZTMD and Z-Dol media for design#2 56

Figure. 4.3.2.4 Summarized modulation regime for design#1 57

Figure. 4.4.2.1 The evolution of LEC and TEC modulations characterize the MR and OR with 1 mW variation among (a) ZTMD and (b) Z-Tetraol lubricated surfaces. TFC power step #10 is the detected TDP. The area covered by blue is MR, and OR is in red. First row represents the LDV modulation, and the second row shows the corresponding AE reading. 59

Figure. 5.2.1 Images from OSA show mogul formation on various lubricated surfaces: (a) Z-Dol 12 Å, (b) W-MD 12 Å, (c) Z-Dol 9 Å and (d) Z-Dol 15 Å. In each sub-figure the top image represents 0 minute load scan, the middle one shows load scan at 7 minutes, and the bottom image shows the thermal protrusion area marked by continuous contacts. By the use of thermal protrusion marks the position of slider can be estimated in each sub-figure.....63

Figure. 5.3.1.1 Illustration of experimental scheme using MATLAB-processed OSA images. The width shown in each loading condition is approximately the dimension of slider's center pad on the TE. A whiter area means a higher lubricant thickness, which is termed mogul in this chapter. In the continuous contact condition, the dark track indicates a groove plowed by the thermal protrusion. 65

Figure. 5.3.2.1 Slider modulation and lubricant modulation are well correlated location-wisely. Purple data represent the lubricant's circumferential profile radially averaged over 40 microns. 66

Figure. 5.3.2.2 Mogul evolution as touchdown progresses. The insertion is a zoomed-in view of the mogul being observed. The mogul originates from a flat lubricant profile and then grows in height and width. When a height of 5-6 angstrom is reached, the mogul seems to be sheared towards the down-track direction. 67

Figure. 5.3.2.3 Mogul shows a reserve trend under successive 5 mW TFC overdrives/overpushes. The mogul "spreads" in the down-track direction. 68

Figure. 5.3.3.1 Representative lubricant deformation history under continuous contacts 69

Figure. 5.3.3.2 Lubricant depletion thickness over time (left), and the normalized depletion with respect to overall thickness, (right) among different lubricant designs. The 19-minute data represent lubricant recovery after 15-minute TFC overdrives, which suggest lubricant replenishment. 69

Figure. 5.3.4.1 Demonstrative mogul profiling result. The insertion shows the numerically found mogul profile at different scans. 70

Figure. 5.3.5.1 Moguls' dimension evolution as a function of touchdown passes 72

Figure. 5.3.5.2 Normalized MR and dTDP as a function of touchdown passes 73

Figure. 5.4.1 First touchdown attempt of a slider after a 15-minute passive flying. When the slider approached the existing mogul developed previously, slider modulation started developing from approximately 2-3 mW away from TDP. This directly shows the possibility of slider modulation sensing moguls. Second rows are zoomed-in data plots for modulations. 75

Figure. 5.4.2 MR evolution from TD to overdrive.....76

Figure. 5.4.3 dTDP evolution from TD to overdrive 76

Figure. 5.5.1 Raw OSA image showing touchdown induced mogul formation (middle) on a Z-Dol 9 Å sample. (top) Topography of passive flying at 11 minutes, (middle) approximately 30 touchdowns and (bottom) continuous contacts in 900 seconds. Touchdown-induced moguls are circled in read. 78

Figure. 5.5.2 Raw OSA image showing touchdown induced mogul formation on Z-Dol 15 Å sample. (top) Topography of passive flying at 11 minutes, (middle) approximately 30 touchdowns and (bottom) continuous contacts in 900 seconds. Note the sheared mogul formed due to contacts (circled in red) are different from the moguls form outside the thermal protrusion area. 79

Figure. 5.5.3 Raw OSA image showing touchdown induced mogul formation on Z-Dol 12 Å sample. (top) Topography of passive flying at 11 minutes, (middle) approximately 30 touchdowns and (bottom) continuous contacts in 900 seconds. The contact-induced moguls' (circled in red) dimensions are different form the ones formed in passive flying. 80

Figure. 5.5.4 Raw OSA image showing touchdown induced mogul formation on W-MD 12 Å sample. (top) Topography of passive flying at 11 minutes, (middle) approximately 30 touchdowns and (bottom) continuous contacts in 900 seconds. Contact-induced mogul (circled in read) is much smaller in area when compared to Z-Dol samples. 81

Figure. 6.2.1.1 Experiment set-up diagram 84

Figure. 6.2.2.1 dTDP as a function of TD cycle under different levels overdrive power. 86

Figure. 6.2.2.2 AES COC wear and dTDP as a function of TFC overdrive. 86

Figure. 6.2.2.3 AES COC wear as a function of dTDP. 87

Figure. 6.2.2.4 Wear resistant performance of ZTMD lubricant (lube A) and D-4OH (lube B) lubricant under TFC overdrives. Multidentate lubricant induced more wear during slider-disk contacts.....88

Figure. 6.2.2.5 Lubricant dependence on AES COC wear as a function of dTDP. 89

Figure. 6.2.3.1 HGA#1 wear under SEM inspections: (left) showing 10 mW TFC overdrives and (right) 20 mW TFC overdrives against Z-Tetraol lubricated surfaces. SEM images were credited to Kaynam Chun at WDC. 90

Figure. 6.2.3.2 HGA#2 wear under SEM inspections: (left) showing 10 mW TFC overdrives and (right) 20 mW TFC overdrives against Z-Tetraol lubricated surfaces. SEM images were credited to Kaynam Chun at WDC. 91

Figure. 6.3.2.1 Typical temperature response of TDS from flying to contact. 93

Figure. 6.3.2.2 Representative TR curves as functions of TFC powers up to TDP with different amounts of wear 94

Figure. 6.3.2.3 PtTR and wear readings from dTDP.....94

Figure. 6.3.2.4 PtTR and dTDP correlation 96

LIST OF ABBREVIATIONS

ABS	Air Bearing Surface
AFM	Atomic Force Microscopy
AES	Auger Electron Spectroscopy
BPM	Bit Patterned Media
CML	Computer Mechanics Laboratory
COC	Carbon Overcoat
DLC	Diamond-Like Carbon
FEA	Finite Element Analysis
FFT	Fast Fourier Transform
HAMR	Heat-Assisted Magnetic Recording
HDI	Head-Disk Interface
HDD	Hard Disk Drive
LDV	Laser Doppler Vibrometry/Vibrometer
OSA	Optical Surface Analyzer
MR	Modulation Regime
PFPE	Perfluoropolyether
PMR	Perpendicular Magnetic Recording
SMR	Shingled Magnetic Recording
SEM	Scanning Electron Microscopy
TDMR	Two-Dimensional Magnetic Recording
TD	Touchdown
TDP	Touchdown Power
TFC	Thermal Flying-Height Control

ACKNOWLEDGEMENTS

The summer in 2015 marks the full five year since I landed the United States pursuing my doctoral degree at University of California at Berkeley. It has been an unforgettable adventure which I would not have been through without supports from people around me.

The days fulfilled with research would not have been so motivating and intriguing without my advisor, Prof. David B. Bogy. Prof. Bogy supports me financially throughout my doctoral study and has been generously providing me flexible resources towards experimental staging and businesses traveling. Under such a worry-free environment, I could focus on my research and strike for a balanced life. He has an open-minded yet strict research spirit which affects me deeply. I learned from him that research-wise everything is possible and the purpose of research is keep advancing the front-line knowledge; life-wise we should treat people precisely-reasonably as we do to ourselves. Both are not easy but Prof. Bogy is one of the geniuses that excel them. In addition, Prof. Bogy is always on the side of his students. I thank him for being my great advisor.

Part of the requirements for Ph.D. is course study, and I thank professors giving lectures to my major and minor disciplines. Special thanks to my dissertation committee: Prof. Steigmann interrogates me with his nutritious solid mechanics knowledge and Prof. Strain delivers numerical techniques with a great sense of humor. I thank Prof. Zohdi and Prof. O'Reilly for serving as committee members in my qualifying exam.

Research in HDDs are highly industry related, and certain achievements cannot be done with profound advices, suggestions and material supports from HDD companies. I would like to thank people from Hitachi GST (now HGST, a WD company), Dr. Run-Han Wang for equipment advises. Dr. Aravind. Murthy and Dr. Remmelt Pit mentoring me through my summer Co-op in 2012. Kevin Hunter and Karl Flechsig for staging supports. Special thanks to Aravind, and Kevin for working with me on Candela OSA 5100 donation to CML and Dr. Rohit Ambekar for VENA environmental chambers.

Engineers in Western Digital Corporation play an unrivaled role in my research project through 4 years WDC-CML collaboration. Special thanks to Dr. Jih-Ping Peng for serving the principal investigator from WDC for my research projects. Jih-Ping has been very helpful, friendly and generous in sharing his perspectives in HDD research and fatherhood. Jih-Ping also introduces several experts in different realms of HDD tribology to me. Dr. Shaun Chen and Dr. Yasuo Sakane supported me with special media requests, Tzhong-Shih Pan for HGA supports and Kaynam Chun for SEM investigations.

I would like to thank Seagate Technology, who donated a Candela OSA at the time we needed it the most in 2011. Big thanks to Minh Lee for passing her experience in measurement.

Equipment vendors' contribution cannot be left behind. I would like to thank Eric Lawrence from Polytec Inc. for supporting me with OFV-534 and OFV-551 loaners back and forth. Eric also shares his valuable experience with me regarding using the laser Doppler vibrometer efficiently to maximize research throughput.

Hysitron Inc. has been helpful by providing me with the most advanced nanoindentation technology. I would like to thank Dr. Douglas Stauffer, Dr. Anqi Qiu and Richard Nay for hosting me when I was doing experiments at Minnesota. Special thanks to Douglas for working with me on the testing of xProbe all along.

Lab mates are always supportive. From my first few years, senior CML lab members Jinglin Zheng, Liping Li, Joanna Bechtel, Sripathi V. Canchi and Rahul Rai have been providing me with resourceful solutions to research and course works. Visiting scholars Jia Zhao, Yuliang Liu, Dequan Shi and Fabio Azilazian showed their enthusiasms from different research realm. Most of my doctoral studies were accompanied by Shaomin Xiong and Alejandro Rodriguez Mendez. Shaomin Xiong always shares his excellent experiment skills with me, and Alejandro has been my homeboy from a fresh Cal student to a fresh Ph.D. We have attended several international conferences together and studied on the same course subjects for endless nights. Material group in CML broadens my research view. I thank Na Wang, Jun Xie and Jozef Matlak for sharing their knowledge in carbon films with me. Young students in CML are always energetic. I thank Soroush Sarabi, Amin Ghafari, Haoyu Wu and Yuan Ma. I especially enjoy staging and discussing and sharing my experience with Yuan Ma and Haoyu. I have to mention our lab manager Dolf Mardan. He has been an excellent helper in all lab associated issues and skillful in software/hardware maintenance. Thomas Clark and Rene are staffs in ME department that I cannot forget to mention for their hardware/software advisory.

I was fortunate enough to have a few very good intern students during my Ph.D. career. I thank Snigdha Sharma, Ye Han and Delara Mohtasham for giving me the opportunity to be a mentor. I feel blessed learning Snigdha attending CMU and Ye joining Prof. Carpick's group soon. Special thanks to Delara for staying with me for three semesters studying lubricant modulations.

My friends nourish my life. I especially thank Chih-Ming Lin and Jun-Chau Chien for not only keeping me from being a dull boy but provide me with their own expertise to help conduct my research.

Last but not the least; my family is the genesis of all my achievements. I have a big family including mine and my wife's. They provide unconditional support and accompany all along. Special thanks to my wife, Yu-Chu, for supporting me and our family with enormous dedication and love.

Chapter 1

Introduction

This chapter briefly introduces the hard disk drive and its head-disk interface, the thermal flying-height control (TFC) technology, and the objective and the organization of this dissertation.

1.1 The basics of a hard disk drive and its evolution

The hard disk drive has become the main stream data storage solution since 1950s, and its name is associated with its physical architecture: coaxial spinning hard disks. Different from other storage strategies utilizing optics or electronics/flash memory, hard disk drive belongs to the realm of magnetic storage. Magnetic bits are stored as either "0" or "1" in polarity on the magnetic layer on the disk, and the spinning disks allow the magnetic read-write transducer to access data over the recording surfaces. Primarily due to the rotating disks and the necessity to position the magnetic transducer accordingly, the hard disk drive involves extensive mechanical engineering, and especially in dynamics, control, mechanics of materials, and tribology [1].This dissertation focuses on the tribological aspects in the mechanical interface where the magnetic data is written.

To achieve a stable tribological interface in HDDs, the head that carries the read-write transducer is required to be precisely positioned with respect to the rotating disk surface. A proper separation between the head and disk surface allows effective lubrication between fast moving surfaces. The planar positioning of the magnetic transducer can be mostly achieved by controlling the rigid-body motion of an actuator; however, the vertical positioning is based on a different strategy. In contrast to planar motions, the mechanical separation between the magnetic transducers and the fast rotating disks requires a stable, adaptive and accurate spacing control to properly position the head at disk proximity.

The requirement for the head to be placed at disk proximity comes from the necessity to sense the magnetic signals from recording surfaces. While smaller head-disk spacing provides a better signal to noise ratio for the magnetic sensory, the intensity of the magnetic fields decrease as the magnetic bits' physical dimensions shrink, which conversely increase the areal density. Because areal density is a direct measure of the capacity, it has been the

Figure 1.1.1 An early Winchester drive around 1975. It works on 14" disks and holds a storage capacity of 20 Mega-bytes. The "brown-orange" material on the disk is the hue of iron oxide particles. Its size is considerably huge compared to a more modern Western Digital 3.5" drive manufactured in 2008 with 40 Giga-bytes capacity on the top-right of the figure.

main indicator of the evolution of the HDD [2]. Under the demand of increasing areal density the definition of "proximity" has evolved from the scale of microns to a few nanometers as of today.

Historically, the very first commercial hard disk drive, IBM 350 [3], was used in a computer named Random Access Method of Accounting and Control (IBM 305 RAMAC) introduced in 1956 by IBM. The RAMAC system was designed to access data (characters) stored in magnetic platters in a "fast" way, with seek times around 600 mille-seconds and with a capacity of 5 million 6-bit characters which totals 3.75 Mega-bytes. The method used to position the head away from recording media was achieved by planar pressurized air bearing sliders at around 20 um spacing. Later a more advanced self-acting hydrodynamic air bearing (IBM 1301 in 1962, and Winchester in 1973) was adopted by forcing the ambient air flow through a designed air bearing surface (ABS), instead of using an external compressed air supply. This improvement made a much smaller head-disk spacings possible and paved the way for today's commercial HDDs [4], as shown in Fig. 1.1.1.

Although the basic operating principle for the HDD has not been changed drastically since 1970, technologies dedicated to the integration of recording media and magnetic sensor never ceased to evolve. Such evolution is a combination of the advancement in materials (giant magnetoresistive materials [5]), mechanics (heat transfer, lubricant, air bearing surface design, etc…) and manufacturing (thin film inductive heads [6] and media [7]). Over a nearly 60-year development, remarkable improvements were made in terms of dimensions, weight, speed, areal density, cost and reliability. The aforementioned RAMAC

305 system weighted over a ton and was larger than a residential refrigerator, and it cost $3200 for a monthly lease back in the 1960s; now one could easily order a commercial 2.5" mobile HDD that weighs less than half a pound with a capacity of 2 TB for $89. Specifically, the term "proximity" has evolved from 20 μm to around 2 nm under writing process.

In fact, many new proposals are made towards a higher overall capacity or areal density in HDDs, including bit-patterned media (BPM) (new media technology) [8], two-dimensional magnetic recording (TDMR) (read-write architecture) [9], shingled magnetic recording (SMR), heat-assisted magnetic recording (HAMR) (new head and media technology) [10] and Helium technology. Among them, the Helium-filled drive has been delivered since 2013 at a capacity of 6TB and up to 8TB in 2014 and 10 TB utilizing Helium with SMR in June 2015; and HAMR has entered the development stage from research level. A demonstration product from Seagate was presented at INTERMAG 2015 conference performing read/write using HAMR technology.

1.2 A tribological challenge in HDDs: the head-disk interface

Regardless of which new technology is going to be implemented in HDDs, the tribological interface remains a challenge. Current hard disk drives operate with air-bearing sliders flying over disks spinning 5400-15,000 revolutions per minute (RPM) with a writing spacing around 2 nm or even lower. The air-bearing sliders are designed to perform the read-write process in a flying condition without contacts. A long-term non-contact recording at disk proximity relies on successful ABS design and media integration. The magnetic transducer is commonly referred to as the "head", which is always carried by an air bearing slider. Therefore, mechanically a head and a slider are viewed as an integrated unit. The interface between the head and the disk is called the head-disk interface (HDI).

The air-bearing technology in the HDI allows the slider to fly stably at a few nanometers away from the disk surface. There are two measures of the flying height; one is the magnetic spacing and the other is the physical spacing, and they differ by the protective layers on top of the magnetic media.

A disk substrate, the "hard disk", is usually made of an aluminum alloy or glass, and it is coated with various under layers and a magnetic layer of approximately 20-30 nm thick. On top of the magnetic layer is the diamond like carbon (DLC) layer ranging from 15Å to 25Å and on top of that a perfluoropolyether (PFPE) lubricant layer of 9Å to 16Å in thickness. The read-write portion of the slider surface is coated with a 10Å to 20Å DLC layer. Each layer comes with its own roughness that is not negligible in view of the nanoscale contact. From the mean top surface of the magnetic layer to the read-write head under the DLC layer is termed the magnetic spacing. From the mean top surface of the PFPE lubricant layer to the mean top of the DLC layer on the read-write portion of the slider is called the physical spacing.

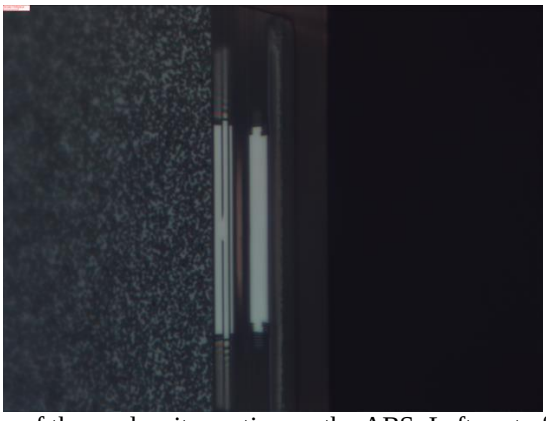

Figure 1.3.1. Zoomed section of the read-write portion on the ABS. Left part of the metal stripes are reader shields, and the writer return poles are on the right.

The typical physical spacing for sliders in current products is about 5 nm to 10 nm with modulations around one nanometers or lower [2, 11, 12], depending on the ABS design and the corresponding RPM. The general low flying attitude makes the DLC and PFPE layers of special importance. DLC layers and PFPE layers provide a reliable wear and corrosion resistant protection for the soft magnetic layer. PFPE lubricant layers featuring low surface energy and high chemical stability provide good surface protection in the event of contacts, and produce a long-term non-contact tribology interface.

In addition to the air bearing, the nanoscale mechanical spacing is maintained together with a delicate suspension structure that positions the slider with a given load against rotating media. Suspension design plays an important role in controlling the slider's dynamic response to environmental disturbances as well as in precision track positioning. A slider is bonded to a suspension through a gimbal structure, and therefore in component level experiments a slider/suspension combination is often referred to as the head-gimbal-assembly (HGA). A detailed explanation for a typical HGA can be found in [13].

In this dissertation we are mainly concerned with the effects of the TFC induced physical clearance change and the corresponding slicer and lubricant dynamics.

The challenge in studying the HDI is to understand the physics that cannot be directly observed through optics or electronic microscopy due to the extremely narrow physical spacing. We can, at best, perform experiments that are designed to measure relevant quantities and deduce the physics from the results. An interesting yet challenging feature of the research in HDI is fact that the HDI involves a several interfaces of materials with dimensions ranging from a few angstroms to tens of micro-meters. The separation of the length and possibly time scales can make simulations/experiments hard to accomplish.

1.3 The thermal flying-height control technology

Traditionally the reduction of the slider's flying height was achieved by the ABS design. However, the reduction of the flying altitude by the ABS design brings the whole slider's trailing end to almost the same level, causing more of the ABS to interact with surfaces below through intermolecular forces, electrostatic forces, topography modifications and direct contacts. A recently commercialized technique is the thermal flying-height control (TFC) technology. The TFC architecture uses a resistive heating element to deform a local region around the read-write head portion (Fig. 1.3.1) of the slider, bringing it closer to the disk [14, 15]. The physical spacing may be controlled by changing the power supplied to the TFC heater, and the control is capable of producing nanometer variations in physical spacing using powers in milliwatts.

One of the designs of the ABS and the heater used here is shown in Figs. 1.3.2. In general the heater protrusion is a very "blunt" bulge because its horizontal dimensions are on the order of tens of microns whereas its vertical dimensions are in tens of nanometers. Fig. 1.3.2 (b) shows a representative ABS pressure profile with an 11 nm thermal protrusion. Fig. 1.3.2(c) shows a representative thermal protrusion with a maximum height around 11 nm on the trailing edge of the ABS.

Although TFC technology improves HDI reliability and spacing control, it complicates the mechanics of the HDI by introducing a non-negligible amount of heat flux into the existing mechanical interface. A thermal protrusion has to be optimized in terms of location, geometry, associated actuator power and the induced temperature field. Since the thermal problem has to be solved in a mechanical interface, a TFC slider inevitably involves thermo-mechanical coupling in modeling and experiments.

From research point of view, the local protrusion provides a confined area of contact, and this feature is very useful in studying the dynamics and wear in the HDI. Because the local protrusion can be viewed as a probe, TFC sliders can be devised as a fast probing technique that may be used to explore different properties of lubricants and DLC layers at ultra-high shear rates.

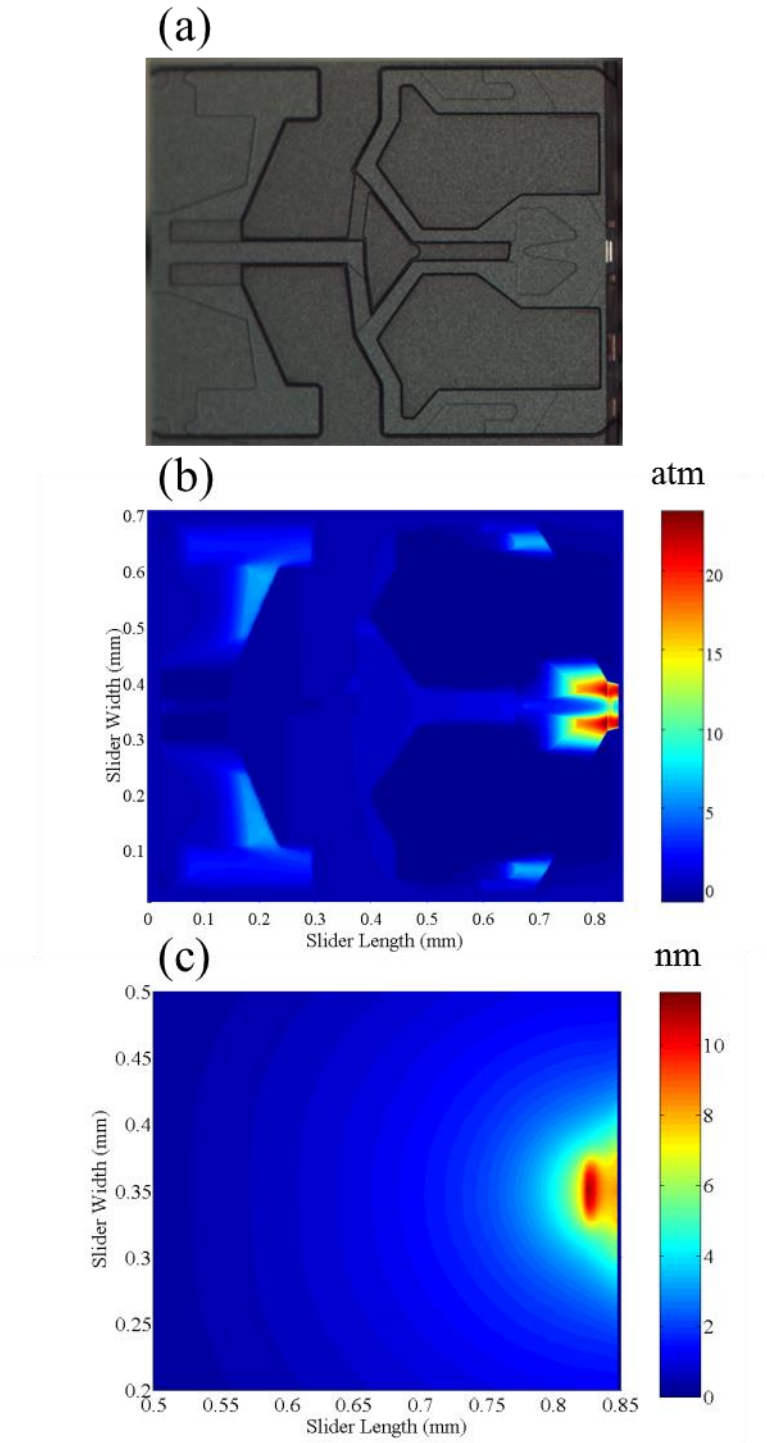

Figure 1.3.2 (a) Photograph of one of the ABS designs used in this dissertation, (b) simulated ABS pressure and (c) the representative heater protrusion profile at a maximum height of 11 nm.

1.4 Objective of this work

The objective of this dissertation is to advance the knowledge of the head-disk contacts by investigating the interactions between the top lubricant layers on the disk surface and the air bearing slider over various contact regimes by experiments with simulation.

1.5 Organization of the dissertation

This dissertation is composed of seven chapters. Chapter 1 gives a brief introduction of HDD basics, the HDI, the TFC technology, the dissertation objective and organization. Chapter 2 provides a preliminary outline to the study of HDI. It presents fundamental methodologies of instrumentation and experiment design as well as rationales for the following studies covered in this dissertation. Chapter 3 focuses on slider-disk contact detection using slider dynamics at contact proximity as a transition from flying to light contacts. Multiple degrees of freedom in slider dynamics are measured using fine focusing lens and dedicated numerical simulations are used to support and interpret the experimental findings. In Chapter 4 the slider dynamics is further analyzed to characterize head-disk contacts. It is found that head-disk contact detection is sensitive to slider/media match and a reliability measure is proposed to evaluate media performance. Chapter 5 investigates in detail the slider-disk contact in the view of lubricant modulation. Chapter 6 discusses the head wear caused by slider-disk contacts beyond the touchdown power level. Two TFC-based methods are proposed and calibrated to monitor the amount of head wear. The newly proposed method using a temperature sensor attempts to measure head wear without incurring contact. Chapter 7 concludes the dissertation by summarizing the significant observations/findings and proposing future works.

Chapter 2

Preliminary study of the head-disk interface with TFC slider

This chapter presents a preliminary investigation of head-disk interaction. It reports different interference stages of slider contact against lubricated surfaces in terms of slider dynamics. In addition to the findings from experiments and simulations, detailed description of the experimental setup and the specifications of the equipment and experimental samples are provided, if applicable. Part of this chapter is devoted to explaining the calibration procedure of the optical surface analyzer (OSA) as well as its importance in quantifying the PFPE lubricant thickness changes.

2.1 Introduction

A successful read-write process relies on a stable HDI. Driven by storage demands, the ever increasing areal density dictates a lower flying height. Before TFC technology was implemented into commercial HDDs, the efforts in advanced ABS design were focused on achieving a low fly-height slider that can operate without contacts throughout its designed lifespan. Nonetheless, a flying height of 5 nm or below had been a threshold for stability because of surface roughness and force interactions. Decreasing the spacing below 5 nm often produces instabilities. Instabilities at disk proximity are attributable to intermolecular forces, electrostatic forces and menisci formation, to mention a few [16]. Although instability is not desirable in industrial applications, it is of academic and research interest. Prior to 2008, most experimental instability investigations were done by bringing the head to the disk surface through either reducing the RPM of the disk or the ambient air pressure in a chamber [17].

The way instabilities were studied reflects a problematic nature of a low fly-height slider: a massive contact/interference area, even considering the trailing edge only, can significantly scale up the attraction force. In view of the disk, a low fly-height slider with relatively large areas at disk proximity also enhances the lubricant transfer from the disk to the slider. The introduction of TFC technology resolves these disadvantages by reducing

the proximity area through the use of localized joule heating, resulting a confined thermal protrusion that reduces the flying height only locally.

While the TFC technology currently enables a lower writing spacing of around 1-2 nm, it requires an additional understanding of the concept of contact so that a desired spacing, say 2 nm, can be precisely set. Therefore, contact detection serves as one of the most important internal calibration procedures in a HDD, and contact detection is not expected to be performed more than about 10 times during a drive's lifespan.

Since the most obvious way to determine head-disk contact is to cause it, a head-disk contact is then inevitable, and its understanding is essential for HDD reliability. Prior to establishing the most sensitive detection scheme, an overview of slider-disk contact behavior would benefit the research starting from a fundamental investigation. One way to understand head-disk contacts is to perform an in-situ slider-disk interaction while monitoring it from flying to the initiation of contact and beyond that to a more severe contact. One reason for studying the slider-disk interaction beyond contact is to probe the possibility of contact recording. Contact recording, means the mechanical spacing is reduced to zero, and this is one way to maximize areal density under existing perpendicular media recording (PMR) [2, 11].

One idea proposed for contact recording was called "surfing" which is considered to be theoretically possible for a slider's thermal protrusion to skim through the lubricant layer but not contact the carbon layer [25, 26 and 27]. Nonetheless, surfing is seldom experimentally observed with all supporting data, including slider dynamics, interfacial forces and lubricant modulation [29]. In this chapter, "experimental surfing" is defined and its feasibility is evaluated. The characteristics of bouncing including the onset of contact and the corresponding oscillation modes are explained with simulation support.

2.2 Experimental Setup

The experiments are performed on a stage capable of making in-situ measurements using an acoustic emission (AE) sensor, a laser Doppler vibrometer (LDV) and an OSA, which is based on high resolution scanning ellipsometry [18] (Fig. 2.2.1). The AE sensor detects the elastic-stress waves in the actuator arm transmitted from the slider and suspension caused by slider-disk contacts, the LDV measures the vertical velocity of the slider at the its trailing edge center (TEC), and the OSA monitors the modulation of the lubricant layer coated on the disk surface [20].

2.2.1 Laser Doppler Vibrometer

The LDV used here is made by Polytec Inc. and it contains three main parts: the electronic controller (OFV-3000), the interferometer (OFV-512), and the probe head (OFV-101). The

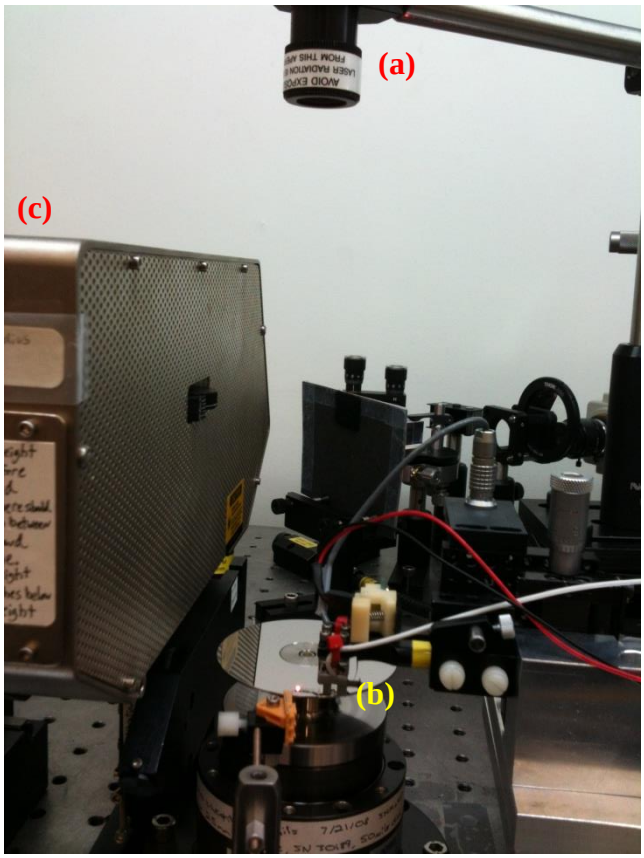

Figure 2.2.1 The experiment setup contains (a) LDV, (b) AE sensor and (c) OSA for in-situ measurements.

controller performs the signal processing and decoding. The interferometer hosts all of the optics and the laser. The probe head focuses the laser spot to the desired dimension. The OFV-512 is a differential interferometer, and when it is used in "single ended" mode, the reference end must be optically grounded with a calibrated mirror, which may not be used interchangeably with other similar LDVs. A proper fiber alignment is required to give an output power at 1 milliwatt (mW), and it is a good measure of the system's condition.

2.2.2 Acoustic emission sensors

The AE sensor is composed of a piezoelectric plate of lead-zircon-titanate (PZT) with conductors on its faces, and it is designed to detected high frequency (> 10 kHz) elastic wave signals that propagate through the slider-suspension structure. AE sensors are very sensitive even though the signal is quite small, and a proper pre-amplifier plus an amplifier are required to perform contact detection. The AE sensors used in this chapter are manufactured by Acoustic Emission Technologies (AET). The gain setting on the amplifier is also important for obtaining reliable results. Too large a gain picks up too much environmental noise while too small a gain loses the sensitivity. In the contact detection

application the contact signal shows a repeatable result at gains equal to 50 dB with a multiplier of 0 on the amplifier panel. Larger gains can make false detections by amplifying electronic noise. AE sensors manufactured by Physical Acoustics Corporation are used from chapters 3 through 6, in addition to the AET sensors.

2.2.3 Optical Surface Analyzers (OSA)

The OSA used in this research was manufactured by Candela Instruments around 1998 and this model is based on the Candela-2100 but with a more advanced scanning head that has the feature of the Candela-5100, such as the scribe and topography channels, and it is installed in an open platform, capable of adding other measurement tools on an air table. The planar resolution is better in newer models; however, the vertical resolution stays equally good between the different models.

The OSA is an optical tool that uses ellipsometry to investigate thin film profiles. The film being scanned must be transparent to some degree so that the phase shifts of the reflected laser beams can be analyzed, and a calculated "reflectivity" is produced as a result of the film thickness. The OSA has several different channels, and each of them is optimized for certain features on the film [18].

2.2.4 Load cell and strain gauge

The load cell refers to an assembly of beam structures that can sustain loads, and strain gauges glued to the machined surfaces on the beam. The load cell used in this experiment is scavenged from a HGA holder made by TTi Inc. The signal conditioner is from Vishay Precision Group. The strain gauges were configured as a Wheatstone bridge circuit.

2.2.5 Data acquisition and flying-height control

The data were acquired by a National Instrument (NI) USB-6211 DAQ device and a high speed PCI acquisition board by Measurement Computing (PCI-DAS4020/12). NI USB-6211 is used to feedback control the TFC voltage by sensing the voltage from its analog output terminals. The PCI-DAS4020 features simultaneous data acquisition up to a 20 MS/s sampling rate and is used to capture dynamic signals from the slider. A customized Labview program is written to calculate and control the TFC power with sub-mW resolution; a software, Ultrafast, developed by TTi Inc., is used to control PCI-DAS4020 at an acquisition rate of 1MS/s.

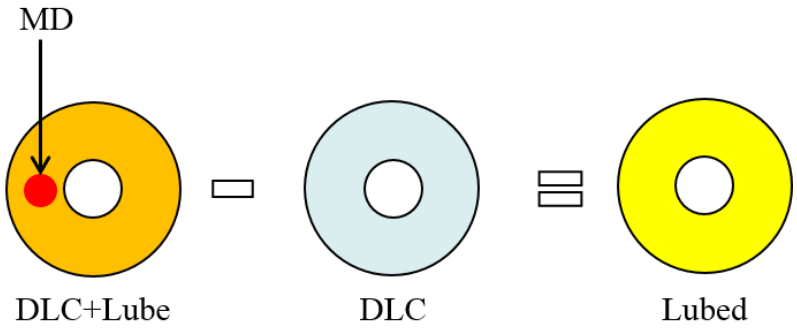

Figure 2.3.3.1 Representative diagram showing the Pre/Post Lube calibration procedure.

2.3 Calibration Procedures for the Optical Surface Analyzer

In this work, we use the Q phase of the OSA, which is an optimized combination of P polarization and S polarization lights at an incident angle close to the Brewster's angle, to perform PFPE film thickness measurements. However, the OSA can only present the relative "reflectivity" all over the surface to the machine's optical ground, thus a calibration procedure is essential in converting the OSA readings to the true thickness variation of a specific type of film.

2.3.1 Sample Preparation

The samples were manufactured with the help of Western Digital Corporation (WDC). Eight disks with bare DLC layers were first made for background scans, and then the same disks were dip-coated with Z-Tetraol lubricants to produce thicknesses from 9Å to 20 Å. The disk substrates were glass of 0.8mm thickness and 65mm in outer diameter and 20mm in inner diameter. The lube thicknesses were measured using Fourier transform infrared spectroscopy (FTIR) in WDC.

2.3.2 Calibration Procedure

Eight disks with bare DLC layers (no lube) were first scanned using the Q phase channel on both sides. The reason for scanning the DLC layers is to collect the background variations due to the waviness and roughness of the disk. Since the background variations and waviness are disk surface dependent, the eight disks with 16 surfaces were marked with different patterns using the scribe function on the OSA scanning head for reference.

The 16 surfaces were later sent back to the media site of WDC where they were dip-coated with Z-Tetroal lubricants from 9Å to 20 Å. Each surface was then re-scanned with the lubricants on it. The scanning radii were from 20mm to 24mm (middle radii, MD) with 4 microns resolution in the radial direction and approximately 4~5 microns in the circumferential direction. The averaged reflectivity reading of the un-lubed DLC disks at the MD was recorded and subtracted from the lubricated ones on the same surface with references to the scribed marks.

The differences in the readings before/after dip-coatings result from the different thicknesses of lubricants less the DLC contributions on the background. The 16 differential readings were analyzed by least-squared linear curve fitting, and the slope of the linear approximation line is the reflectivity/Å conversion ratio. This calibration procedure is called the Prelube/Postlube method

2.3.3 Calibration Results

The analyzed result is shown in Fig. 2.3.3.2. A good calibration result was obtained and it supports the feasibility of using the OSA for measuring PFPE film thickness variations. Theoretically different types of PFPE films may have different reflectivities, and to precisely describe the amount of lubricant modulation a calibration should be performed using the specific PFPE lubricant of interest. The negative slope results from the fact that the thicker the lubricant layer, the less reflective light will be detected by the OSA. This result is used as a reference number for all Fomblin-Z PFPE lubricants later in this dissertation. However, the variation between lubricant types may not exceed an error of 15% [22], and the calibration is more system-specific.

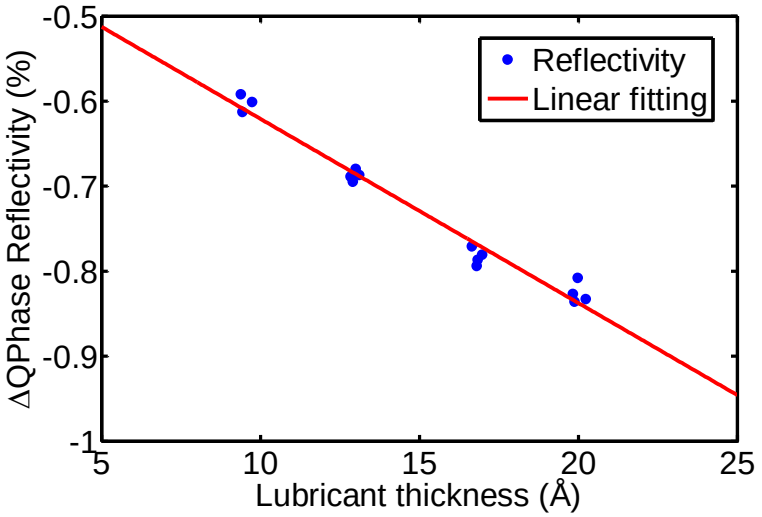

Figure 2.3.3.2 The calibration result using the Prelube/Postlube methods. The slope of the linear fitting line is -0.0217% with R^2=0.9739

2.4 Methodology

In order to investigate the slider-disk interaction and to find the interference levels of interest, we implemented a series of experimental schemes to identify the slider-disk contact characteristics. A Polytec LDV, an AE sensor and an OSA are used to monitor dynamic signals from the slider and lubricant surface.

2.4.1 Experimental schemes

Experiments were performed using the TFC power control with a custom programmed Labview code and a USB-6211 multifunctional data acquisition board with a voltage follower circuit. We observed three distinct dynamical phases during a continuous stair-up TFC power scheme (Fig. 2.4.1.1), and the three power schemes are used to investigate the dynamics at each phase. The LDV measures the vertical velocity signal of the slider at the trailing edge center (TEC) from its back-orifice on the suspension (Fig. 2.4.1.2). Contacts are identified by the touchdown power (TDP), which is based on the abrupt modulation in the AE signals.

The first test scheme applied a step-up power history with 30 milliseconds (ms) dwelling time at each power step from 0 mW to a certain power level that demonstrates a typical light touchdown in the AE signal. With this scheme, we are able to detect and define the TDP, set up the particular power levels of interest and observe the overall light contact dynamics.

The first test scheme provides three phases that characterize the light touchdown, including the value of the TDP, and the power range within which each phase is defined. Therefore, we can choose three distinct power values that are representative of each phase: TDP-5

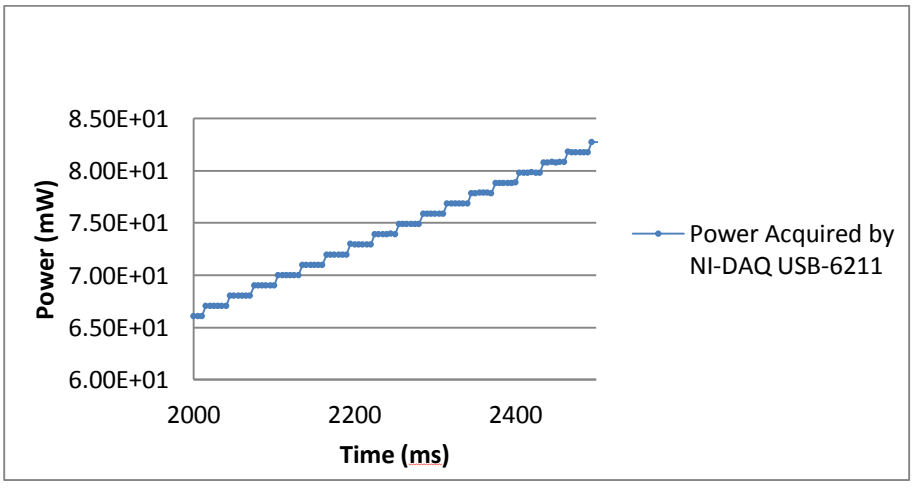

Figure 2.4.1.1 Step-up power history with 30 ms dwell time

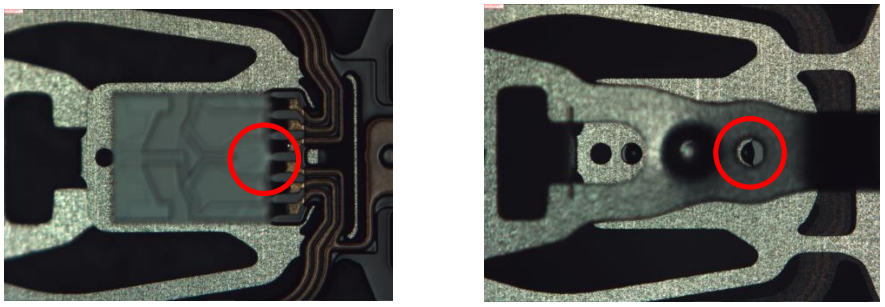

Figure 2.4.1.2 (left) Part of the suspension from the ABS side's view (in the background) (right) Top view of the suspension in part. TEC is marked using a red circle, where the LDV takes the measurement.

mW (P1), TDP+5 mW (P2) and TDP+55 mW (P3) which represent phases I, II and III respectively. In the second test scheme, the power history was similar to that in the first test scheme but remains at each distinct power level, P1, P2 and P3, for 1000 ms to investigate the slider dynamics at each level. The dwelling time at each power step is 30 ms for P1 and 15 ms for P2 and P3. The reason for the dwelling time change in this scheme is to demonstrate that the change from 15 ms to 30 ms is sufficiently long for the system to reach its steady state at each power step as suggested by the repeatable experimental results.

To explore more of the physics of phase III we set up the third test that is similar to the second scheme but with P3 at TDP+65 mW and P1 at TDP-5 mW kept fixed for twelve minutes to investigate its stability and interactions with lubricants.

2.4.2 Numerical simulation

While the slider-disk interaction has been experimentally identified using AE, LDV and OSA, the frequency spectrum presented by the LDV requires a physical explanation. Most experimental studies attribute these observed vibration modes to the slider's 1st pitch and 2nd pitch modes by experience and rationale, but in this dissertation a numerical simulation using a detailed HGA model together with the effect of the ABS is implemented to further understand these experimental modes.

The numerical simulations essentially follow the approach proposed by Zeng [30] but with slight modifications. A full finite element model of the HGA with the air bearing is subject to harmonic analysis to determine the frequency responses of the entire dynamical system. The stiffness of the air bearing is evaluated for 18 nm of TFC protrusion, where the slider is still flying, and this is incorporated into the HGA model as an elastic element with one end fixed at the slider's mass center and the other end fixed at the disk node. This full model is chosen to represent the same suspension and ABS designs as those used in the experiments. A 10 mN excitation force is applied at the slider's TEC in the in-plane

direction (x-direction) for the 1st case, and in the out-of-plane direction (z-direction) for the 2nd case.

2.4.3 Data processing

The signals from AE, LDV and OSA are processed using a customized code in MATLAB. The AE and LDV signals were both analyzed in the time domain and frequency domain. In the time domain, the oscillating nature of the dynamic signals was characterized using 3-sigma over each 15-30 milliseconds period. In the frequency domain the spectra are calculated using a fast Fourier transform (FFT) at each power step. The results are comparable with those obtained using the TTi data analyzer, Ultrafast, and MATLAB program. Friction force is processed by a moving average over each power step.

The OSA images were acquired by its computer at circumferential acquisition rate around 2 MS/s. For accurate film modulation studies, a background image before each test is performed and is subtracted from the modulated lubricant images to remove the background noise, disk clamp chuck induced distortions and disk run-outs.

2.5 Results and Discussion

In this section the results obtained from the different experimental schemes are discussed.

2.5.1 Slider dynamics and acoustic emission sensor

It was revealed from the first test scheme that a light touchdown contains three distinct phases. As shown in Fig. 2.5.1.1(a), phase I contains low AE and LDV signals, and phase II begins with sharp spikes in the AE signal and then drops to a certain level that is much larger than in phase I. In the same period, the LDV signal grows gradually and has similar trends in magnitudes as the AE signal. In phase III, the amplitudes of both of the LDV and AE signals reduce to nearly constant values that are small compared with those in phase II but still somewhat larger than in phase I. For the time domain analysis, we use three times the standard variation of a vibration signal over a period to quantify the magnitude of the vibration, and it is termed as the 3σ. Since the power history remains constant for 30 ms at each step, we can compute the 3σ plot over every 30 ms period for both the AE and LDV signals with respect to each power step, as shown in Fig. 2.5.1.1(b), where the three phases are clearly presented. We therefore define the TDP as the power where the first AE spike is observed in its 3σ plot. Furthermore, with the joint-time frequency analysis using the FFT with resolution of 0.0625 kHz, we can also observe three distinct phases in the frequency domain that correlate well with the phases classified in the time domain, as shown in Fig. 2.5.1.1(c). In the frequency domain results in Fig. 2.5.1.1(c), phase I shows no obvious peaks even with the heaters turned on. However, phase II, which starts with

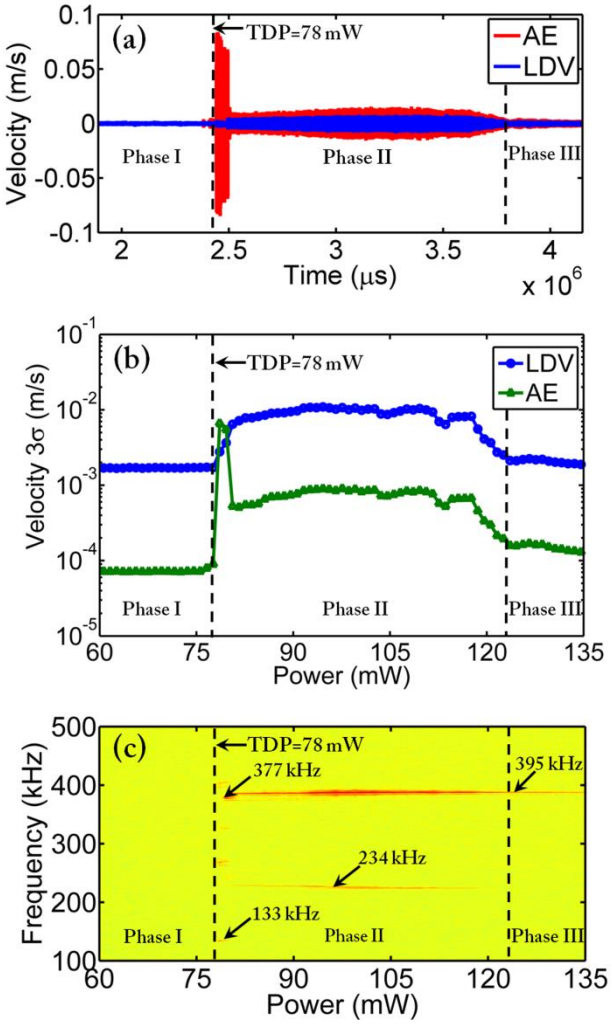

Figure 2.5.1.1 (a) Dynamic signals in time domain and (b) the 3σ of time domain signals with corresponding powers (c) the frequency spectrum at different powers

sharp AE spikes in the time domain, is rich in frequency content. Within its first 3 mW increments beyond TDP, a peak with frequency of 133 kHz and its second the third harmonics are observed. These peaks are soon suppressed at higher powers, and are replaced by two frequency peaks appearing at 234 kHz and 377 kHz. In the middle of phase II, stronger and more stable peaks located at 234 kHz and 390 kHz are observed, and in the late phase II, the peaks around 234 kHz gradually disappear and the peaks around 390 kHz shift slightly to a higher value at 395 kHz with a suppressed magnitude. Phase II shows a complex frequency content as well as transition, and it correlates well with the vibration time domain signals. In phase III, only the high frequency content from phase II remains with relatively low magnitudes, and it is consistent with the low AE and LDV signals in the time domain. Fig. 2.5.1.1 shows good agreement in the dynamical phases between the different measurement methods.

It is shown by the second test scheme that three phases and their dynamical characteristics are clearly presented by P1, P2 and P3. For P1, which is 5 mW below the TDP, we see no time domain signal changes and no obvious peaks in the frequency domain; thus it is termed the “flying state” even when the heater is on as shown in Fig. 2.5.1.2(a). For P2, which is 5 mW beyond TDP, a rich frequency content is observed, as shown in Fig. 2.5.1.2(b). As indicated in the first test scheme, initially a peak at 137 kHz is excited as well as its harmonics, and then it is soon replaced by two dominant peaks at 234 kHz and 382 kHz when the power is kept at P2. Phase II, where a rich frequency content and vibration signals are observed, is therefore termed the “bouncing state”. For P3, the transitions of peaks and time domain signals in the power up process correlate well with previous observations, and only a weak, yet distinct frequency peak at 391 kHz, remains when the power level reaches P3, as shown in Fig. 2.5.1.2(c). It is worth noting that in phase III, the frequency domain results indicate a slightly higher frequency vibration mode than the bouncing state without the 234 kHz mode, meaning that the contact condition experiences a significant change in transition from phase II to phase III. Another observation from the time domain signal also suggests that a steady but weak vibration occurs in this phase.

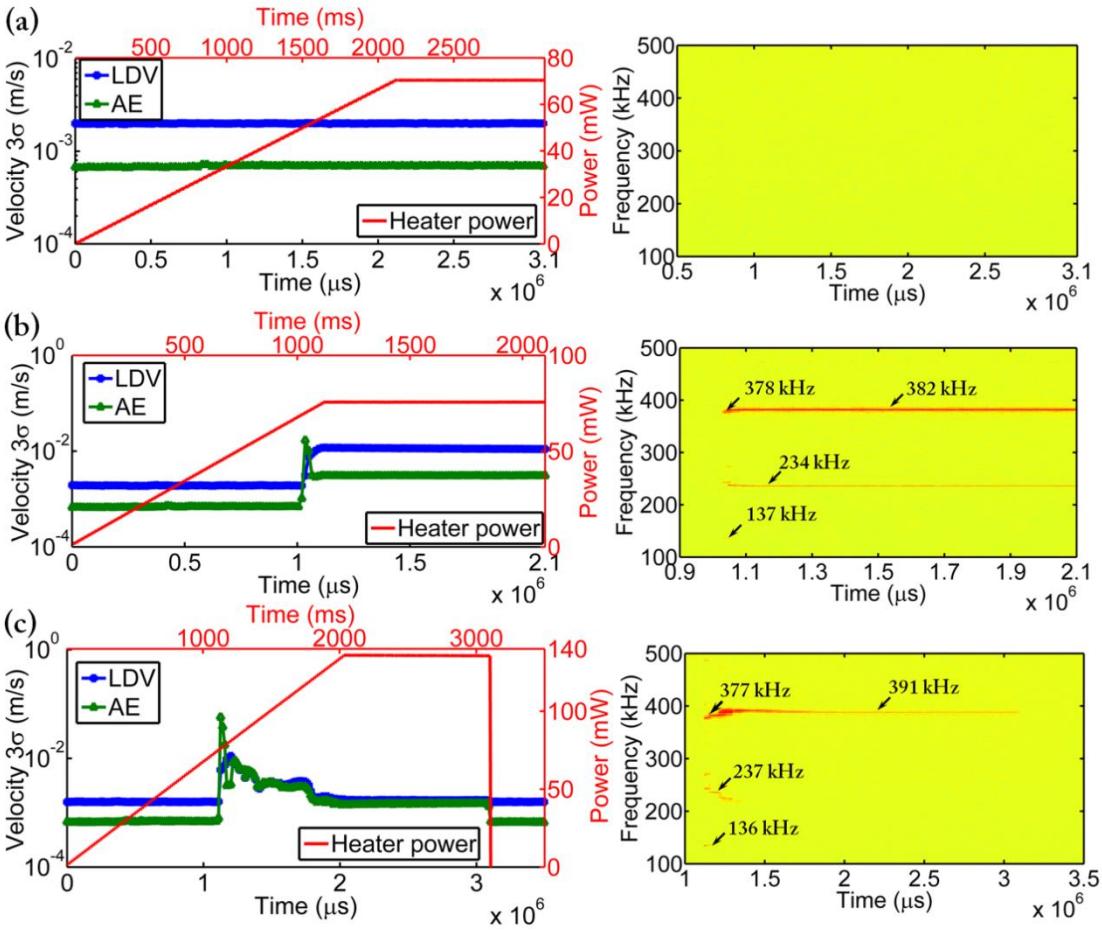

Figure 2.5.1.2 Comparison of dynamical behaviors in both time domain (left) and frequency domain (right) at different heater powers (a) P1, (b) P2 and (c) P3, respectively. Dominant peaks are indicated by arrows.

2.5.2 Lubricant response

It is found from the twelve-minute test using the OSA, P1 shows negligible lubricant modulation while P3 shows prominent lubricant modulation right under the thermal protrusion area. Such modulation evolves with time, as directly shown in Fig. 2.5.2.1, where the lighter yellowish area indicates a thinner lubricant layer and darker area represents accumulation. The in-plane resolution of the OSA images are of micron meters. Therefore, the thinning/thickening of lubricant layers can be viewed as an averaged measure over a large number of molecules, considering a typical Z-Tetraol molecule's length is at tens of nanometers. Significantly, the lubricants deform into a cross profile with two ridges and one groove. The overall lubricant thickness is 12 Å, and the mobile layer is 6Å thick. Carefully calibrated OSA readings show that the profile's peak to valley thickness change is about 1.2 Å, as shown in Fig. 2.5.2.2, which suggests the interaction between the thermal protrusion and the lubricant only exists in the mobile layers of the lubricants. Thus, we designate phase III as the "surfing state".

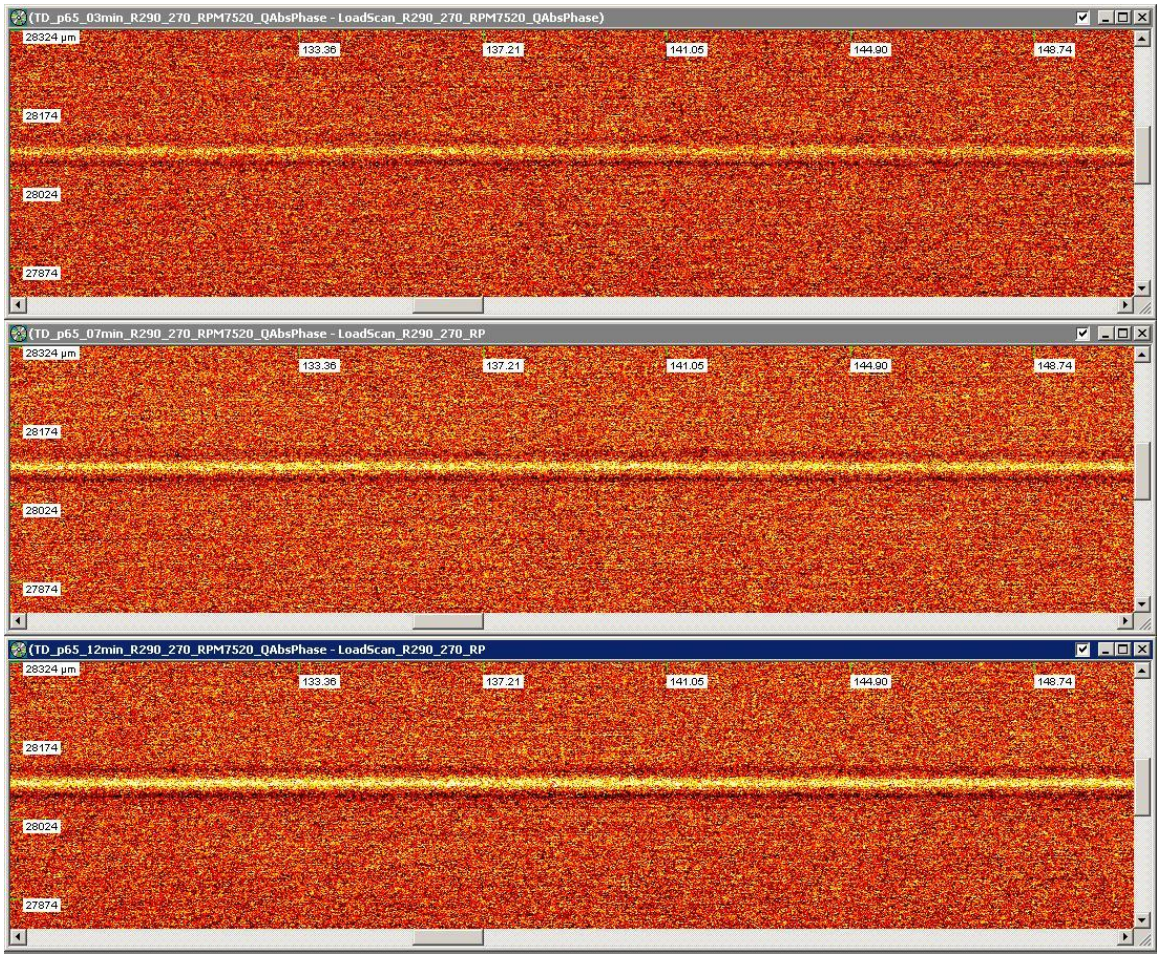

Figure 2.5.2.1 OSA raw data showing lubricant depletion under Phase III at 3 minutes, 7 minutes and 12 minutes separately.

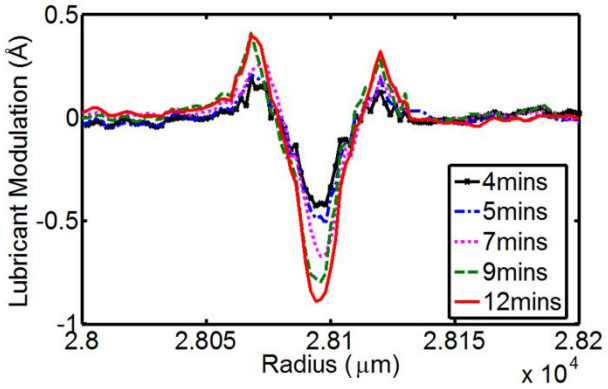

Figure 2.5.2.2 Lubricant modulation profile along the radial direction ranging from 4 minutes to 12 minutes in phase III.

2.5.3 Numerical simulations

The system's frequency responses in the z-direction at the slider's mass center for the two cases are shown in Fig. 2.5.3.1(a). It is interesting to note that the dominant dynamical modes vary with the direction of the excitation force. In particular, for the x-direction excitation the dominant modes have frequencies at 122 kHz and 152 kHz. On the other hand, the 324 kHz mode becomes dominant under the pure z-direction excitation. Therefore, it is reasonable to expect that different modes become dominant at different touchdown stages as the force combinations vary with touchdown status. Fig. 2.5.3.1(b) shows the nodal lines corresponding to the modes shown in Fig. 2.5.3.1(a). Comparing these results with the observations in the experiments, we conclude that the repeatedly seen peaks around 130 kHz to 140 kHz are related to the peaks located at 122 kHz and 152 kHz, and because the nodal lines are located at the trailing edge of the slider, as shown in Fig. 2.5.3.1(b), these modes are considered related to the slider's first air bearing pitch mode. The high frequency components around 377 kHz to 395 kHz are evidently related to the 324 kHz peak obtained in the simulation, which has a nodal line located at the leading edge as shown Fig. 2.5.3.1(b), and is associated with the slider's second air bearing pitch mode. The frequency of this mode is 50~70 kHz lower than what is seen in the experiments. However, considering that the simulation is done on an air bearing stiffness evaluated at a flying state, we expect this frequency to increase by several tens of kilohertz if we further push the slider to touchdown. Another interesting observation is that the experimental mode at 234 kHz, which is neither a pure air bearing mode, nor a pure suspension mode, also is found in the simulation with a nodal line located closer to the trailing edge of the slider and off the slider body where we can conclude it is a suspension-air-bearing coupled mode and is able to be excited under certain conditions. Not all peaks obtained from the simulations are observed in the experiments because the real excitation force components may not be as simple as those applied in the harmonic analysis. Nevertheless, the simulations do explain why different modes show up at different touchdown powers, and

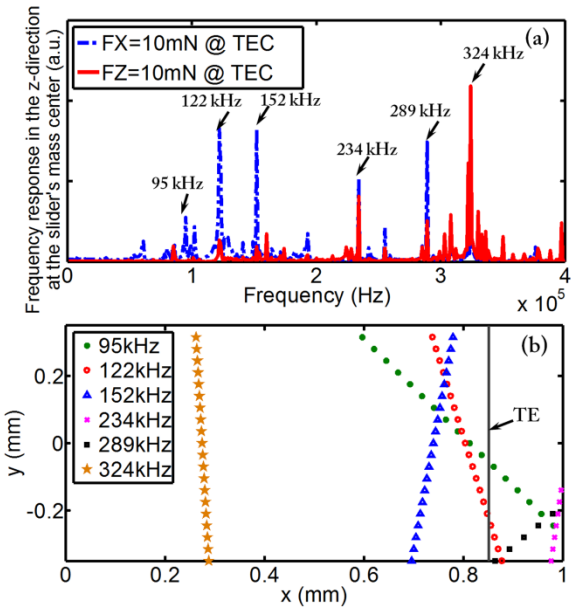

Figure 2.5.3.1 Simulation results on (a) frequency response and (b) corresponding nodal lines of dominant frequencies plotted on the ABS. The solid line located between 0.8 and 1 indicates the slider's trailing edge (TE).

they recover the modes observed in the experiments that cannot be explained by using either simple air bearing or suspension models.

2.5.4 Interfacial friction force: comments on the feasibility of surfing

In order to determine the repeatability of the surfing phenomenon, several HGAs were studied under high TFC powers to observe surfing. While the phenomenon of surfing can be repeated on different HGAs, the required additional TFC power beyond TDP varies among them. These values range from 15 mW to 120 mW. In addition to the large variations in surfing power (with relatively similar TDPs around 70-80 mW), the frictional forces are non-negligible during a surfing sate. It is worth noting that even though both the LDV and AE signals dropped to significantly lower values than in its bouncing state, the strain gauge signal stays at the value prior to entering the surfing regime. It means a strong surface interaction is still present, but with much smaller vibration amplitudes. Interestingly, the friction force does not increase monotonically with the power. Even though the friction force stopped increasing, the existence of the friction force suggests a possible development of wear if a slider stays in surfing for a long time. The non-negligible friction force in the experimental surfing state makes the idea of contact recording via surfing less practicable.

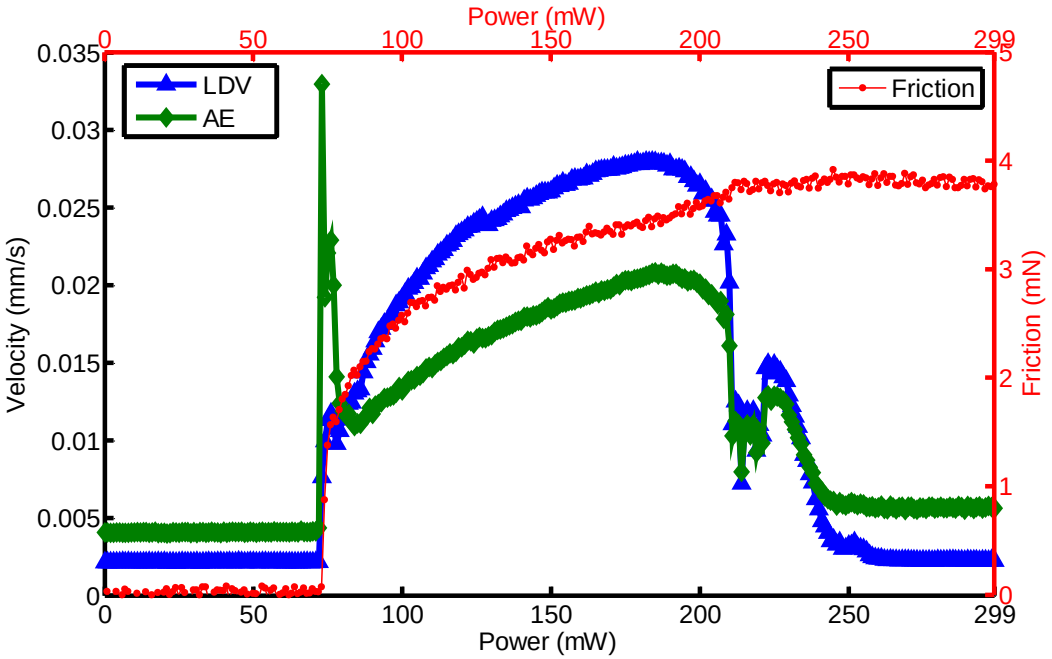

Figure 2.5.4.1 Data with friction force measured.

2.6 Summary and Conclusion

Three distinctive slider-disk interaction stages are identified experimentally and are explained with simulation support. Rich dynamical contents are found in the bouncing state and surfing state.

The bouncing state is an important phase in the light touchdown because its frequencies reflect not only its inherent air bearing modes but also the suspension-air-bearing coupled modes, which may be excited by different interfacial forces. The existence of suspension-air-bearing coupled modes suggests that under a well-controlled power supply process, the bouncing state initiates from extremely light contact induced natural vibrations and progresses to a forced vibration condition as the heater protrusion grows. This indicates that lubricant-induced vibrations affect the bouncing state.

The surfing state is also supported by multiple in-situ measurements using the AE sensor, LDV, and OSA. It is worth noting that we observe the slider reaching its surfing state with both AE and LDV signals of low magnitude but with a distinct, slightly–shifted higher second air bearing pitch mode compared with the bouncing state. And most importantly, the Angstrom-level modulation of the lubricant surface with heater power higher than that

at the TDP strongly suggests the state of surfing. The suppressed AE and LDV signals indicate a stable dynamical phase with light contacts, and the weak second air bearing pitch mode suggests that the slider is partially supported by the air bearing.

This chapter classifies the dynamical phases of a slider's light touchdown, and most importantly it characterizes its surfing state using multiple measurement techniques. The measured slider's dynamical frequencies in the bouncing state correlate well with the simulation results, indicating that suspension-air-bearing coupled vibration modes can be excited by different contact conditions with lubricants and thermal protrusion. Therefore, it is essential to take the suspension-air-bearing coupling effects into consideration when touchdown occurs. It is also crucial to design a reliable and controllable interface for the state of surfing, which is defined as having a distinct 2nd air-bearing pitch mode yet having low amplitude AE and LDV signals. And the surfing is expected to occur only in the mobile layers of ultra-thin PFPE lubricants. The surfing phase with the evolution of deformation of mobile layer lubricants with time shown in Fig. 2.4.2.2 suggests that the deformation mechanism and mechanical properties of mobile layer lubricants may be essential for future theoretical constructions and simulation works of this phenomenon.

Although the surfing condition has been presented with OSA data, there are several challenges for such phenomenon to be practically utilized in a real HDI. One challenge is that a touchdown power may not be predicted for each HGA, nor the TFC power of a surfing state. Therefore, before a stable surfing state being reached, very likely the bouncing state will take place. The disadvantages in bouncing state are self-explanatory, and the priority in HDI studies should be focused on the detection for contacts without exciting the bouncing state.

The second challenge is the difference between the theoretical model that suggests surfing and the experimental surfing established in experiments [23, 25, 26, 27, 28, 31, 39]. In modeled surfing conditions, several potentials are assumed as a function of spacing and lubricant film thicknesses, which can be evaluated arbitrarily as long as they are physically feasible. Therefore, an equilibrium may exist, ideally, at any head-disk spacing/film thicknesses as predicted. However, such assumptions are usually violated in experimental conditions. As suggested in the surfing states observed here, the depletion of the lubricant film is at a rate of sub-angstroms per minute. Even for an aggressive TFC overdrive the depletion rate should not exceed one angstrom per minute. This means the thermal protrusion may not be able to reach a desired interference without the consideration of film depletion rate. The experimental surfing, as a result, could be understood as more of a steady contact against hard substrates mediated by lubricant films. The effect brought by the lubricant modulation in the HDI is another important topic for further understanding.

As thin as the PFPE film is, at the molecular level it may not be able to be fully depleted, even under a high TFC overdrive power. The lubricant-DLC bonding is strong enough to withstand head-disk contacts; however, it does not guarantee full lubricant coverage over the DLC layer. Lubricant depletion can cause less lubricant coverage, leading to asperity

contacts between the disk and slider's DLC layers [32]. As a result, the third challenge for surfing is mechanical wear. Wear monitoring and control is critical for a reliable HDI.

Although surfing and bouncing are not desired in the HDI, this chapter indicated three important topics for future studies: contact detection, lubricant modulation and wear. Contact detection will be discussed in chapter 3, the effects of lubricant modulation will be addressed in chapters 4 and 5, and chapter 6 presents the head wear study.

Chapter 3

Thermal protrusion-induced slider's flying height modulation at contact proximity

This chapter presents detailed measurements using the LDV to capture the slider's behavior at contact proximity in order to understand the slider's dynamics at the onset of contact. With the introduction of TFC technology, contacts were made by thermal protrusions. To study the dynamics at proximity, a more sophisticated data acquisition scheme and sampling rate were adopted. The slider's dynamics was captured using a fine-focusing laser interferometer which decomposed the slider's rigid body motion into three degrees of freedom. Numerically the slider's displacement fields under different forcing conditions are carried out using FEA, CMLAir [36] and CML parameter identification program [37].

3.1 Introduction

Thermal protrusion induced slider-disk contacts have been widely investigated experimentally, theoretically, and by simulations. Slider dynamics at contact were experimentally explored at different interference heater powers using laser Doppler vibrometry (LDV) [38], [39]. These investigations indicated a certain correlation between the slider's vertical dynamic signals and a modulation of the disk lubricant layer in the regime of contact. However, in drive-level applications, the dynamics at first contact or approaching contact is of more interest. Recently several studies have focused on identifying the excitation source of the contact signal using LDV [30] and acoustic emission (AE) sensors [40]. In component-level studies, AE sensors are often used to detect contact-induced elastic waves. The contact criterion varies according to the researchers' preferences, but it is usually based on the increase in the magnitude of the AE signals' root mean square (RMS) value over a period of time [40], [41], or a sudden spike in a time domain window [38], [39]. Therefore, the correlation between the increase in the AE signal and the interference between the head and disk surface requires further investigation. In this chapter, we use a direct observation of the slider's dynamics to choose the threshold

manifesting a transition from proximity to contacts.

Moreover, among the recent studies regarding HDI contacts the LDV was applied at several locations according to the researchers' choices: trailing edge, trailing edge center [38], [39], leading edge [42], suspension or gimbal legs [30]. A recent paper [30] reported the different touchdown stages by making separate measurements on the trailing edge center and gimbal legs. This suggests that the slider's vibration measured with LDV is indeed location sensitive, and a more realistic description of slider motions may be obtained by observing the slider's dynamics in multiple dimensions [43]. It is thus essential to understand the slider's dynamics by taking measurements at multiple locations of the slider body, in order to provide a determination of which location deserves the most attention for determining the early onset of contact.

In this chapter, the slider's dynamics at contact proximities are measured at the TEC, leading edge center (LEC), and in the down-track direction (DTD) to investigate the slider's behavior in transition from flying to light contacts. Such light contacts are also found to be disk surface dependent. Results show that the instabilities in the DTD and LEC are more sensitive to the transition from disk proximity to the onset of contact than on the TEC. At the defined contact event, DTD modulation dominates the vibration in the in-plane direction whereas the LEC modulation dominates the vertical instability, leaving the TEC rather stable. The higher sensitivity to contact events in the DTD with little modulations on TEC suggests that the DTD modulations can be used as a contact detection criterion prior to severe TEC modulations that can cause mechanical wear.

Numerical simulations were implemented to investigate the thermal protrusion induced slider-disk modulation at contact proximities. Two different HGA designs were used to study the transient dynamics of sliders in transition from flying to the onset of contact. Simulations considering both air-bearing and suspension designs were carried out using finite volume (CMLAir) and FEA (ANSYS).

Experimental results and simulations are in good agreement, and therefore reasonably explain the possible source of instabilities and its associated excitable modes. The results also suggest that the dynamics varies among the HGA designs.

3.2 Experiments

Experiments were performed on a customized spin-stand capable of executing *in-situ* measurements with an AE sensor, an LDV and an optical surface analyzer (OSA) which is similar to the stage used in chapter 2 but with certain modifications to improve accuracy of the contact study.

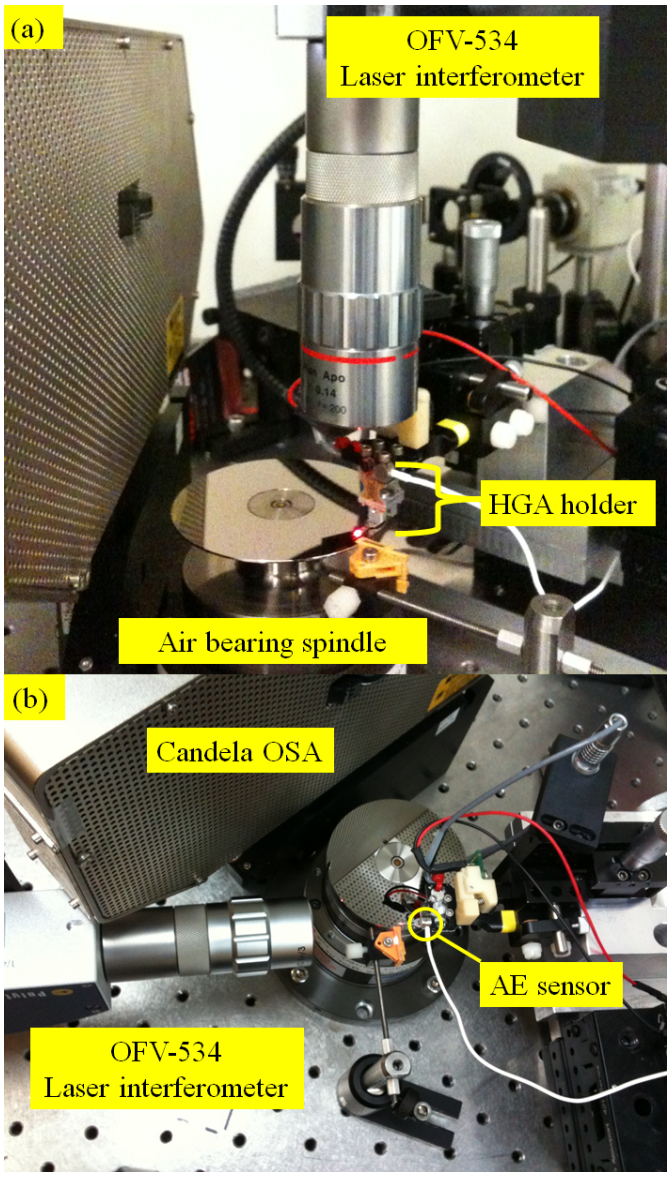

Figure. 3.2.1.1. Experimental setup for *in-situ* measurements on (a) vertical dynamics, and (b) down-track dynamics.

3.2.1 LDV measurement system update

The OFV-512 with OFV-3000 LDV setup was capable of finding slider dynamics under different contact conditions. However, when a more dedicated measurement is aimed at discovering the subtle transition from flying to the onset of contacts, its resolution is limited to the analog controller, OFV-3000. In this regard, a digital controller, OFV-5000 with digital decoders VD-06 and VD-09, was used for slider dynamics in this dissertation hereafter. The VD-06 and VD-09 have cut-off frequencies of 350 kHz and 1 MHz,

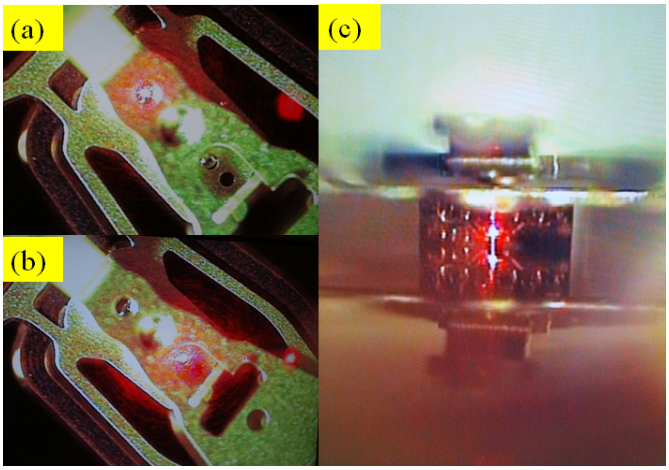

Figure. 3.2.1.2. Laser spots focused on (a) TEC, (b) LEC, and (c) DTD. The brightest red dots are the focused laser spots, which are surrounded by scattered lights.

respectively. However, it was verified by the VD-09 that the dynamics of interests were below the frequency bandwidth of 350 kHz, so only the results using the VD-06 are presented in this chapter.

Besides the improvement of the digital controller, an update in laser interferometer can also increase the signal to noise ratio by integrating an in-line camera and a close-up lens that provides a finer focus spot. The OFV-534 interferometer with a 5X/10X microscope lens was used to provide in-situ laser spot images and a spot of 5-7 um in diameter at a working distance around 30-50 mm.

Figs. 3.2.1.1 (a)-(b) show the vertical measurement configuration and down-track measurement configurations separately. The locations of the laser spots on the head-gimbal-assembly (HGA) used in the measurements are shown in Figs. 3.2.1.2 (a)-(c).

Another solution that provides a similar solution is to use OFV-512 and a microscope lens OFV-130-5 that can focus the measurement spot down to 5 micron. In this configuration, an external camera with proper optics is required to visualize the laser spot as shown in Fig. 4.2.2.

3.2.2 Visualization of the laser spot

Realizing that slider vibration possesses multiple degrees of freedom, we set up the proper optics for visualizing the laser spot. For the OFV-534 with in-line cameras, no additional setup is required. However, if a fine-focused laser spot is to be visualized, care needs to be taken. The Navitar lens assembly with a 1.33x adapter (model # 1-61448) and a fine focusing body tube (model # 1-61449) were used to provide a field of view (FOV) for 2.00 mm by 2.67 mm with a working distance around 92 mm and a magnification rate of 2.4x. Such FOV was determined together with the diagonal CCD dimension (1/2 inch) of the

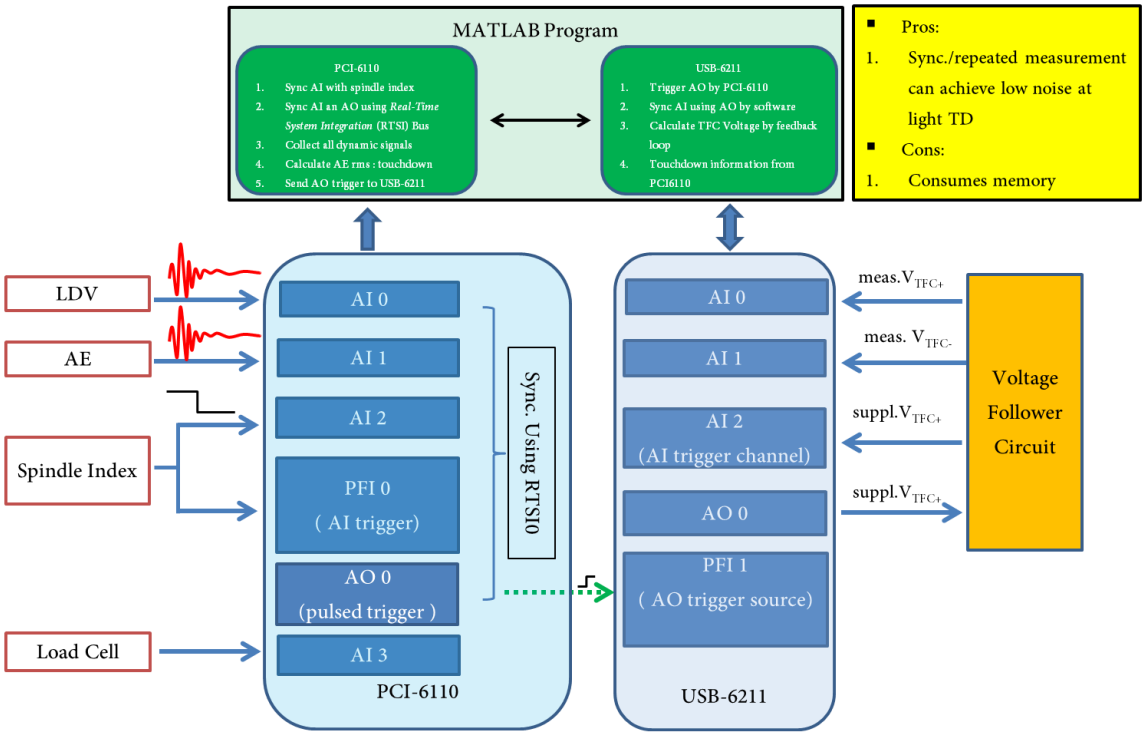

Figure. 3.2.3.1. Representative data acquisition diagram used in this chapter. On PCI-6110, AI 0-3 are synchronized analog input channels.

corresponding digital camera, Hitachi KP-D50 was used in this dissertation. Laser spots are usually smaller than could be observed, due to the scattering light. There are two ways to enhance the contrast of the laser spot. One is to use fiber optics to locally lighten the neighboring space of the HGA; the other way is to apply optical filters to reduce the glare and enhance the contrast. A long wavelength pass color filter from THORLABS, FGL665M, was used in this dissertation with the OFV-512/OFV-551 interferometer.

3.2.3 Data acquisition update

An updated data acquisition is used in this chapter. The data acquisition and TFC heater power supply are controlled by use of a customized MATLAB program synchronizing the TFC heater power supply and dynamic signal acquisition to the spindle index. All dynamical data were acquired using a National Instrument (NI) data acquisition card, PCI-6110, at 5MS/s sampling rate, and the heater power was feedback-controlled by an NI USB-6211.

The PCI-6110 can perform 5MS/s sampling rate simultaneously for 4 analog input channels. This important feature assures no delay between acquired dynamic signals. A diagram representing the data acquisition scheme is shown in Fig. 3.2.3.1. On PCI-6110, the analog input engine is triggered by feeding an OSA spindle index into the PFI0, and

the analog input and output engines are then synchronized via RSTI0. The synchronized analog output channel, AO 0, is then used as a pulsed trigger for USB-6211's analog output engine. The USB-6211's analog input engine is later triggered after the data acquisition command. This procedure ensures the same timing on the spindle index, PCI-6110 data acquisition and the TFC heater power supply.

3.3 Methodology

Both experiments and simulations are performed to investigate the HGA behavior at contact proximity. Different HGA designs and media are used to explore the efficacy and repeatability of the method of contact detection.

3.3.1 Rationale

Recently it was reported that LDV measurements at the TEC during slider-disk contact events revealed two interesting phenomena. One is that the observed TEC vibration consisted primarily of the 2nd pitch mode [39, 40, 43]. The other one is that the TEC vibration to some degree, could be affected by the gimbal structures at low frequencies (<50 kHz) [46]. However, the same measurements were done on the gimbal legs as well [30], suggesting that an earlier detection of contact could be observed at that location, compared with the responses on the TEC. The above-mentioned studies indicated that the LDV-based contact definition may depend on the measurement location, and therefore, a more detailed study of the transition from contact proximity to a possible contact event is necessary.

3.3.2 Samples and Experimental Schemes

The experimental procedures and specifications of the samples are as follows. HDD 2.5 inch disks covered with a thickness of 1.2 nanometers of Z-Tetraol or Z-Dol lubricants with 70% bonding ratio were used. Equivalent linear speeds of flying sliders over disks were kept around 22 m/s with approximately zero slider skew. Slider-disk contacts were established by increasing the voltage supplied to the TFC heaters, and the voltage pulses are referred to as "TFC pulses" hereafter. Each TFC pulse started and ended with a 1 ms half sine-wave rising or falling profile which was held constant over the duration of 15 ms in between. Data was acquired for 25 ms and synchronized with each TFC pulse. AE signals were analyzed in real time using the RMS value during the TFC pulsed period as contact indicators. The dynamics recorded during the TFC pulse on/off period over the same measurement window were used to study how the TFC heaters could affect the slider dynamics using both frequency spectra and time domain displacement modulations. All slider samples were examined by the scanning electron microscope (SEM) for indications of wear.

The TFC sliders used in this study were designed to fly at about 11 nanometers passively, and with thermal actuation efficiencies ranging from 0.14 to 0.18 nm/mW. The LDV measurements were taken at the TEC, LEC and DTD on the same slider sequentially. To exclude any concerns about the measurement sequences, the orders were changed over different slider samples in the experiments. Furthermore, the variation of contact TFC heater power was required to be within +/- 1 mW on the same slider among the change of LDV positions, to insure repeatability. Results for the contact powers were measured from 5 to 10 times at each location when TDP settles down to a variation below 1 mW. The air bearing spindle run-out was around +/- 1 μm at the test radii.

3.4 Simulations

Simulations were done in three separate steps. First, the air-bearing stiffness was evaluated using the dynamic air-bearing simulator CML Air and the CML PIP. Second, the air-bearing stiffness was used together with an ANSYS finite element model of the HGA to perform harmonic analyses, by which the mode shapes and frequency response were obtained. Third, transient analyses were implemented to find excitable dynamics at contacts.

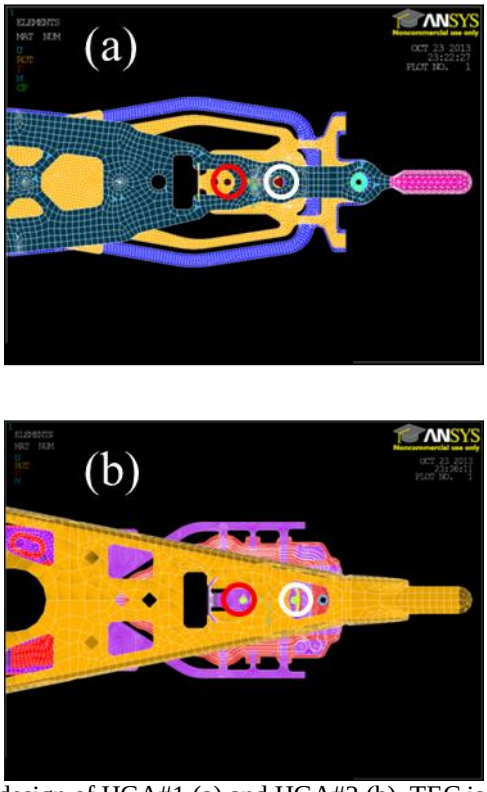

Figure. 3.4.1.1 Suspension design of HGA#1 (a) and HGA#2 (b). TEC is circled in white and LEC is circled in red for both figures.

3.4.1 Finite Element Modeling

Detailed finite element (FE) models are used for structural analysis. The reason for using FE models is to accommodate the complexity introduced by current HGAs. Although the effect of HGAs can be simplified to 6 DOFs or even lower, those models are usually not capable of recovering experimentally observed modes. The benefits of FE analysis is understood from chapter 2, and in this chapter a similar idea is taken. However, a slight modification is made to the slider modeling. Instead of replacing the slider body using a single node attributed to element MASS21 with inertia parameters, in this chapter a slider body of real dimension and density is built in the model. The slider's motions were solved by attaching an addition mode to the slider's mass center attributed to MASS21 with no inertia effects. By adopting this method, the slider's inertia effects are retained by the solid model and its interaction with disks can be linked through the added node.

3.4.2 Estimation of the effect of air-bearing stiffness

The air-bearing stiffness was evaluated at the slider's minimum flying-height of around 1.5 nm with a certain amount of thermal protrusion applied to the ABS. Two HGA designs that differ in both ABS and suspension structure were used in the simulation and experiments to compare the results. The element type, MATRIX27, in ANSYS is used as the spring element that connects the slider's mass center and disk node.

3.4.3 Transient and harmonic analysis

The applied excitation force was 1 mN for both harmonic and transient analysis. In order to simulate the forcing condition at slider-disk contacts, we applied excitation forces as point loads at the slider's TEC on the air-bearing surface (ABS). The magnitude of excitation force was chosen from the scale of experimental findings in chapter 2. In the harmonic analysis, the frequency sweep was from 1 kHz to 400 kHz with 1 kHz increments. In the transient analysis, a square pulse of 0.2 μs width was used to approximate the transient interaction between the thermal protrusion and the media below.

3.5 Results and Discussions

In this section the detailed definition of AE-based contact and the general dynamical interpretations of LDV and AE signals at contact events are presented and analyzed in both the time and frequency domains. The results from Z-Tetraol and Z-Dol samples lead to the same conclusion. All sliders used in this chapter showed no SEM detectable mechanical wear after the tests. It is noted that the contact events are also referred to as touchdowns (TD) by most researchers and the corresponding TFC heater power is called contact power or touchdown power (TDP). A heater power level exceeding the TDP is called an "over-push" or "overdrive", and is referred to as a "back-off" when it is reduced below the TDP.

Simulation results from ANSYS are post-analyzed in the frequency domain and the corresponding mode shapes of the whole HGA and the slider body are investigated.

3.5.1 Experiment

Acoustic emission signals and contact definition

Conventionally, a slider-disk contact event is determined by an increase in the RMS value of AE or LDV signals in component-level testing [30], [38]. In this chapter we use a similar criterion, RMS value of the AE signal, but with an observation in the time domain to help clarify the definition of contacts using a threshold AE RMS value. The contact TFC heater power was determined by the AE patterns based on our postulated slider-disk contact scenario. In a transition from contact proximity to contact, the disk surface asperities just contact the slider's thermal protrusion area instead of the process in which the slider bounces on the disk. The former represents a light contact condition which is mainly attributable to the overall effect of surface asperity distribution and disk run-out [40]. The latter is viewed as a more severe slider bouncing. Differing from the light contacts that are related to surface features that excite the slider's instability at specific disk locations, slider bouncing is regarded as the condition when the slider's vibration amplitude is large enough to cause it to randomly contact the disk surface regardless of the disk surface features. It has been reported that disk surface features such as disk waviness (μ-waviness and nano-waviness) can change the head-disk spacing when the sliders fly passively [47], and at the much lower spacing considered in this study, the perturbation becomes comparable to the flying-height and may contribute to the instability. The RMS values of the AE signals used to identify the transitions were calibrated for different slider-disk matches, and the AE threshold was found to be in the range of 1.15 to 1.3 with normalization to an AE RMS value in the sliders' flying state. As shown in Fig. 3.5.1.1 (a), a proper choice of AE RMS threshold provides a repeatable contact power, and Fig. 3.5.1.1 (b) shows the corresponding time domain history. It is also shown in Fig. 3.5.1.1 (b) that the AE signals, in general, contain both periodic and slightly non-periodic contents from one disk revolution to another during contact events. The excitation magnitudes are not exactly the same, but the periodic signatures are location specific. The non-periodic parts are attributed to the slightly varying excitation magnitudes of the location specific AE signals, and also a result of transitions from contact proximity to the onset of contact.

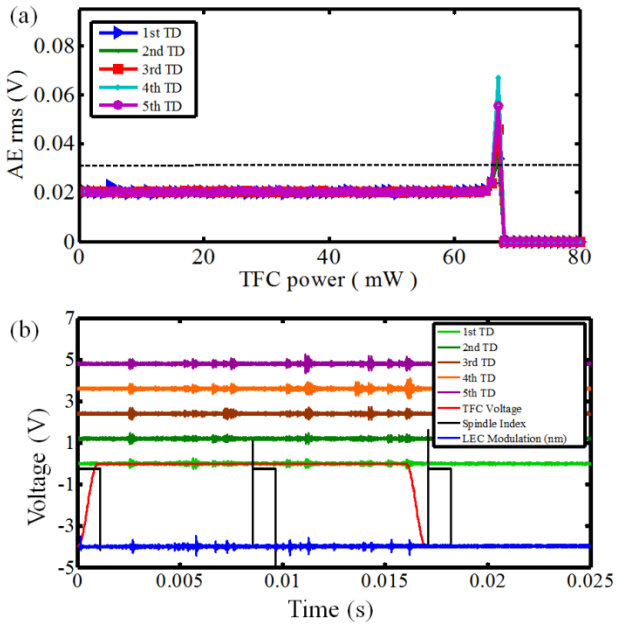

Figure. 3.5.1.1 A typical AE-based contact detection scheme. (a) Five consecutive TD tests at the same contact power with dashed AE threshold line. (b) The corresponding time domain traces with post-processed LEC modulations.

The justification for defining the transitions using AE is illustrated in Figs. 3.5.1.2 (a)-(c). At the defined contact power, the AE signal consists primarily of location specific excitations together with minor non-periodic contents, as shown in Fig. 3.5.1.2 (b). However, at 1 mW back-off, as shown in Fig. 3.5.1.2 (a), the AE signal contains weaker and fewer location specific pulses compared with the contact case. In contrast to the contact and 1 mW back-off events, Fig. 3.5.1.2 (c) shows the AE signal when the power is at 1 mW overpush. The AE signal modulation is much larger over the period with the TFC heater powered on, and it no longer features the location specific patterns. The LEC displacement modulations also follow this pattern. We define this as the transition from slider-disk contact proximity to the onset of slider-disk contacts.

Time domain laser Doppler vibrometry dynamic signals at contact events

The synchronized and simultaneous data acquisition scheme described above ensures the accurate timing with disk revolutions and minimum delays between acquired dynamic signals. Fig. 3.51.3 (a) shows a typical measurement result with the synchronized spindle index, LDV, AE signals, and TFC pulses. As shown in Figs. 3.51.3 (a)-(b), generally the velocity modulations, if observable, occur prior to the AE signals, and this difference represents the time delay of elastic wave propagating through the structures to the position of the AE sensor. A closer inspection of the LDV signal reveals that the velocity modulations at the LEC, though subtle, are larger than those at the TEC, at the same locations on the disk. These subtle and location specific velocity modulations also suggest

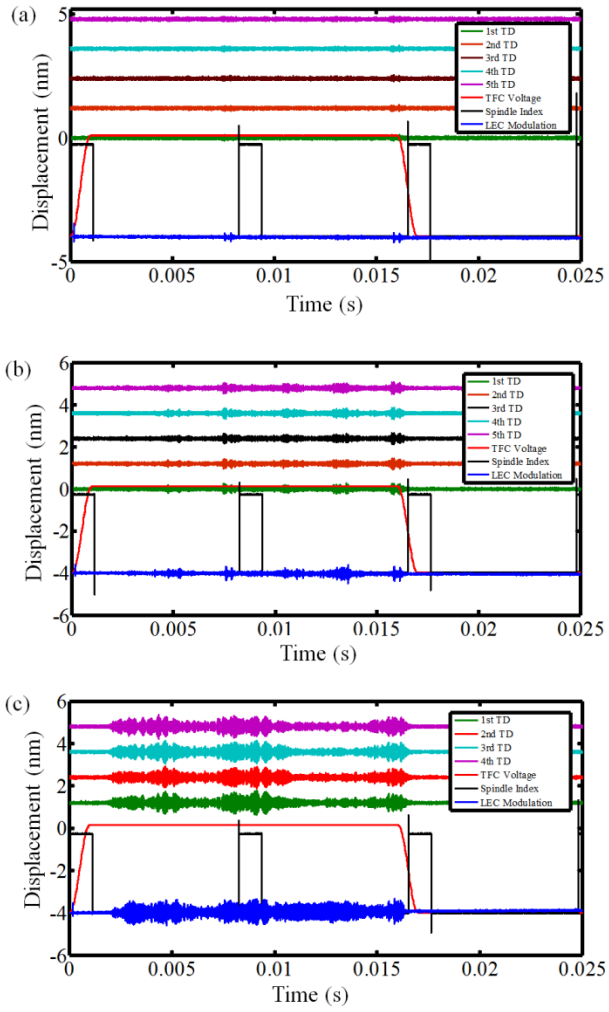

Figure. 3.5.1.2 AE dynamic patterns transitions from (a) 1 mW back-off to (b) TD to (c) over-push using the same HGA in five consecutive power-up cycles. Over-pushes are applied four times after TDs. Repeatable patterns could be observed from cycle to cycle, but the location specific patterns vanish at (c).

that a transient measure of vibration amplitude rather than an averaged RMS value over the entire TFC actuated duration should be used to quantify the instability. More detailed comparisons of the time domain results at the TEC, LEC and DTD are shown in Figs. 3.5.1.4 (a)-(c). The displacement modulations are numerically integrated from the band-pass filtered (50 kHz-350 kHz) LDV signal, and the AE signals shown are also processed through the same filter. The LEC displacement modulations are larger than those at the TEC, the same as the velocity measurements; however, the modulations at the DTD are even larger than at the LEC, for both velocities and displacements. The above-mentioned phenomenon requires a frequency analysis, and an analysis of modulation evolution from contact proximity to the onset of contacts to decompose the dynamic contents.

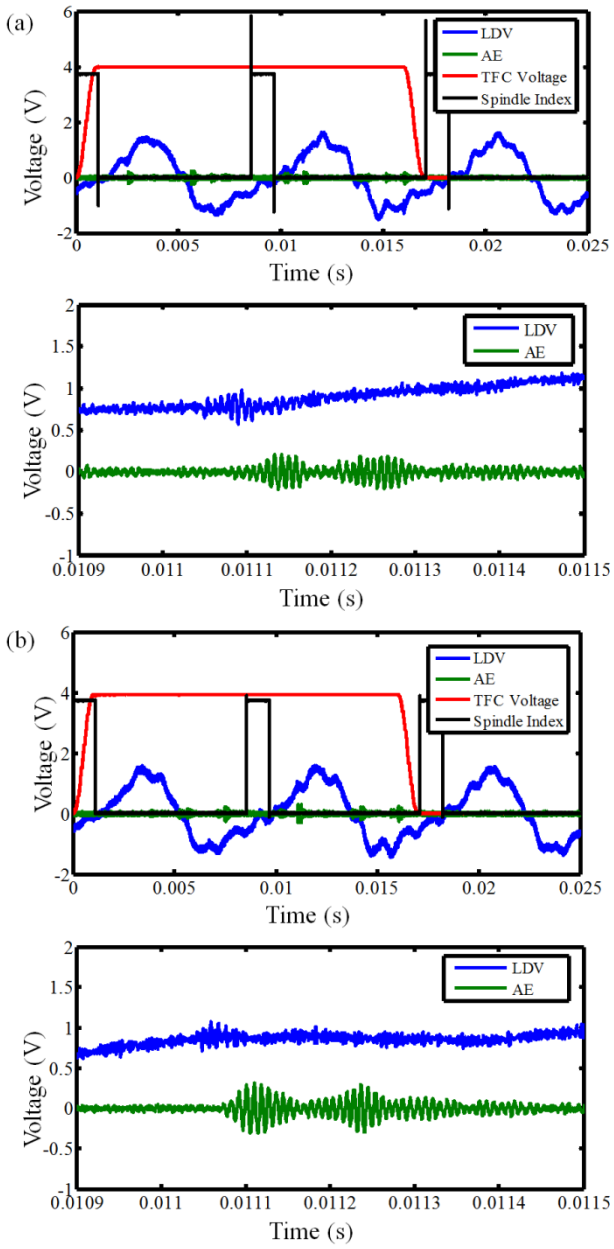

Figure. 3.5.1.3 Typical synchronized measurement results on (a) LEC and (b) TEC. TFC pulses are synchronized to spindle indexes. Closed-up figures from 0.0109 s to 0.0115 s are presented to show the differences between LEC and TEC velocity modulations in time domain.

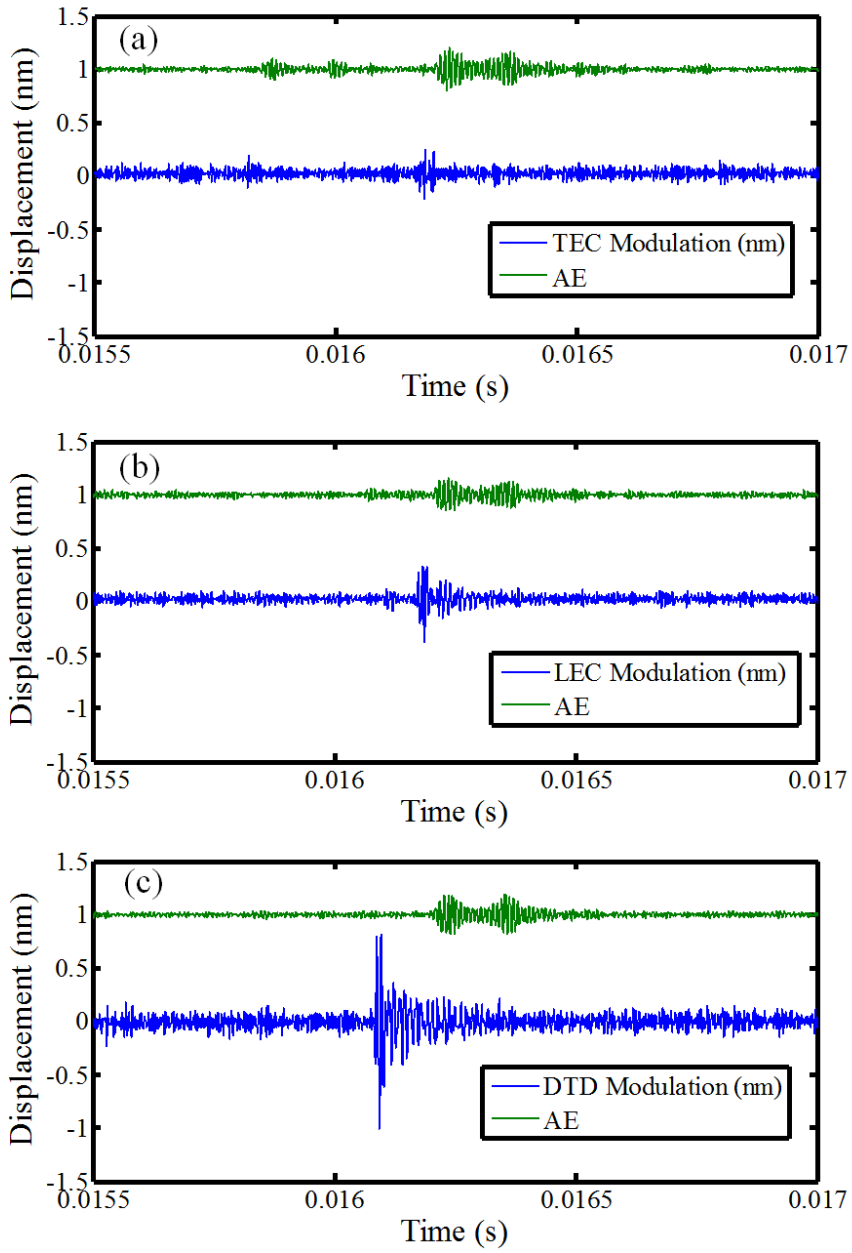

Figure. 3.5.1.4 Comparison of displacement modulations on (a) TEC, (b) LEC, and (c) DTD with AE signals as references.

Frequency spectrum analysis and explanations

The frequency spectra for comparing the slider dynamics with/without a TFC pulse are obtained using the Fast Fourier Transform (FFT) in MATLAB. An FFT is applied to each 5 ms period with the TFC pulse on/off. Although the magnitudes of the dynamic signals are subtle, the contrasts between the TFC pulsed period and passive flying period are obvious. As shown in Figs. 3.5.1.5 (a)-(b), the LEC spectrum features a group of conspicuous frequency peaks from 85 kHz to 140 kHz, whereas the TEC spectrum is rather silent with weak frequency modulations around 240 kHz and 320 kHz. Fig. 3.5.1.5 (c) shows the DTD spectrum, which shares prominent frequency peaks at 86 kHz and 117 kHz with the spectrum of the LEC, but it also features a distinguished peak around 76 kHz. Fig. 3.5.1.5 (d) shows the AE spectrum at contact events for reference. For the purposes of slider dynamics discussion, the low frequency components below 50 kHz are not included, although they may contain effects pertinent to the TEC dynamics. Compared with a recent study [46], the LDV response at the TEC in this paper is considered to be smaller at least by half in displacement modulations, suggesting a contact regime of less interference is being observed here. In the AE spectrum, the frequency content is observed to be a combination of LEC and DTD, suggesting that the AE sensor collects all elastic stress waves transmitted through structures to its position, and therefore shares frequency contents with the LDV measurements on LEC and DTD in part.

The frequency contents can be further explained by harmonic analysis of the HGA used in the experiments, and the simulation procedure is similar to that in recent papers [30], [39]. By experimentally comparing the TEC, LEC and DTD spectra, we conclude that the frequency peaks ranging from 90 kHz to 140 kHz are related to the 1st pitch modes. This range was analyzed in a recent paper [30] using simulation by the finite element method. The frequency modes ranging from 75 kHz to 90 kHz are reasoned to be related to suspension and air-bearing coupled modes in the DTD.

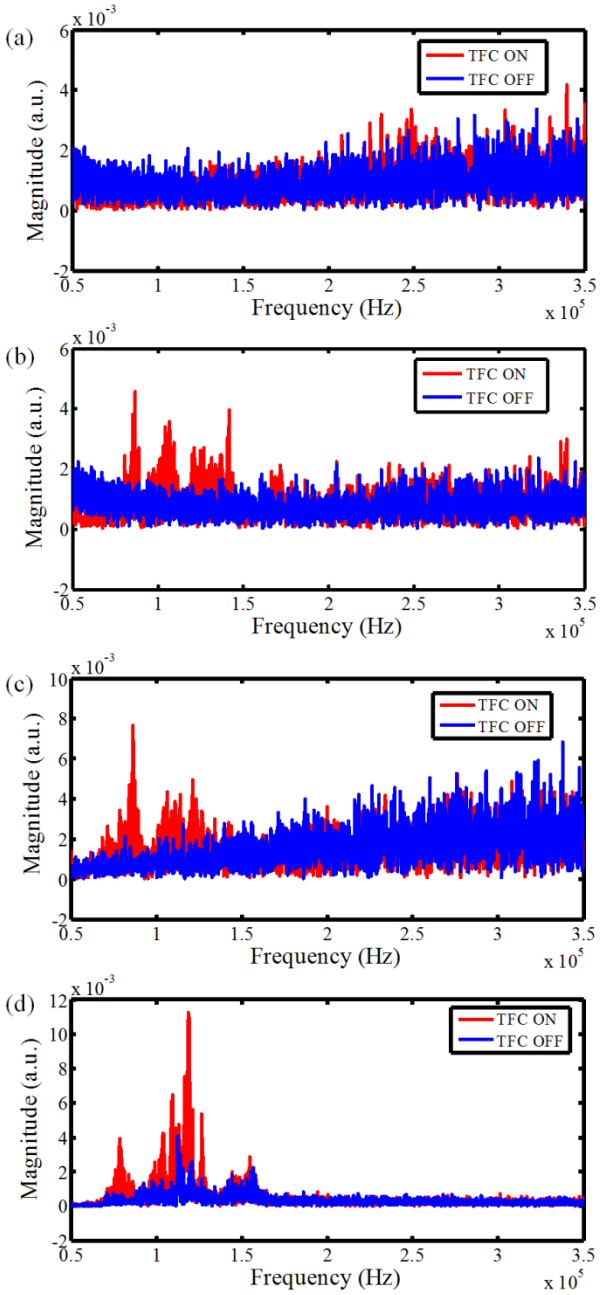

Figure. 3.5.1.5 Frequency spectra on (a) TEC, (b) LEC, (c) DTD, and (d) AE signals at a typical slider-disk contact event.

Evolution of flying-height modulation at contact proximities

Next, the maximum 3-sigma value of displacement signals representing the maximum peak to peak modulations are analyzed from 14 mW back-off to the contact power. Figs. 3.5.1.6 (a)-(b) show a representative evolution of displacement modulations and the corresponding

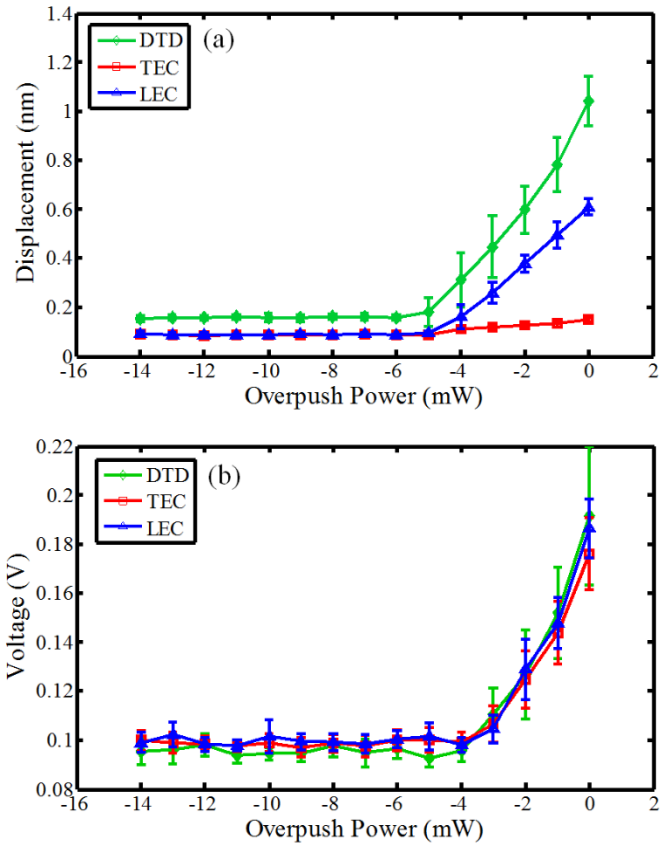

Figure. 3.5.1.6 Representative evolutions of (a) maximum 3-sigma displacement modulations on LEC, TEC, and DTD; (b) corresponding AE modulations. Solid marks are the averaged value and the error bar indicates plus/minus one standard deviation from 10 TD tests.

AE modulations from 10 consecutive TD tests. The 3-sigma value is chosen from the maximum computed 3-sigma values over every 20 μs in order to capture the transient peak-to-peak modulations. The displacement modulations start to grow at around 5 mW back-off at both the LEC and DTD, which implies that the instability started to occur at approximately 1 nanometer away from the contact surface level, which is interestingly close to, but slightly smaller than the critical clearance that initiates lubricant transfers [33]. Although the LEC and DTD modulations continue to increase as the heater power increases, the TEC modulations are almost comparable to those at the flying state with very little increase. Despite the modulation amplitude differences among LEC, TEC and DTD, the corresponding AE modulation amplitudes are almost identical, which implies that these measurements are under similar contact conditions. It should be emphasized that the 3-sigma displacement modulation in this paper quantifies the maximum transient peak-to-peak vibration amplitude over one disk revolution, but it is not an averaged measure such as would be obtained using the RMS value over all TFC durations. Much lower modulation values would be expected using the RMS value of the LDV measurements.

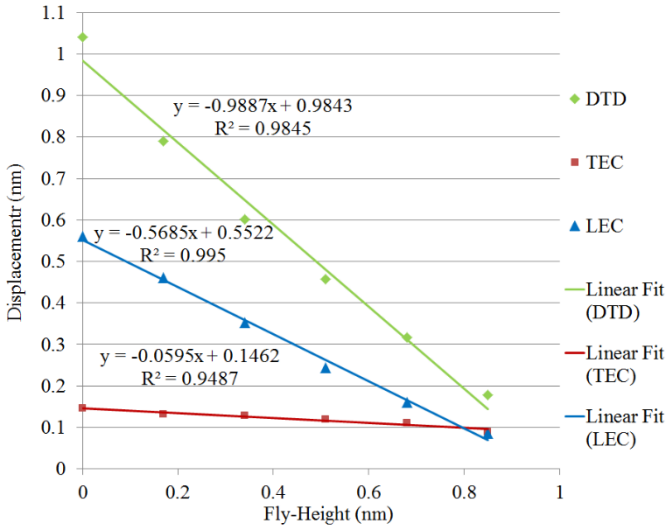

Figure. 3.5.1.7 Modulation growth rate with respect to the decrease in flying-height of LEC, TEC and DTD

Slider dynamics at the onset of contacts

Using the time domain information, the frequency spectra and the evolution of displacement modulation analysis we can interpret the dynamics of the slider from contact proximity to the onset of contact. As shown in Fig. 3.5.1.7, modulations at the DTD, LEC, and TEC all start to grow when the heater protrusion area is approximately 1 nanometer away from the defined contact. However, the modulations grow at different levels of head-disk spacing. Considering that 1 mW increase in heater power corresponds to approximately 1.7 Å decrease in flying-height, the growth rate in a dimensionless factor (increase in modulation/decrease in flying-height) is 0.99, 0.57 and 0.06 for DTD, LEC and TEC, respectively. The growth rate indicates the sensitivity of the modulations at contact proximity, and shows that DTD possesses the highest sensitivity whereas the TEC is the least sensitive to contact. The linear growth of modulation suggests a gradual increase in the vibrations until the onset of contact at the DTD and LEC, and they are viewed as the main contribution to the instability of the AE-based contact detection, whereas the TEC modulation plays a less dominant role in terms of slider dynamics during such transition.

The instability at contact proximity has previously been considered to be a result of force interactions between the HDI, and it has been extensively reported in numerical investigations [16], [48], [49]. Such force interactions are essentially dependent on the physical clearance between the slider's air-bearing surface (ABS) and disk and therefore mainly concentrate on the thermal protrusion area that is close to the TEC. Forces dependent on the head-disk spacing are usually reported in the vertical direction but in this study the vertical vibration at the TEC is not prominent; instead, the DTD shows a strong in-plane motion that suggests the horizontal excitations play an important role in slider-disk contacts. The direct measurement result of DTD is also consistent with a recent paper

[30], which suggests that a TD prior to TEC modulations is attributable to the in-plane excitations.

3.5.2 Simulation

Harmonic analysis

The harmonic analysis of HGA#1 subjected to 1 mN down-track excitation and the corresponding nodal lines are shown in Fig. 3.5.2.1 and Figs. 3.5.2.2 (a)-(c). Fig. 3.5.2.1 shows the frequency response from the LEC, TEC and DTD. It is seen that the DTD trace features two prominent peaks at 75 kHz and 79 kHz that are not seen on TEC and LEC, and they are associated mainly with the whole structure's longitudinal extension mode in the DTD. These DTD modes are almost orthogonal to the vertical modes, and therefore no substantial component can be observed in the vertical plane. Its orthogonality results in nodal lines on the ABS appear as those of roll modes, as shown in Fig. 3.5.2.2 (a). The LEC trace features a peak at 126 kHz, and the TEC trace possesses stronger responses at 275 kHz. According to the nodal lines shown in Figs. 3.5.2.2 (b), these specific modes, which are only prominent in one trace, are the typical 1st pitch and 2nd pitch modes.

However, there are several frequency peaks that are prominent in more than one trace. Such contents are shown in Fig. 3.5.2.2 (c), and they are labeled as suspension-coupled modes to distinguish them from typical pitch/roll modes. Since the slider itself has little effect on mode coupling, we consider the coupling as coming from the suspension. These suspension-coupled modes may not have nodal lines inside the slider's ABS domain, and may be observed simultaneously at multiple locations over the slider body. These suspension-coupled modes are found less prominent at contact proximity, but they can appear (especially components at around 240 kHz and 333 kHz) when a more engaged contact occurs [39], as a result of a more complex forcing condition being achieved.

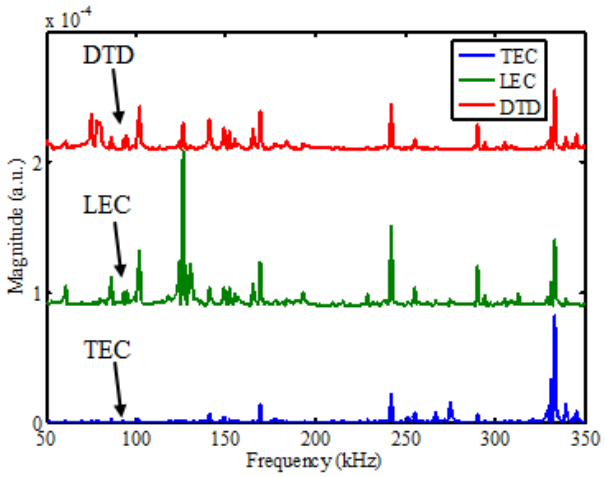

Figure. 3.5.2.1 Frequency response of harmonic analysis for HGA#1.

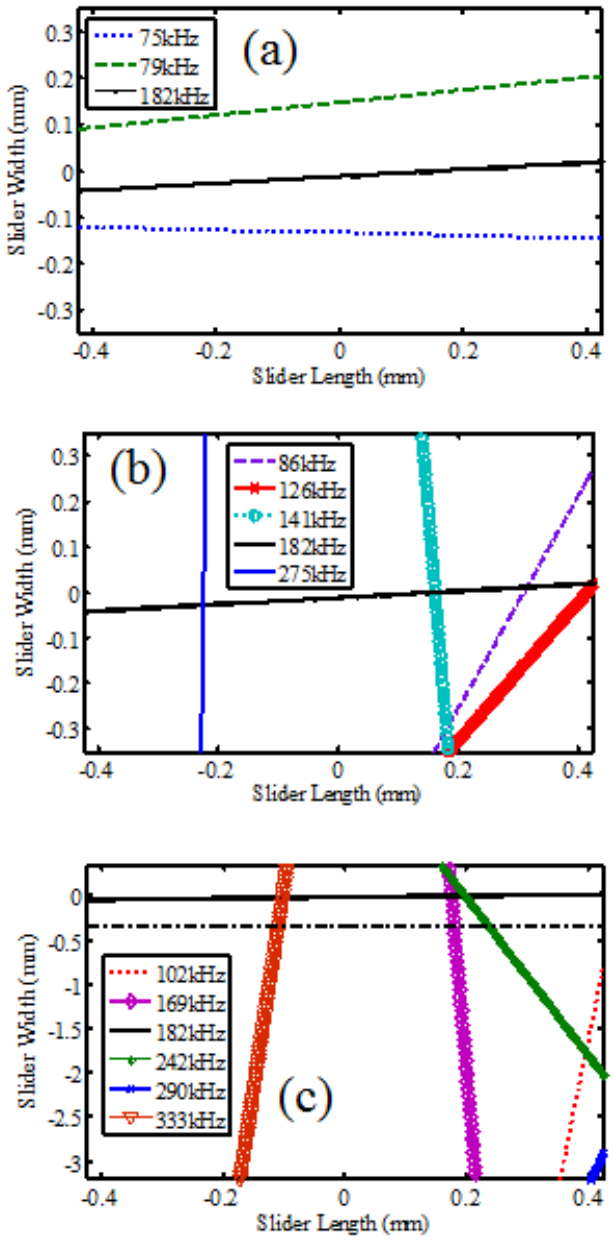

Figure. 3.5.2.2 Nodal lines on the slider ABS extracted from harmonic analysis of HGA#1 showing DTD and roll modes (a), typical pitch modes (b), and suspension-coupled modes (c).

The results for HGA#2 are shown in Figs. 3.5.2.3 (a)-(b). With a different suspension and ABS design, HGA#2 shows less frequency contents above 100 kHz, and the dominant modes at 72 kHz and 80 kHz are viewed as 1st pitch modes in the vertical direction. Nonetheless, these two modes are stronger in the DTD, which suggests LEC-DTD coupled modes. As a comparison to HGA#1, the DTD modes of HGA#2 are mechanically coupled with LEC modes so that strong DTD modes are observed as 1st pitch modes vertically, rather than roll modes.

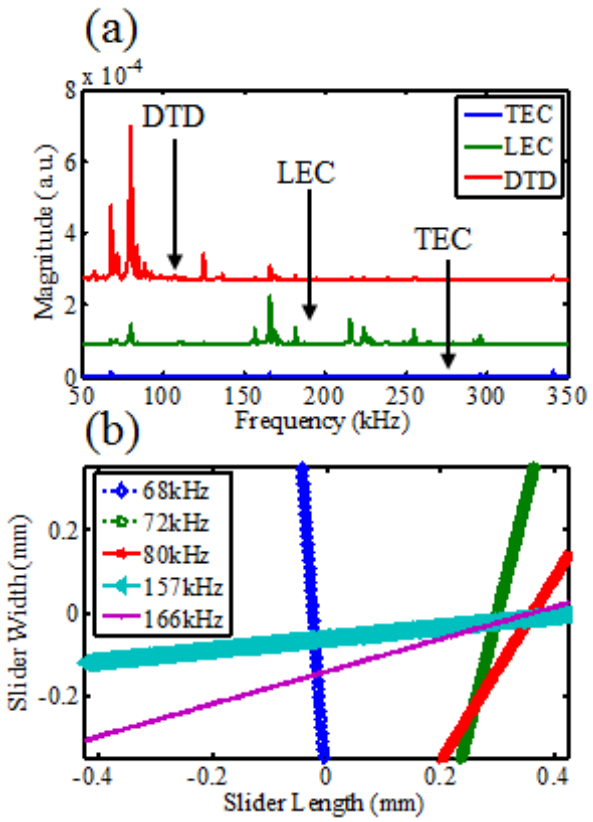

Figure. 3.5.2.3 Frequency response of HGA#2 from harmonic analysis (a) and the corresponding nodal lines on slider ABS (b).

Transient analysis

The spectra of HGA#1 under transient excitations for vertical, off-track and down-track directions are shown in Figs. 3.5.2.4 (a)-(c). It can be inferred from the spectra that vertical excitation produces a prominent 2nd pitch mode, whereas off-track excitation arouses roll modes, 1st pitch modes and DTD modes. The down-track force excites the strongest DTD modes as well as 1st pitch modes. Since the slider's transient response differs according to the direction of excitations, the slider's vibration modes can serve as a useful benchmark in determining possible sources of excitations.

Experiment-simulation correlation

The dynamics of two HGA designs with down-track excitations are presented in Figs. 3.5.2.5 (a)-(c) and Figs. 3.5.2.6 (a)-(c), respectively. They contain the spectra of simulated responses and experimental spectra at touchdown from the LEC and DTD. Experimental results of the TEC are not presented here due to their reduced presence at contact proximity, which is also suggested by the simulations. The simulated transient results show that the down-track forces excite the prominent peaks at around 70 kHz-80 kHz for both HGAs, whereas excitations in the off-track and out-of-plane directions contribute different spectra

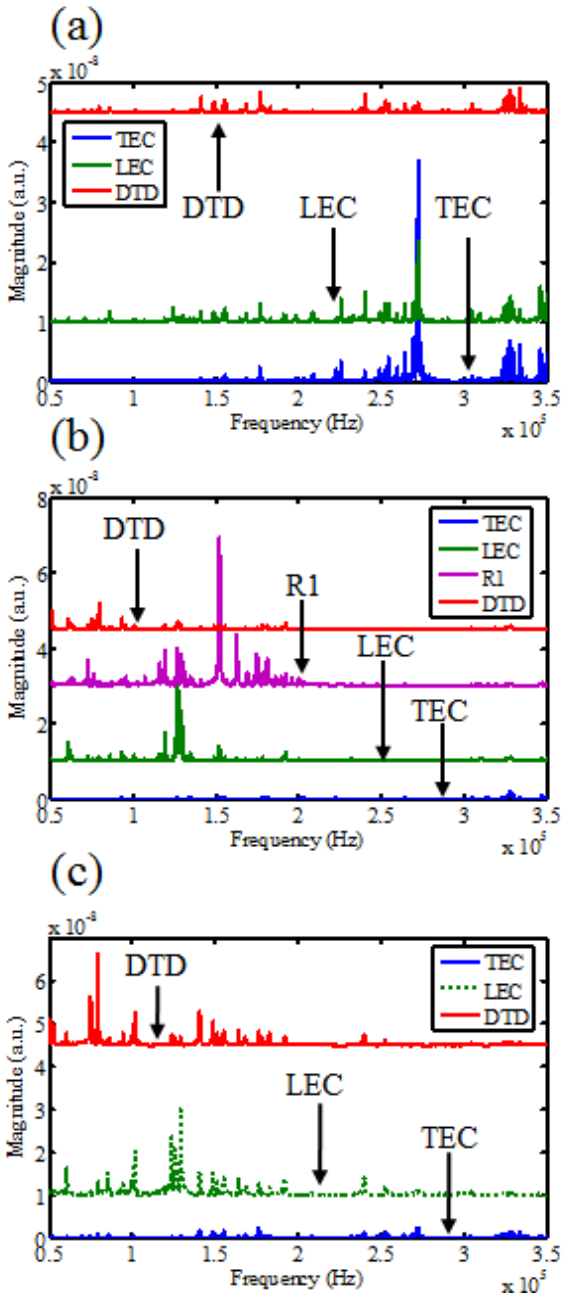

Figure. 3.5.2.4 Frequency spectra from transient analysis with vertical excitation (a), off-track excitation (b) and down-track excitation (c). R1 in (b) denotes the location on the slider that represent roll modes.

from those experimentally observed. Simulations also predict the differences between the HGAs in the frequency range of the 1st pitch modes. HGA#1 has its 1st pitch and related suspension-coupled modes in the 85 kHz-140 kHz range, whereas HGA#2 has only shared 1st pitch modes from the DTD. The results suggest the importance of DTD modes and therefore the in-plane forces at contact proximities.

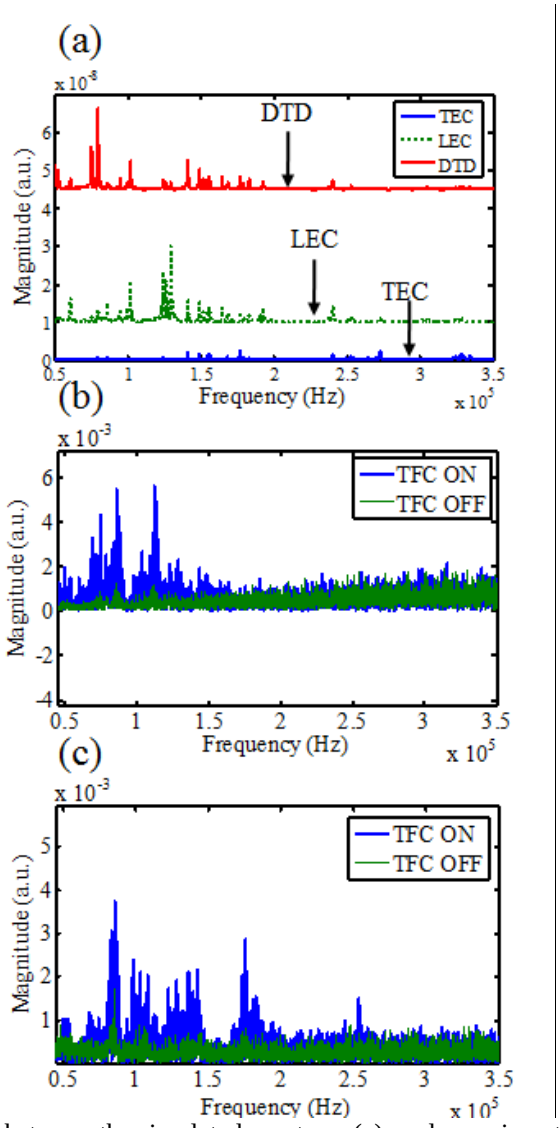

Figure. 3.5.2.5 Comparison between the simulated spectrum (a), and experimental spectra at DTD (b) and LEC (c) for HGA#1 subjected to DTD excitation.

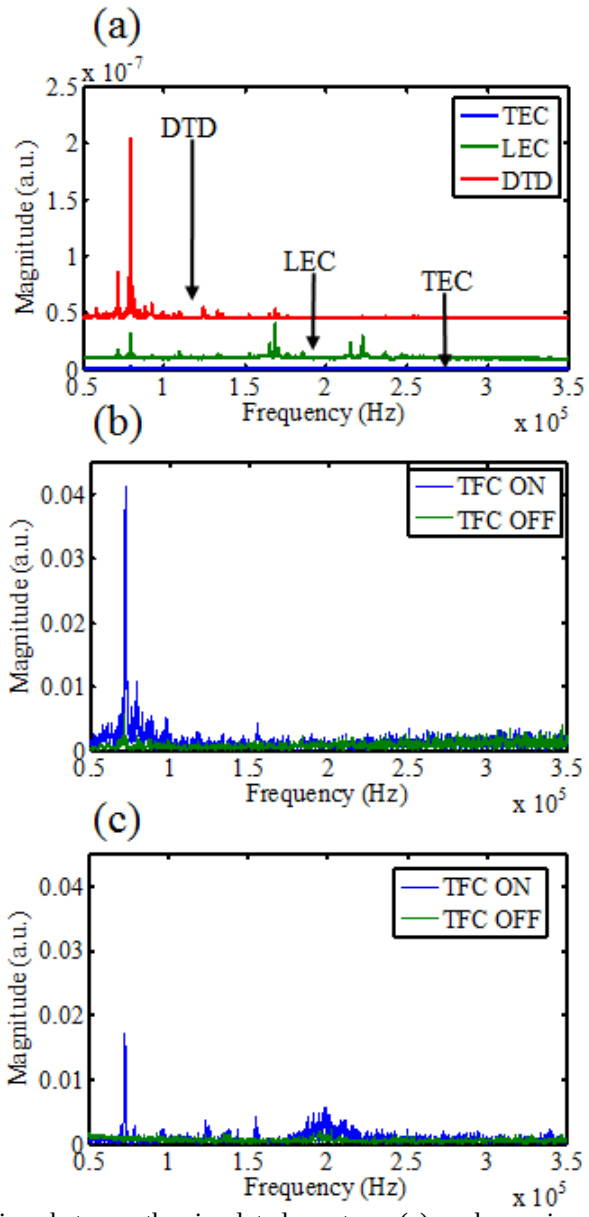

Figure. 3.5.2.6 Comparison between the simulated spectrum (a), and experimental spectra at DTD (b) and LEC (c) for HGA#2 subjected to DTD excitation.

3.6 Summary and Conclusions

In this chapter the dynamics of sliders at contact proximity are investigated. The definition of contact is considered from a dynamics point of view, and it is post justified by the instability of the AE signal, LDV signals and SEM wear inspection. The transition from the onset of instability to contact is presented to give a physical picture of the dynamical behavior of a slider approaching its contact regime. Forces exciting the instability come mainly from the in-plane components. The experimental results suggest that in order to study the onset of thermal protrusion induced instability of a TFC slider with minimal interference between the head and the disk surface, more attention should be placed on the LEC and DTD, or other positions rather than the TEC. It may be suitable for contact detection purposes to choose the TEC as a primary point of measurement; however, it risks overlooking a more lightly engaged slider-disk contact. In either the drive-level or component-level studies, the development of embedded in-plane motion displacement sensors is expected to be important for achieving reliable contact proximity detections.

By extracting the mode shapes with their associated frequencies from the simulation and comparing them with the experiment results, we conclude that at thermal protrusion induced contact proximity the in-plane force is the most important excitation. This can also be inferred from the similar DTD modes shared by the different HGA designs. The similarity of the DTD modes among the HGA designs can be a good contact detection indicator that is less design dependent than the modes detected in the other directions, and designing to reduce the LEC coupling from DTD excitation is essential for slider stability.

The modulations in slider motion are usually not able to be detected as experimentally demonstrated in this chapter. In a real HDD, the modulation of slider motion may be detected via magnetic read-back signals, and the understanding in the contact mechanism helps interpreting various signals obtained in drives. Concluding from the observed phenomenon, decoding the magnetic signals among 70 kHz-100 kHz may be the most sensitive frequency band to the onset of contacts; alternatively, a friction-based sensor with high sensitivity could improve the contact detection in HDI.

Chapter 4

Characterization of slider-disk contacts

This chapter presents a method to effectively characterize the slider-disk contacts. From the study of contact detection, it was found that not only at touchdown power can the slider dynamics be triggered, but also at a few power steps before TDP. This is defined as the modulation regime and is critical for the determining minimum stable flying height, or the stable back-off spacing, in terms of drive terminology. The modulation regime has been experimentally verified to be a measure of spacing, and is highly media dependent. By using the same HGA design over various media, the effects of lubricant type and thickness were investigated.

4.1 Introduction

While a reduced low-flying area improve the reliability of the head-disk interface (HDI), the interactions between the thermal protrusion and the disk surface requires a further investigation to push the stable low-flying limit of TFC sliders.

Current HDDs use certain signal thresholds to define head-disk contacts, based on which read-write flying height is set by certain TFC power back-offs from the defined contact power. Therefore, it is important to elucidate how the head-disk contact is defined, and how a stable back-off power can be chosen. Recent publications have been dedicated to the slider-disk interactions in the regime beyond the onset of contacts. The dynamics of TFC sliders in different heater power overdrives [38, 39] and at disk defects [42] indicated that prominent slider vibrations can be excited, and therefore raised a reliability concern. Simulations addressing intermolecular force interactions between the slider and lubricant layers were also studied [16, 48, 49, 63] to characterize the slider's behavior when it contacts with the lubricant layer and the materials below. The study at the regime of slider-disk contacts is important to component-level evaluations of product performance, but in drive-level applications the slider behavior before contact occurs, i.e. at contact proximity, requires a further investigation.

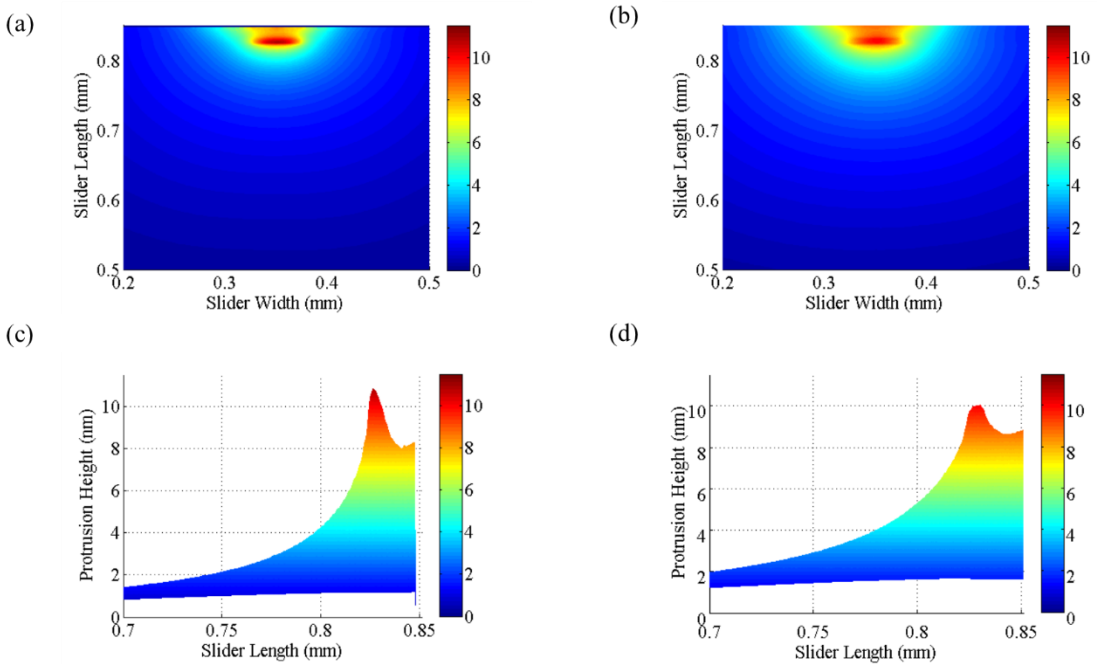

Figure. 4.2.1 Representative heater protrusion at around 10 nm for (a) HGA#1 and (b) HGA#2 when viewed from the ABS surface and from sides (c)-(d) respectively. It is noted that HGA#1 is much sharper and therefore possesses smaller contact area. The sharper profile also increases the thermal actuation efficiency. The scale of the color bar is in nm.

In this chapter, both the effects of heater designs and lubricant types on contact detections are discussed. It is suggested that for lubricants with high chemical affinity to the diamond-like carbon layers, less detectable perturbation occurs and a lower stable flying-height can be achieved by a TFC slider. Moreover, heater designs mainly affect the thermal actuation efficiency before contact occurs. A heater with lower thermal actuation efficiency increases the sensitivity to contact proximity but renders a rather gradual increase in vibration signals. By the inspection over lubricant surfaces, it is also suggested that part of the contact signal could come from the "lubricant asperities or moguls" [35]. The stable minimum achievable flying-heights depend on a proper match of thermal efficiency and choice of lubricants.

4.2 Experiments

Experiments were performed on an *in-situ* spin-stand equipped with an optical surface analyzer (OSA), a digital LDV and an acoustic emission (AE) sensor from chapter 3. Instead of using OFV-534, the combination of OFV-5000 with interferometer OFV-512, OFV130-5 and proper optics were used to visualize laser spots as mentioned in the last chapter. The laser beam was focused on the LEC to characterize the slider's modulations.

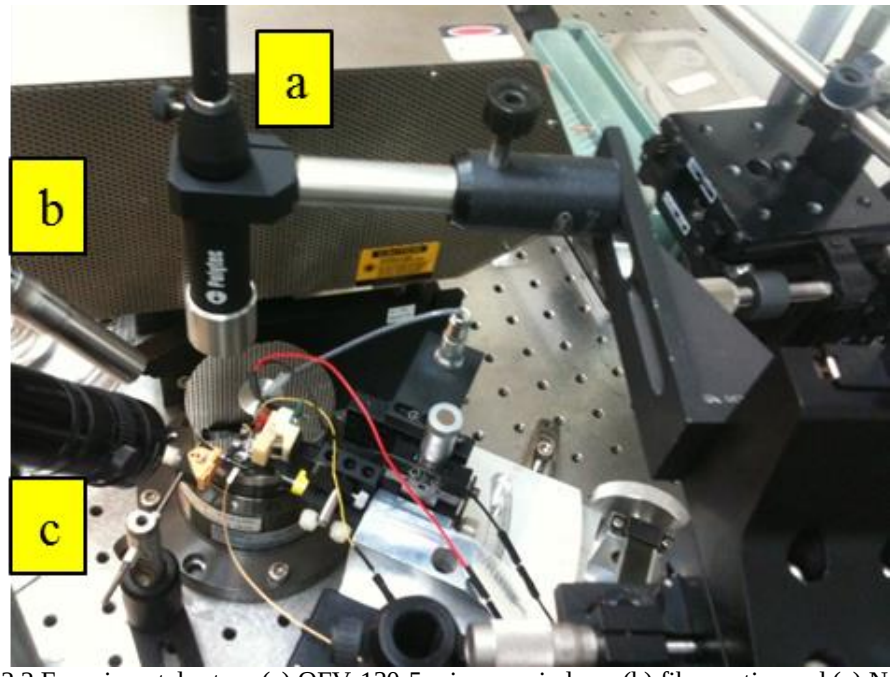

Figure. 4.2.2 Experimental setup: (a) OFV-130-5 microscopic lens, (b) fiber optics and (c) Navitar lens with filter.

In this chapter, as shown in Fig. 4.2.1, two HGA designs (Design#1 and #2) that only differ in the heater's thermal actuation efficiency were used, and touchdown detection experiments were performed over disks with different lubricants. Disks coated with ZTMD (80% bonded, 10 Å), Z-Dol (70% bonded, 9 Å and 12 Å) and Z-Tetraol (70% bonded, 12 Å) were used. Fig. 4.2.2 shows the experimental setup used in chapters 4-6.

4.3 Modulation Regime

From chapter 3, the slider modulations in all directions have been observed to start growing a few power steps prior to the defined contact, which is referenced to AE signals. The growth in modulations are most prominent in DTD and LEC, and therefore the modulation regime (MR) is defined as the number of range of power steps from the growth of DTD or LEC modulations to the touchdown power. In the next section the physical meaning of this modulation regime will be discussed before it is applied to examine the effect of lubricants. The MR is calculated as the power difference between that power corresponding to modulation growth reaching 130% of the noise floor and TDP.

4.3.1 Physical meaning of modulation regime

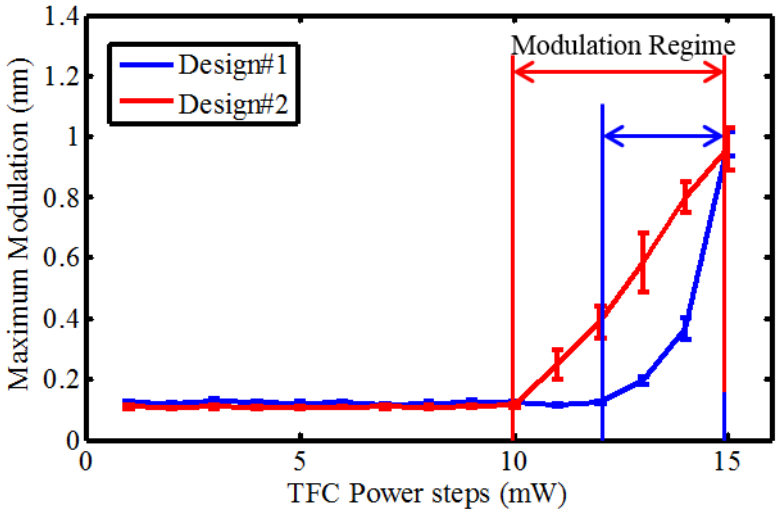

Figure. 4.3.1.1 Representative modulation regimes for different HGA designs over ZTMD disks. The 15th TFC power steps indicates touchdown here.

To understand the meaning of the modulation regime, we first applied the touchdown detection scheme to ZTMD disks using the two different HGA's that differ in thermal actuation efficiency only. ZTMD lubricant is known for its superior stability in terms of lubricant transfer and mogul formation [54, 55], and therefore the modulation regime can likely be attributable to non-contact interactions such as intermolecular forces. Design #1 possesses a TDP around 65 mW and design #2 it is around 120 mW. According to the thermal actuation efficiency, design #1 has almost twice the efficiency as design #2. As shown in Fig. 4.3.1.1, it is found that on the same ZTMD media, design #2 experiences a broader modulation regime than design #1. It is noted that the two designs reached a similar displacement modulation at touchdown on the same media.

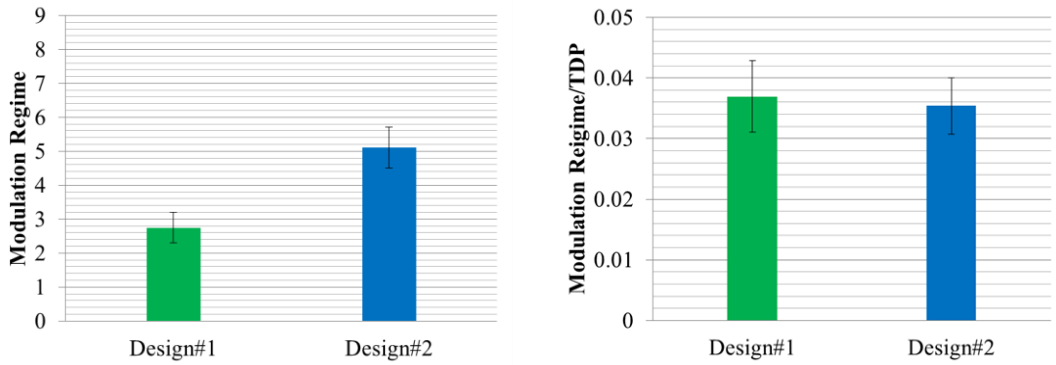

Figure. 4.3.1.2 (left) Summarized modulation regime observed on design #1 and #2. The error bar indicates the +1/-1 standard deviation among the 7 samples for each design. (right) Normalized MR shows a similar value between designs.

Experiments were repeated over seven HGAs for each design, and their results are summarized in Figs. 4.3.1.2. The modulation regime for design #1 has an average value around 2.75 while it is 5.11 for design #2. However, when the modulation regime is normalized by the corresponding TDP at each test, the differences between design #1 and #2 becomes subtle. Typically the normalized modulation regimes are of value 0.0369 and 0.0356 for design #1 and #2, respectively.

In comparison to the non-normalized cases, which values differ by a factor of two, the normalized modulation regimes for the two designs are essentially the same. This result suggests that the modulation regime sensed by slider modulations is a measure of mechanical spacing. Therefore, the modulation regime can be further interpreted as the minimum spacing a slider can achieve without modulation.

4.3.2 Lubricant effects on the Modulation Regime

In this section the modulation regime is investigated over various media designs. The modulation regime has been verified on ZTMD using two different heater designs to show it coincides with mechanical spacing, and the next step is to extend the study to Z-Dol 12 Å samples. Fig. 4.3.2.1 shows the representative modulation regime evolution as a function of power steps for design #1 on both ZTMD and Z-Dol 12 Å. It can be inferred that ZTMD possesses a shorter modulation regime and a more abrupt increase in modulation amplitudes, whereas Z-Dol yields a smoother and longer modulation regime. Both design #1 and design #2 are tested over ZTMD and Z-Dol 12 Å for complete comparison on the effect over designs and media types. Results are shown in Fig. 4.3.2.2 and Fig. 4.3.2.3, which suggest that the prolonged modulation regime on Z-Dol is a general trend for both designs. Therefore, only design #1 is used for further investigations on Z-Dol 9 Å and Z-Tetraol 12 Å. As shown in Fig. 4.3.2.4, the differences in modulations can be clearly attributed to the lubricant properties. Comparisons between the results for Z-Dol 9 Å and Z-Dol 12 Å demonstrate the thickness effects on the modulation regime, and it shows that a thinner lubricant layer can effectively reduce the modulation spacing. Z-Tetraol 12 Å and Z-Dol 12 Å, on the other hand, show the effect of molecular structure. It is worth noting that in these experiments, all samples, except for ZTMD, are made from the same process and the production same time frame, therefore all possible variations not related to experimental designs are minimized. Z-Tetraol, at the same or similar thicknesses to Z-Dol, reduced the length of the modulation regime by almost a factor of 2, which leads to a similar but slightly larger value than ZTMD.

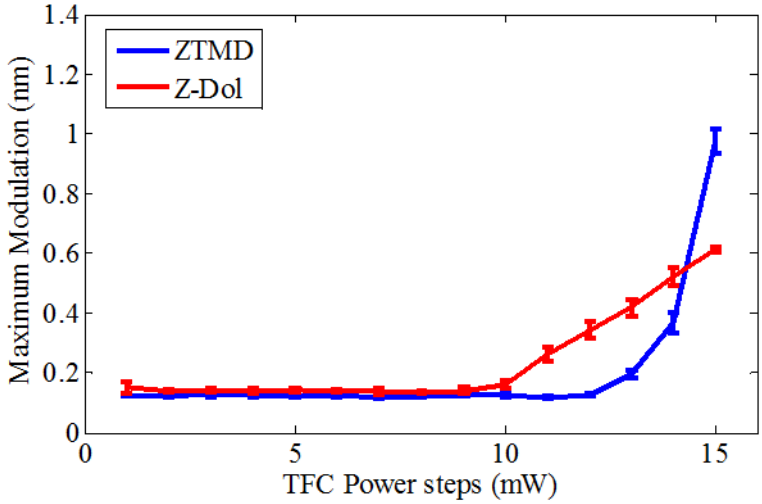

Figure. 4.3.2.1 Representative modulation regimes for design #1 on Z-Dol 12 Å and ZTMD media. Z-Dol 12 Å results in a much larger modulation regime. TFC power step #15 is the defined touchdown power.

The minimum "back-off" spacing, therefore, can be determined by the modulation regime as a "back-off clearance gain" indicator. Conventionally the "clearance gain" refers to the increase in the passive flying height of a slider, and it has been proven that a lower lubricant thickness, a shorter molecular backbone and more polar end-groups are lucrative to HDI reliability by providing more mechanical clearance.

However, in this chapter, the concept of minimum back-off spacing is a measure of how close a head can fly without dynamics being triggered. From the view of slider dynamics, the smaller the minimum "back-off clearance" the closer the operational spacing a HDI can

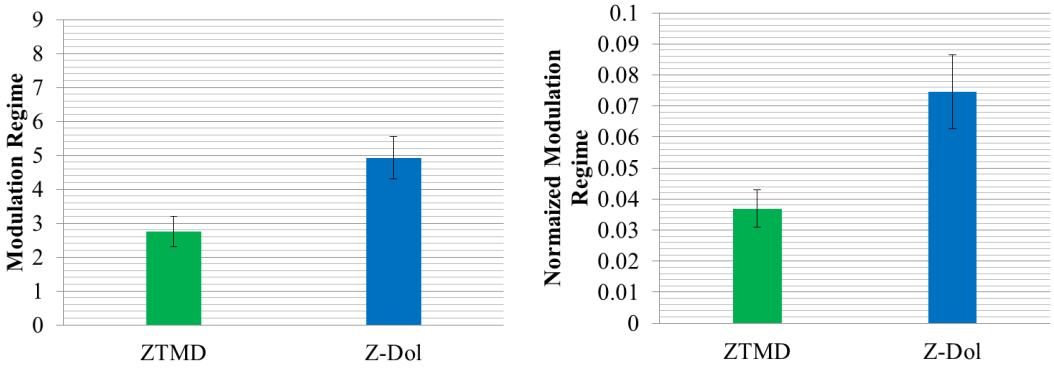

Figure. 4.3.2.2 Summarized modulation regime on ZTMD and Z-Dol media for design#1.

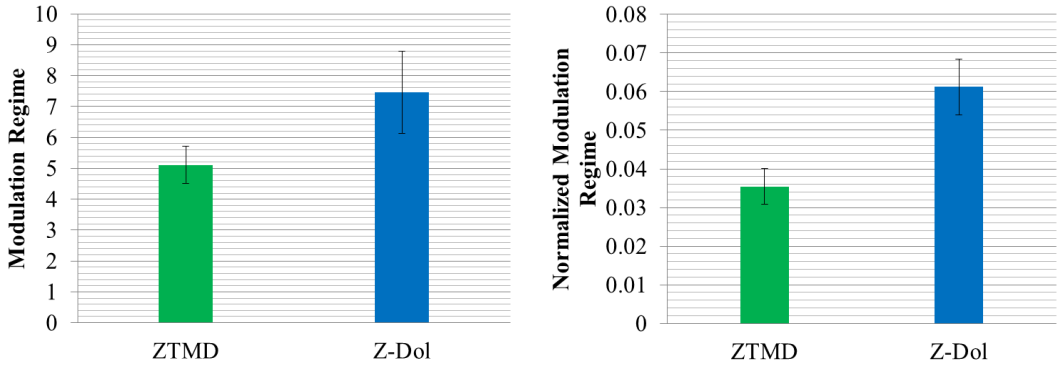

Figure. 4.3.2.3 Summarized modulation regime on ZTMD and Z-Dol media for design#2

achieve. In this regard, by increasing the number of polar end-groups, Z-Tetraol gains approximately 2.6 mW in the MR compared to Z-Dol (Z-Tetraol is 3.2; Z-Dol is 5.8), and a thickness decrease from 12 Å to 9 Å gains 1.8 mW in the MR (Z-Dol 9 Å is 4). The HGST patented/invented multidentate media, ZTMD, shows the best performance by having two pairs of adhesion end-groups amid its main chain and a lowest thickness (note: thickness measure may slightly vary by disk providers, so WDC media and HGST media may be offset by 1 Å). It is concluded that a decrease in thicknesses and an increase in bonding end-groups are both effective methods in allowing a head to interrogate the disk surface at a smaller spacing without perturbation.

4.4 Post-verification of the MR using TFC overdrives

The effects of lubricants on slider-disk proximity have been investigated using MR which is determined by slider modulations on the LEC. However, a remaining question is; how can it be verified as a unique feature for the HDI at contact proximity? Considering AE as was first set as the threshold for the onset of contact, and MR was observed based on it; there is no reason to believe the trend of MR only exists prior to AE-based contacts. An possible scenario that can easily overturn the efficacy of the MR is: after an AE-defined contact, the linear growths in modulation in the LEC and DTD keep increasing, causing the "length" of MR to be indeterminate.

In other words, to prove MR can be used for proximity characterization, eventually the evidence based on the dynamics after the defined contact should be presented to back up the authenticity of MR. Therefore, in this section a TFC overdrive scheme, which means a TFC power higher than defined TDP, is used to investigate the contact behavior.

4.4.1 Introduction to TFC overdrive

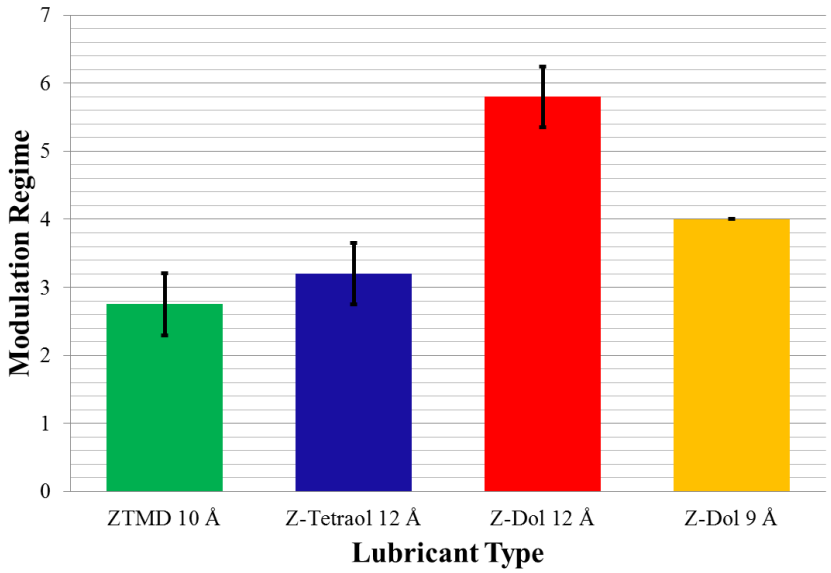

Figure. 4.3.2.4 Summarized modulation regime for design#1

When a value in TFC power is over the defined TDP, it is called an overpush or overdrive. Ideally in commercial HDDs, TFC overdrives are not favored and can only occur by erroneous detection of contacts. In component-level or drive level tests, however, TFC overdrives can be used for accelerated stressing evaluation. In this section, TFC overdrives are introduced intentionally to create more engaged contact conditions and to post-verify the use of MR for proximity sensing.

The MR is derived from chapter 3 and it is a repeatable regime from one touchdown to another with similar TDPs. A similar TDP suggests a similar or comparable contact condition is achieved. Nonetheless, it is not the case when for TFC overdrive. It is understood that under TFC overdrives, the HDIs are subjected to surface modifications due to a stronger mechanical interference. Surface modifications can result in DLC removal (head or disk) and lubricant modulation and/or transfer. The reduction or increase in surface profiles will inevitably change the TDP. Therefore, to study the overdrive dynamics in a repeatable manner, the slider modulations have to be averaged over several overdrive cycles in which the TDPs are kept unchanged. This can be achieved by driving the head wear through the so-called “running-in effect”, which will be shown in chapter 6. When the TDPs are not changing during the TFC overdrive cycles, the contact conditions are assumed to be the same from one overdrive cycle to another. Thus, the slider modulation in TFC overdrive can be investigated repeatedly as it was done in chapter 3 for touchdown only tests. Modulations were measured using LDV on both the LEC and TEC under a TDP variation within 1 mW.

4.4.2 Modulation regime and overdrive regime

Results from a 5 mW TFC overdrive experiment using design #1 and ZTMD media are shown in Fig. 4.4.2.1(a). As suggested from chapter 2 the slider vibration may contain high frequency contents after touchdown, so the data here were recorded using VD-09 filtered by a low-pass filter at 500 kHz. The regime covered by translucent blue indicates the MR as previously defined and the regime covered with translucent red is now termed the "overdrive regime". Here the amount of modulation on the LEC grows linearly in MR until it reaches 1 mW TFC overdrive. The TEC modulation, on the other hand, started to grow prominently after the 1 mW overdrive. This phenomenon suggests a "switch" in dominant vibration modes and answers the question raised previously. The MR behavior, where LEC/DTD grows linearly and outstandingly modulates at a larger amplitude than TEC, does not hold when TFC overdrive is experienced. When a TFC power passes the TDP, a fast increase in the TEC modulation takes place and becomes comparable to or even surpasses the amount of the LEC modulation. The LEC dominance compared to the TEC transition can be visualized by plotting the LEC/TEC ratio. At flying conditions the amount of LEC and TEC modulations are nearly the same therefore its ratio is around 1. When TFC power drives the head to disk proximity the LEC/TEC ratio starts to increase sharply due to a faster modulation growth in LEC than in TEC. Nonetheless, the ratio drops to a value around 0.5 due to the TEC dominance over LEC in the TFC overdrive regime.

A similar phenomenon can be observed using design #1 on Z-Tetraol. This is shown in Fig. 4.4.2.1(b), and in this particular figure the AE history is included for reference to address possible doubts on the constancy of LEC and TEC measurements taken at different times. In addition to the face that these LEC and TEC measurements were taken at the same/similar TDPs, the corresponding AE histories are also comparable. By sharing a similar AE history and similar TDPs, we assume that sequential measurements of LEC and TEC should not affect the result, and they should be very close to simultaneous readouts from LEC and TEC.

As a review of the efficacy of the use of MR, the overdrive regime (OR), where the general trend in MR reverses, establishes that the MR holds at disk proximity. In fact, the drastic increase in TEC modulation in TFC overdrives suggests a vertical forcing component during head-disk contacts, according to the analysis in chapter 3. Consequently, the transition from MR to OR can be further interpreted as a transition in the forcing condition, and therefore another touchdown definition. If touchdown is re-defined as the transition point from MR to OR, AE signals, by taking proper thresholds, can find a TDP that differentiates MR and OR within a range of +/- 1 mw, as shown Fig. 4.4.2.1.

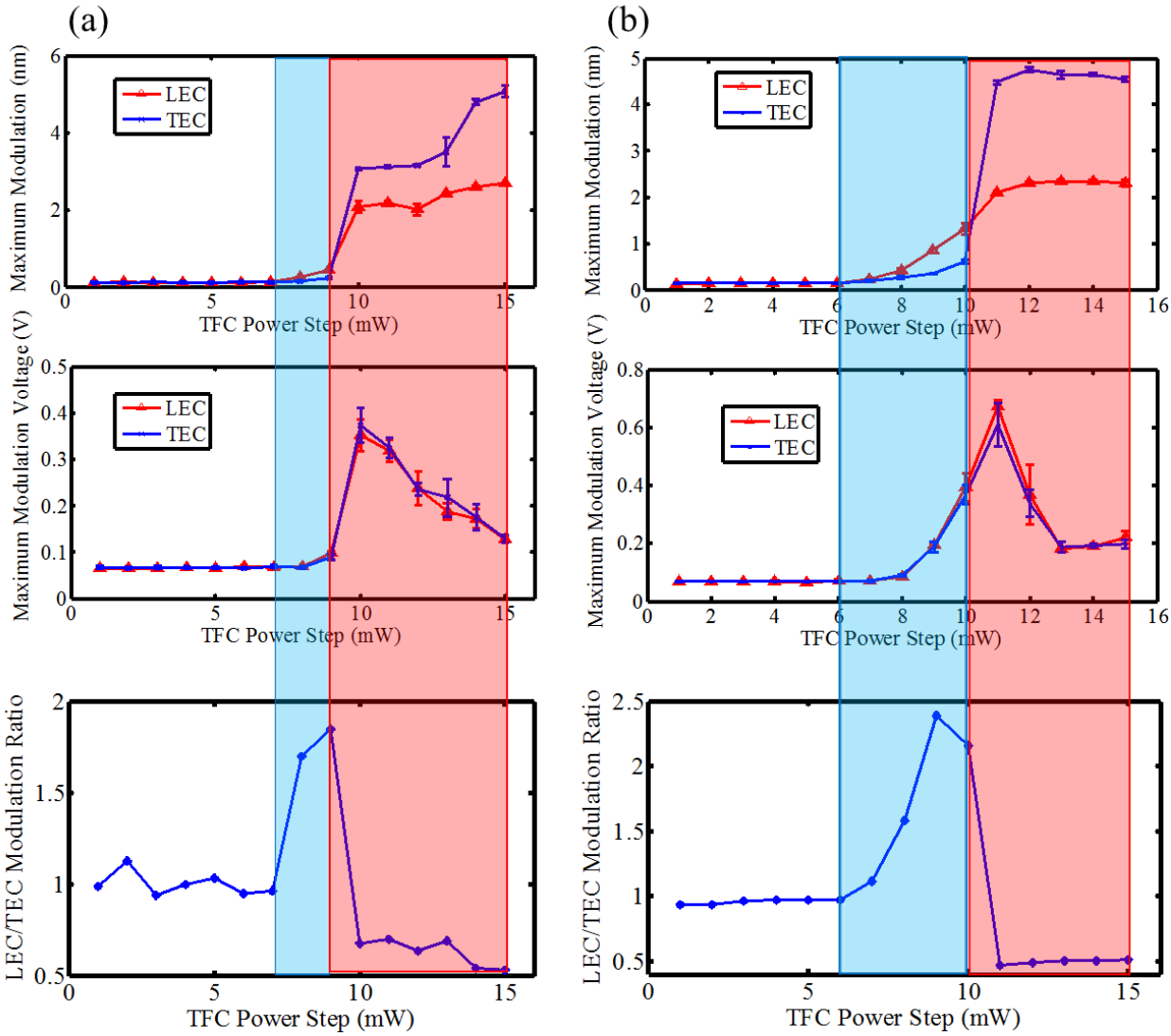

Figure. 4.4.2.1 The evolution of LEC and TEC modulations characterize the MR and OR with 1 mW variation among (a) ZTMD and (b) Z-Tetraol lubricated surfaces. TFC power step #10 is the detected TDP. The area covered by blue is MR, and OR is in red. First row represents the LDV modulation, and the second row shows the corresponding AE reading.

4.5 Summary and Conclusions

In this chapter, the MR is defined and supported by the observation of OR. A further definition of touchdown that the TFC power transitioning from MR into OR is proposed, which results in a close TDP to the method of using an AE threshold. Physically and experimentally, touchdown refers to a forcing condition change: planar excitation transits to out-of-plane excitations.

MR has been verified to be a measure of physical spacing, while OR represents a more engaged interference and is not directly related to clearance. This further justified that MR is a good measure before contact occurs.

By investigating MR over different media using the same HGA design, we conclude that the variation in MR comes mainly from the disk surfaces. The surface effects, according to experiment designs, come from lubricant types and thickness. A thicker, less bonded (by polar end-groups) lubricant film elongates the MR, which equivalently increases the minimum back-off spacing. As a media performance evaluation, MR should be minimized to allow a stable proximity recording. The trend observed using MR is in agreement with the use of AFM in a recent publication [58].

Although the effects of lubricants are investigated by MR, how a lubricant film physically induces MR requires a further investigation. In this regard, a dedicated study focused on the modulation of lubricant films is presented in chapter 5.

Chapter 5

Lubricant modulation under air bearing sliders

From chapter 3 and 4, all experimental data suggest the source of modulation a slider experiences comes from disk surface, and therefore the importance of the lubricant on proximity sensing is self-explanatory. In this chapter, the effect of lubricants on proximity detection is directly investigated using the OSA and LDV. In particular, the evolution of slider modulation in the MR as well as the time domain signals and lubricant topography is established. The experimental findings reported in this chapter advance the understanding of the contact phenomena in the HDI down to interferences in the vertical resolution of angstroms.

5.1 Introduction

The performance and requirements of the HDI has been rapidly advancing in the past two decades. The first direct observation of lubricant modulation was around 2000 when the passive flying height arrived at 20 nm and with the advent of the OSA from Candela Inc. By the use of the OSA, lubricant film changes on spinning disks under flying sliders were able to be observed in-situ. From the past studies, lubricant modulations were classified into two categories: moguls and ripples. Moguls form due to the presence of the air bearing pressures over disk asperities [34], and ripples form as a result of slider dynamics. In addition to non-contact modulations, some researchers who performed continuous contacts refer to a strong lubricant depletion as a “scar” or “lube wear” from engaged head-disk contacts [50]. Despite the efforts made to observe lubricant modulations in the HDI, the effects on lubricants of contact proximity have been studied very little.

The lack of understanding of the lubricant’s behavior at contact proximity comes from several reasons. For example, the spacing in the HDI was previously much larger than the lubricant thickness, and the HDI was designed to have no contacts. Consequently, most of the efforts in lubricant design was to eliminate modulations under passive flying condition by modifying its molecular structures and preparation recipes. It has been proven that

lubricants with lower profiles and less mobility can effectively increase head-disk clearance and reduce the formation of moguls [54]. The mobility of a lubricant can be controlled through adjusting the chemical bonding ratio by UV treatment and baking [57], or by synthesizing different main-chains and different numbers of polar end-groups. In 2008, the concept of "critical clearance" was introduced which established that a significant lubricant transfer from disk to the slider can happen without contacts at low enough spacing [33]. Later it was shown that such transfer is also lubricant-type dependent [51, 74]. While lubricant moguls, ripples and transfers are all important to HDI, they have mostly been studied with emphasis on fly-ability and stabilities at a larger spacing, around a few nanometers.

In this chapter, the lubricant modulation and the slider modulation phenomena at contact proximity and the associated methods developed from chapters 3 and 4 are bridged. By using TFC technology, it is shown that slider modulation can be directly associated with the lubricant topography changes at specific locations, which evolves as touchdown progresses. The values of lubricant modulation are on the order of a few angstroms and can be controlled by tuning the amount of TFC overdrive, which establishes and proves the angstrom-scale interference in the HDI discussed so far.

5.2 Lubricant modulation under passive flying

This section is intended to illustrate the general behavior when a molecularly-thin PFPE film on the disk is subjected to air bearing pressures of a low flying head. Lubricant modulation had been studied for at least 5-6 years prior to the use of TFC technology, and therefore even in experiments using TFC sliders, the results obtained without activating TFC should be in-line with the past reported trends. For completeness and as a reference, we firstly investigated lubricant topographies under passive flying sliders over several lubricant types: Z-Dol 9, 12 and 15 Å, Z-Tetraol 12 Å, and W-MD 12 Å. The newly introduced W-MD is a multidentate lubricant manufactured by WDC.

Sliders were flown passively at a linear speed of about 22 m/s for 10-12 minutes and the corresponding lubricant topographies were recorded in-situ using the OSA. The results are shown in Fig. 5.2.1. The amount of mogul formations follows the same trend as described in a recent paper [35, 56]. Z-Dol lubricants generate moguls for all thicknesses. The 9 Å samples, however, show less mogul formations than the 12 Å and 15 Å samples. Z-Tetraol 12 Å and W-MD 12 Å show insignificant amount of moguls.

The moguls' formations appear to follow the distribution of the air bearing pressure. It should be noted that air bearing pressure distribution itself depends on the slider's flying condition, too. A slider can fly at slightly tilted angles (roll and pitch) off the designed value which may change the expected air bearing distribution; nonetheless, as discussed in a recent dissertation from CML [22], air bearing pressures can cause "tracks" on disks along the circumferential direction by mainly the shearing stress component exerting on

lubricant films. These tracks can be observed in Fig. 5.2.1 and the moguls are found to form mainly on these tracks. While lubricant tracks may be simulated, moguls are hard to be verified numerically [52, 53]. Even though the trend of mogul formation is well observed as a function of lubricant types and parameters, it is hard to find an analytical model that can precisely capture its nature.

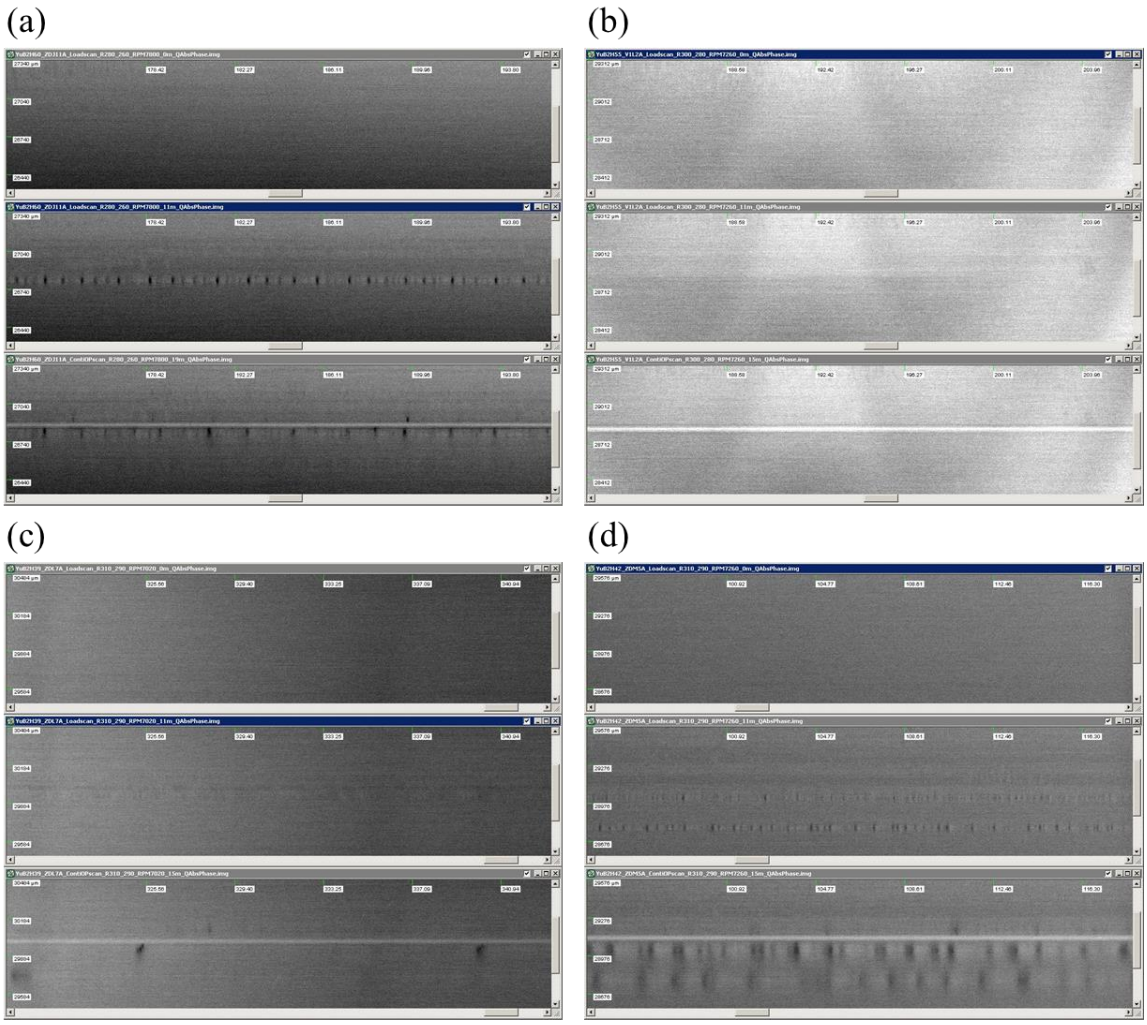

Figure. 5.2.1 Images from OSA show mogul formation on various lubricated surfaces: (a) Z-Dol 12 Å, (b) W-MD 12 Å, (c) Z-Dol 9 Å and (d) Z-Dol 15 Å. In each sub-figure the top image represents 0 minute load scan, the middle one shows load scan at 7 minutes, and the bottom image shows the thermal protrusion area marked by continuous contacts. By the use of thermal protrusion marks the position of slider can be estimated in each sub-figure.

5.3 Lubricant modulation under thermal protrusion-induced slider-disk contacts

The mogul formation under passive conditions has been discussed, and in this section the lubricant modulation due to contacts are investigated. In the past when TFC technology has not been applied to the HDI, the head-disk contacts were hard to correlate with disk topography. The difficulty stems the methods used to control flying-height were limited to adjusting RPM and ambient air pressure. Both of these changes take time on the order of tens of seconds, and do not guarantee a good resolution in flying-height adjustment. They are also not viable in commercial HDDs.

On the other hand, TFC technology can control the flying-height at an angstrom-scale resolution within a few tens of micro-seconds. It provides a flexible way for controlling the flying-height, interference level and duration. As has been demonstrated from chapters 2 to chapter 4, TFC sliders produce distinct observations in contact stages and especially the transitions at proximity. Most importantly, it confines any contact area to the protrusion neighborhood, which is usually to up about 40 microns wide and 20 microns in length. The protrusion area provides a good estimation of contact region. This implies the head-disk contact can be observed with a controlled interference and contact area.

A few experiments studying the slider's interaction with lubricant films were conducted. Slider-lubricant transfer and contacts were performed using half-lubed disks. In transfer studies, a transfer can be observed by having the slider move the lubricant from the lubed area to the de-lubed surface. A similar procedure was used for the contact studies, where a low flying-height was maintained so that contacts only occurred when the slider flew over the lubricated regime. These researches help understand a the macroscopic effects on slider-lubricant contacts due to its massive contact area (half disks), and the associated dynamics are more of an averaged measure [17, 59]. In fact, slider-disk contacts are observed to initiate in a location-specific manner, and therefore a more detailed analysis is required to investigate the contact phenomena without sacrificing the special resolution which should be at least on the order of contact area.

5.3.1 Experiments

To investigate the contact induced lubricant modulation in detail, we set the scanning resolution in the OSA to be 1-2 microns in the radial and approximately 5-6 microns in the circumferential direction (corresponds to 32X in Candela TS software setting). The HGA used in this study is the same that used in chapters 3 and 4. In this study we use a procedure as illustrated in Fig. 5.3.1.1:

1. Scan the designated disk track to ensure a clean surface prior to flying a slider.
2. Load the HGA to the designated track, fly passively for 10-12 minutes taking OSA scans in-situ.

3. Perform successive touchdowns for 50-100 cycles on the designated track, with the LDV focused at the LEC and AE signals acquired at each touchdown cycle and OSA scans every 3-4 minutes.
4. Similar to procedure#3, but perform successive 5-8 mW TFC overdrives for 25 cycles.
5. Perform a continuous contact using a 50 mW TFC overdrive for 900 seconds.

The purpose of observing the passive flying condition for 10-12 minutes was to provide a reference for contact-induced topography changes. As shown in Fig. 5.3.1.1, by comparing the passive loading scan from 5 to 10 minutes and the modulation after touchdown occurs, we see that the moguls can be attributed to the contact events. The reason for doing TFC overdrives is to compare the effect of contact conditions and mogul formations. Finally, the continuous contact using excessive TFC overdrives has two meanings: one for studying the lubricant film's reliability under aggressive contacts, and the other one is to mark the TFC protrusion contact area on the disk. By marking the contact area the actual position of a slider can be determined accurately, which makes the correlation between lubricant modulation and the slider's contact area possible. For demonstration purposes, first the result for –Dol 12 Å from section 5.3.1 to 5.3.3 are used. In section 5.3.4 a summary of the results for all lubricants will be shown.

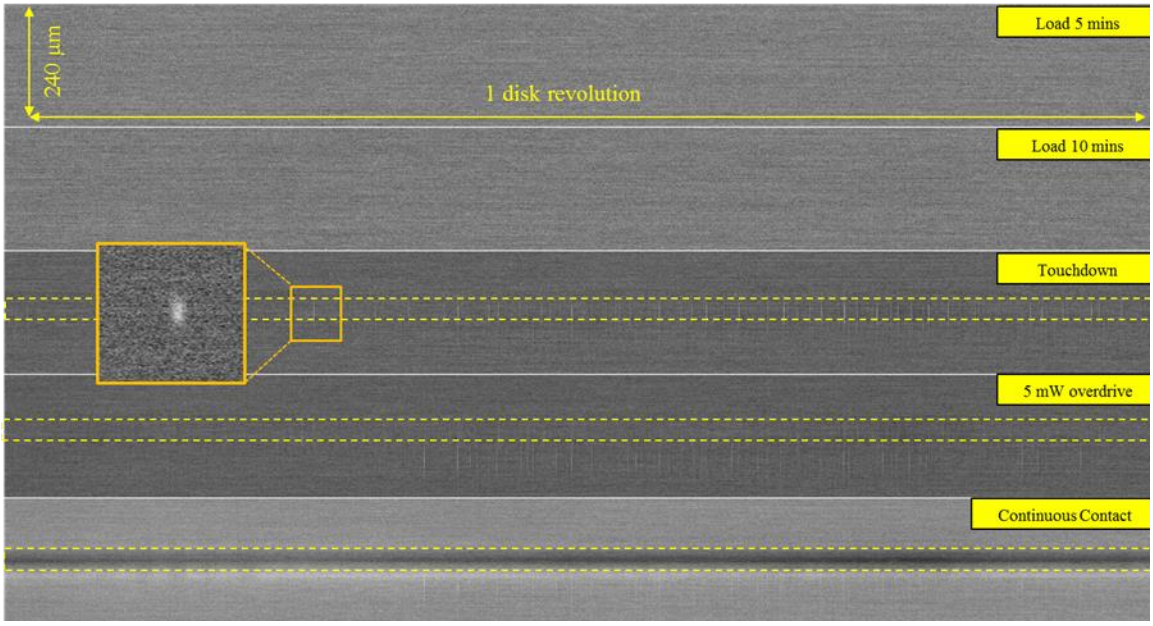

Figure. 5.3.1.1 Illustration of experimental scheme using MATLAB-processed OSA images. The width shown in each loading condition is approximately the dimension of slider's center pad on the TE. A whiter area means a higher lubricant thickness, which is termed mogul in this chapter. In the continuous contact condition, the dark track indicates a groove plowed by the thermal protrusion.

5.3.2 Lubricant modulation under touchdown and overdrive

A quick observation can be made from Fig. 5.3.1.1. The target lubricant surface was clean under the 10-minute passive flying period, and then lubricant modulation appeared in the form of moguls at the area boxed by a dashed enclosure. The modulations disappeared after implementing the TFC overdrives, and the region where the modulation evolves corresponds to the surface right under the thermal protrusion area, according to the groove mark made by continuous contacts. This suggests that such modulation (mogul formation/annihilation) is related to thermal protrusion and contact conditions.

The attempt to correlate slider modulation and lubricant modulation is not new. However, all the previous observations were mostly focused on finding a coherence in the frequency spectra and modulation amplitudes at the length/time scale of disk revolutions. That approach sacrifices the location-specific nature of contact proximity. Instead, in this chapter, the modulation is studied to the resolution no greater than the thermal protrusion dimensions. This results in a new observation that establishes a direct contact correlation between thermal protrusion and the top portion of the lubricant layer.

The slider's flying-height modulation signal taken at the LEC is presented with an artificial DC offset of around 12 angstroms above a lubricant's circumferential profile radially averaged over 40 microns in Fig.5.3.2.1. It is found that the location where the slider modulates the lubricant corresponds to the moguls' positions. The fact that the moguls' pattern could match that of the slider's modulation is very interesting. It suggests that at

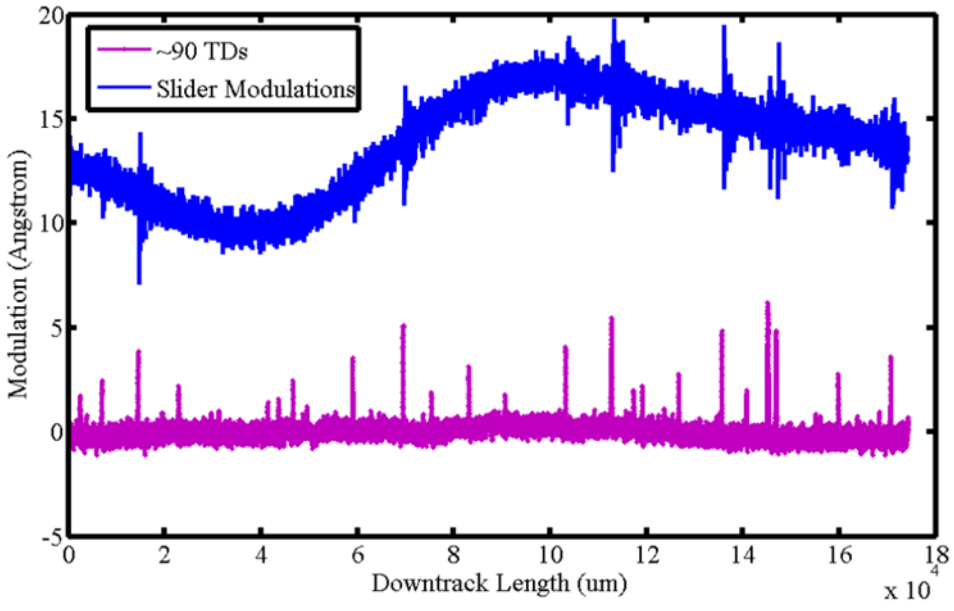

Figure. 5.3.2.1 Slider modulation and lubricant modulation are well correlated location-wisely. Purple data represent the lubricant's circumferential profile radially averaged over 40 microns.

the previously defined touchdown power, sliders can either stroke/pull up the lubricant surface by its protrusion or the slider can sense the newly formed mogul at proximity using its protrusion.

To further investigate the causality between slider modulation and lubricant modulation, successive touchdowns were applied to the HDI with OSA scans every 3 to 4 minutes. It is noted that OSA scans at its own timing which cannot be precisely aligned with touchdown cycles. However, the number of OSA scans and the corresponding touchdown passes can be roughly estimated at 6 touchdowns per scan. By successively applying touchdown and OSA scans, the evolution of moguls can be captured.

As shown in Fig. 5.3.2.2, moguls form after touchdown initiates, and one mogul is chosen for illustration. The blue data on the top is the corresponding slider modulation at the 100th touchdown with a DC offset to show the coincidence between the slider modulation and mogul formation. The mogul not only forms under slider modulations but it also grows. It grows both in height and width significantly in the first 30 touchdowns, after which a significant shear from the top of the mogul can be observed.

However, when the same surface is subjected to successive 5 mW TFC overdrives, the moguls' heights get prominently reduced and sheared further in the down-track direction, which resembles a spreading phenomenon. While moguls spread due to TFC overdrives,

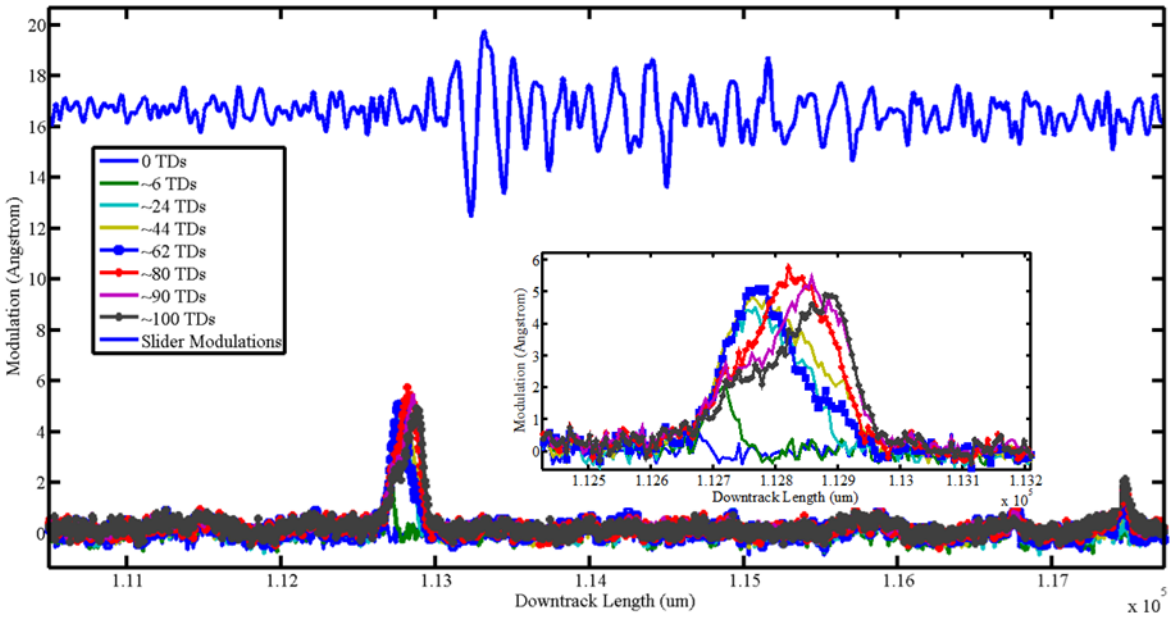

Figure. 5.3.2.2 Mogul evolution as touchdown progresses. The insertion is a zoomed-in view of the mogul being observed. The mogul originates from a flat lubricant profile and then grows in height and width. When a height of 5-6 angstrom is reached, the mogul seems to be sheared towards the down-track direction.

they do not fully vanish. As the demonstrative mogul shows, it retains a height slightly below 2 angstrom.

By monitoring the lubricant's evolution in response to successive touchdowns followed by TFC overdrives, we are able to make the slider-disk contact mechanism at disk proximity much clearer. First, it can be concluded that "touchdown" can generate moguls, and stroke the top surface of the lubricant layer without destroying them. The lateral motion of the moguls follows the shearing direction of the slider. Second, a 5 mW TFC overdrive provides a further interference that can reduce a mogul height to approximately 50% of its maximum height. As a result, from the defined touchdown power to 5 mw TFC overdrive, the interference level is estimated to be a few angstroms only. Note that in this chapter, another interpretation of contact could be derived by the lubricant's response. The phenomenon that a mogul could be generated at touchdown indicates a very light and fast engagement/detachment between the surface of thermal protrusion and the top lubricant layer, whereas the annihilation process suggests a stronger contact with no location-specific pattern. This finding not only elucidates at least one of the slider-disk contact mechanisms, but it also supports the results presented in chapters 3 and 4.

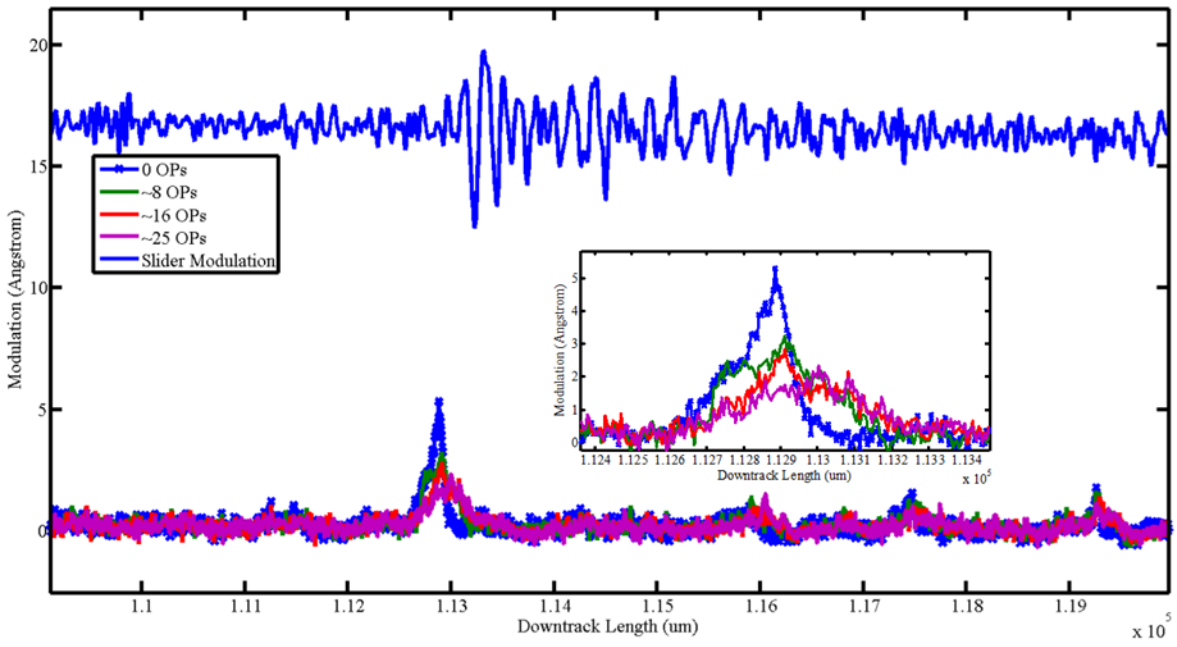

Figure. 5.3.2.3 Mogul shows a reserve trend under successive 5 mW TFC overdrives/overpushes. The mogul "spreads" in the down-track direction.

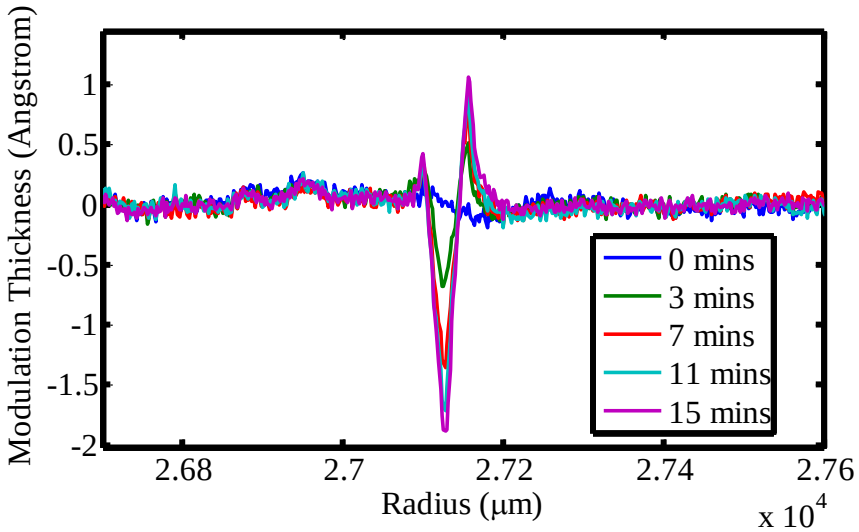

Figure. 5.3.3.1 Representative lubricant deformation history under continuous contacts

5.3.3 Lubricant modulation under continuous contacts

Lubricant contact under 900-second 50 mW TFC overdrives usually forms a groove, which is used to mark the thermal protrusion area in the previous sections, as shown in Fig. 5.3.3.1. Under strong head-disk contacts, there is no location-specific patterns as reported before, nor is there any linear and repeatable procedure that can be applied to the same HGA. However, it is worthwhile to see how much a lubricant layer can be depleted under such an aggressive contact condition.

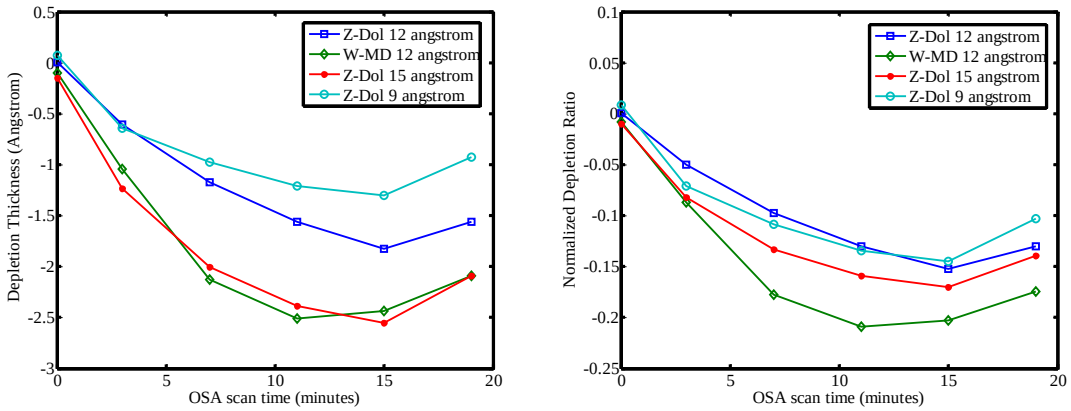

Figure. 5.3.3.2 Lubricant depletion thickness over time (left), and the normalized depletion with respect to overall thickness, (right) among different lubricant designs. The 19-minute data represent lubricant recovery after 15-minute TFC overdrives, which suggest lubricant replenishment.

Interestingly, within the 900-second duration, the lubricants only show a few angstroms of depletion, and it is typically below 20% of its overall thickness, as shown in Fig. 5.3.3.2. The amount of depletion observed during continues contact depends on both the lubricant parameters and contact strength. However, in the present continuous contact experiments we can not precisely quantify contact strength by the amount of TFC overdrive. Therefore, only two conclusions can be made. First, the depletion of the lubricant surface is very slow around at the order of angstroms/minutes, and the maximum depletion thickness is below the designed mobile ratio~25%-30% (calculated from the designed bonding ratio~70%-75%). Second, based on the first observation, the lubricant layer seems to be solid-like, and it is not penetrable by thermal protrusions. Recall the friction force data shown in chapter 2, such friction may come from lubricants plus the asperities contacts protruded from the disk DLC overcoat with less lubricant coverage.

5.3.4 Data Processing

In the following section the effects on touchdowns due to different lubricant types and thicknesses will be discussed. Before those comparisons are made, we present here an illustration of the data processing method on moguls. A customized MATLAB script was used to find the peaks of the last touchdown induced lubricant profile, and these locations were used as the initial guesses to find the peaks in the previous profile, etc. After the peaks in each lubricant profile are found, the moguls' dimensions are determined by finding the

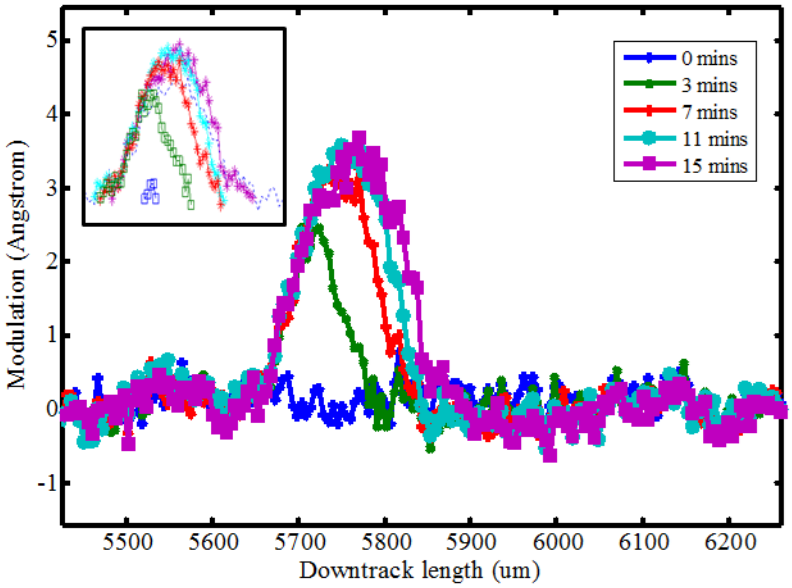

Figure. 5.3.4.1 Demonstrative mogul profiling result. The insertion shows the numerically found mogul profile at different scans.

lobes to each sides of each peak, as shown in Fig. 5.3.4.1, which shows the determination of mogul length, and width is analyzed in a similar way.

5.3.5 Lubricant modulation, TDP and modulation regime

The correlation between slider modulation and the lubricant modulation has been presented in previous sections using Z-Dol 12 Å samples for illustration. In this section, a summary of moguls' dimension evolution as touchdown progresses over different lubricant types (Z-Dol and mulidentate), and thicknesses (Z-Dol 9, 12 and 15 Å) is shown in Fig. 5.3.5.1. The summary presents the averaged moguls' dimensions and their standard deviations at each OSA scan of each lubricant sample.

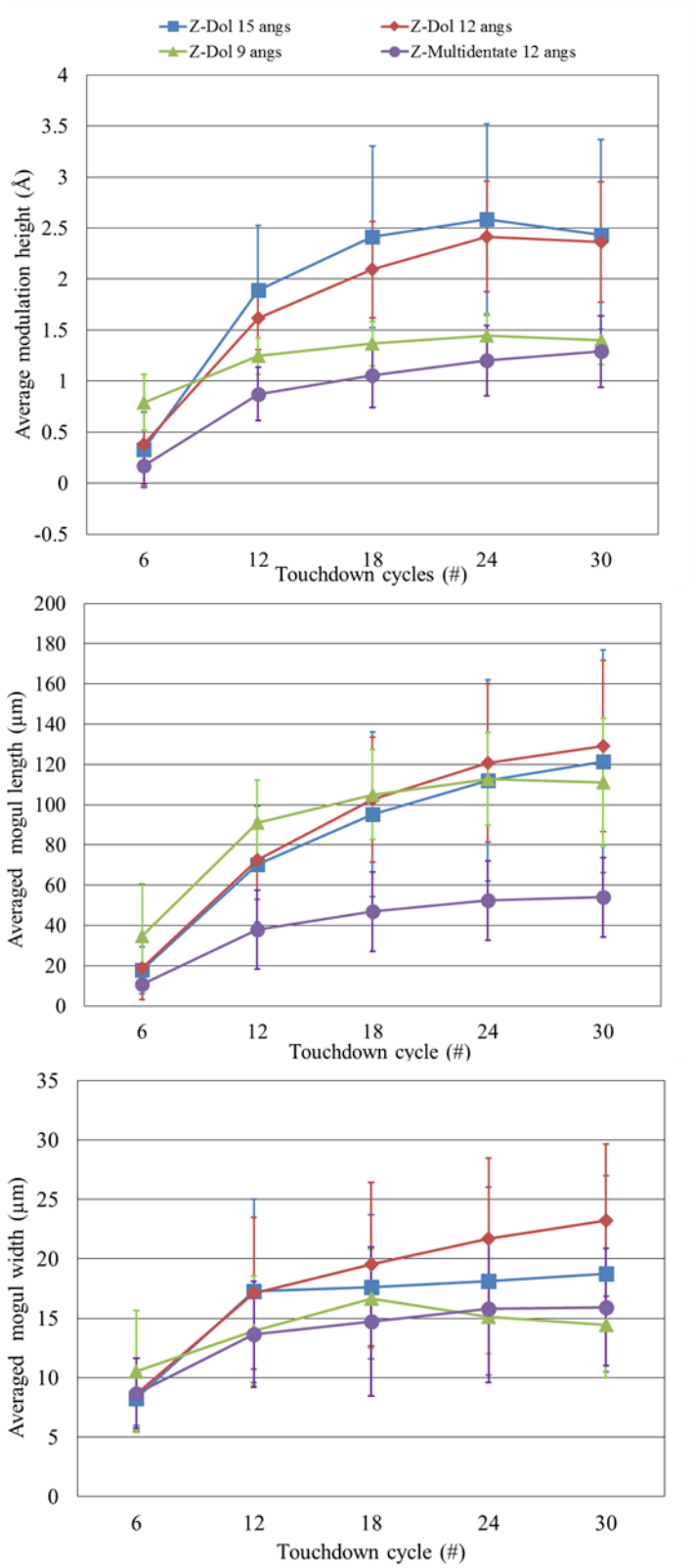

Figure. 5.3.5.1 Moguls' dimension evolution as a function of touchdown passes

Regarding the moguls' heights, all lubricants show trends of growing in the first 30 touchdown passes. However, there are two groups in terms of heights. Z-Dol 12 Å and 15 Å share a very similar growing history, whereas Z-Dol 9 Å is closer to W-MD 12 Å. Therefore it can be concluded that a reduction in thickness and increase in the number of polar end-groups can effectively suppress mogul formation. However, when it comes to the mogul's length, all Z-Dol samples show a similar trend in sheared length, which is much longer than W-MD. Considering the shear length may be related to the lubricant's resistivity to shear stress, W-MD is superior to Z-Dol by bonding strength. While thicknesses variations on Z-Dol samples show no obvious effect in shearing length. Width-wise it is hard to draw any conclusion due to its closeness among samples considering relatively large standard deviations.

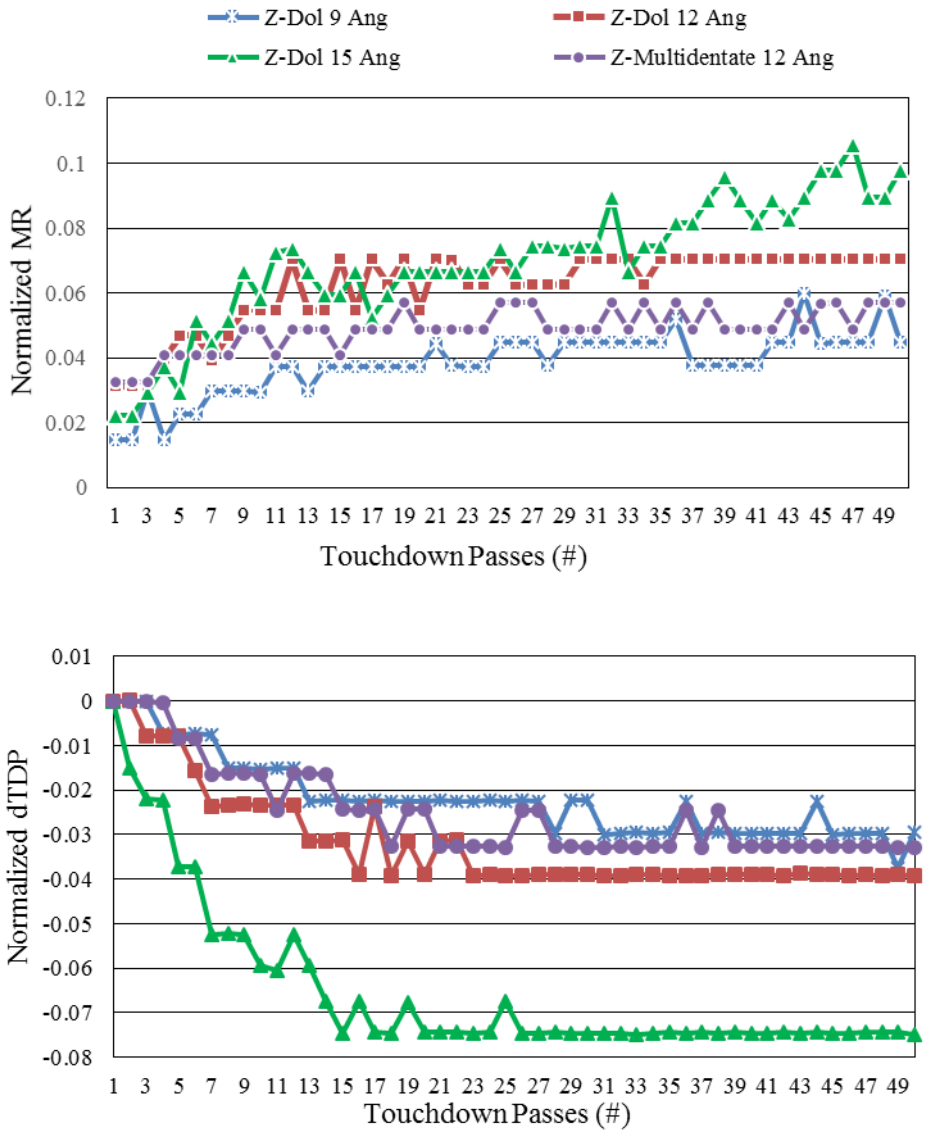

Figure. 5.3.5.2 Normalized MR and dTDP as a function of touchdown passes

However, the width is surmised to be controlled mainly by the thermal protrusion's contact width; although Z-Dol 12 Å and 15 Å seems to have larger widths than Z-Dol 9 Å and W-MD 12 Å.

The above analysis represents the lubricant's property evaluated using the slider's touchdown, and interestingly the effects of thickness and bonding strength can be partly distinguished in terms of mogul heights and shearing length. The next question is whether or not a slider can sense the differences in the lubricants' topography. To answer this, the method of MR developed in chapter 4 is used here. Fig. 5.3.5.2 shows the MR normalized by the corresponding touchdown power (normalized MR) for a direct spacing measure at contact proximity as explained in chapter 4. The normalized MR of each lubricant sample starts at a similar value and then grows as touchdown progresses, and the evolution of normalized MR shares the trend of the moguls' heights. This suggests that the normalized MR senses an increase in the minimum back-off spacing that could be attributed to the growing moguls. Meanwhile, the normalized dTDP (TDP value difference from the fist TDP) indicates a decrease in the mechanical clearance, which suggests that increasing in the moguls' height not only raises the minimum stable flying heights but also the contact reference plane.

It is noted that the normalized MR recovers the observations in chapter 4, where the MR were analyzed at settled TDPs. By comparing the normalized MR and dTDP in Fig. 5.3.5.2, we find that after 30 touchdown passes, the dTDPs and therefore TDPs stabilizes; and the corresponding normalized MR indicates the effect of lubricant thickness and polar end-groups.

Another important point to mention is that thinner and stronger bonded lubricant layers are more resistive to perturbations induced by contacts, from both the MR and TDP's analysis. TDP measures a long-term reliability at passive flying conditions and MR measures the accessibility to proximity.

In addition, the observation related to mogul shear makes an intriguing link to the dynamics study in chapter 3, where the shear excitation was found to be the dominant forcing component at contact proximity. Comparing the moguls' behavior and the contact dynamics, it can be concluded that lubricants can provide a certain shear stress to sliders via the rotating disk.

5.4 Causality of slider modulation and lubricant modulation

It has been shown that slider vibrations and lubricant modulation can be location-wisely correlated. The way the lubricant modulates is in the form of moguls, which can further be correlated to the behavior of the MR and TDP. From the evolution of moguls' dimensions, it is concluded that shearing stress plays the main role and this observation supports the findings in slider dynamics. However, correlation does not represent causality and

therefore the question remains; is slider modulation aroused by lubricant modulation or vice versa?

From the experimental results on the evolution of moguls and MR as touchdown progresses, it is natural to conclude that the lubricant modulation is induced by slider modulation at touchdown. However, since the growth of moguls can later be sensed by the slider causing the increase in the MR, it also suggests that lubricant modulation can reversely affect slider dynamics.

The best way to investigate the causality is to observe the lubricant surface during the passive flying period and the 1st slider's touchdown attempt. Fig. 5.4.1 demonstrates how

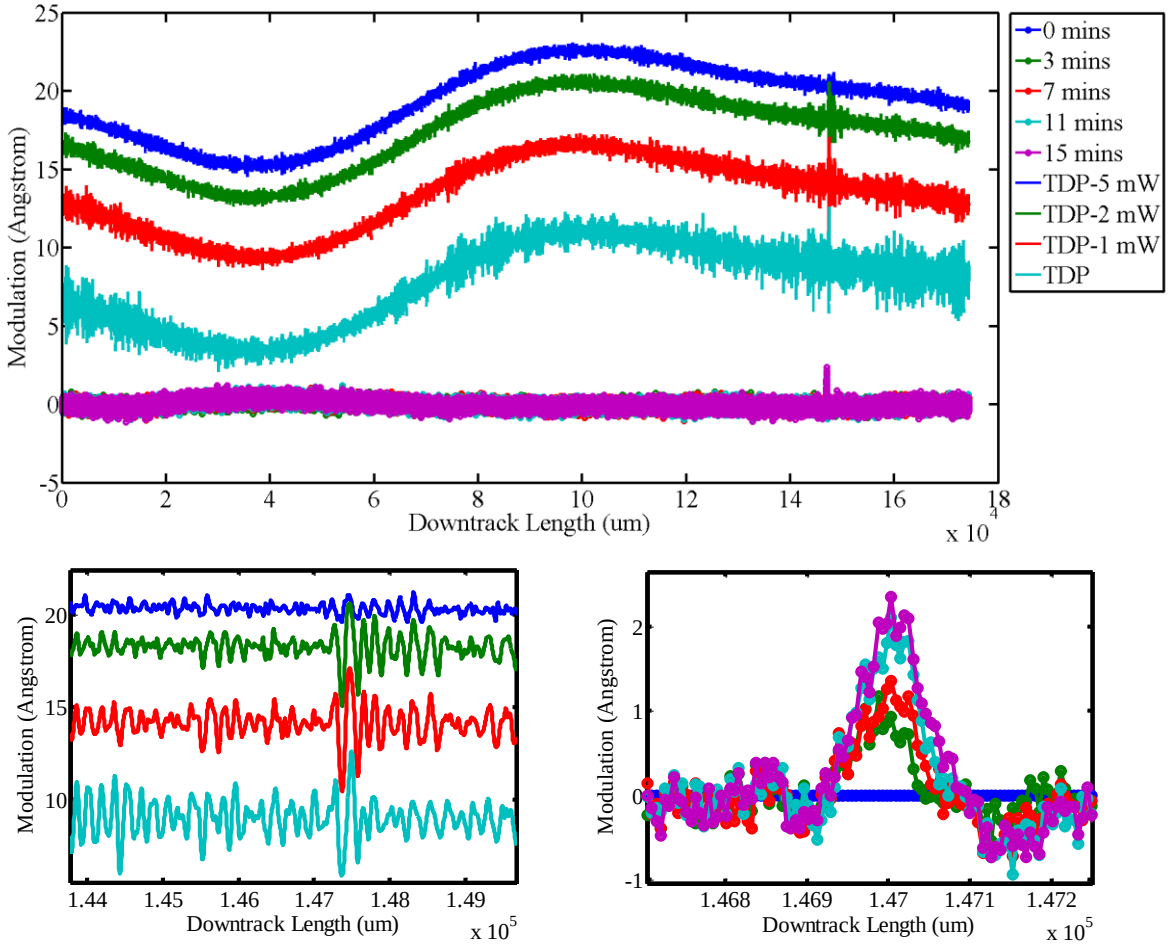

Figure. 5.4.1 First touchdown attempt of a slider after a 15-minute passive flying. When the slider approached the existing mogul developed previously, slider modulation started developing from approximately 2-3 mW away from TDP. This directly shows the possibility of slider modulation sensing moguls. Second rows are zoomed-in data plots for modulations.

an existing mogul can affect the slider's modulation. In conclusion, they are highly dependent on each other, and here an experimental proof is provided.

Cases when contact-induced moguls cannot be identified do happen occasionally. It occurs when contacts are made with a large number of existing moguls, which lead to a more complex contact behavior. The contact pattern is partly due to existing moguls. Under such condition, the lubricant modulation may not be easily identified as contact-induced, and a contact event may bring up some moguls while suppressing others due to the irregularity

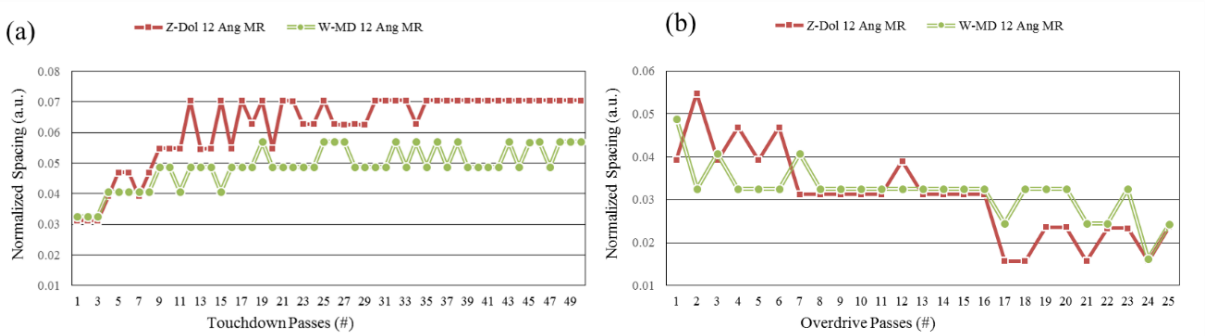

Figure. 5.4.2 MR evolution from TD to overdrive

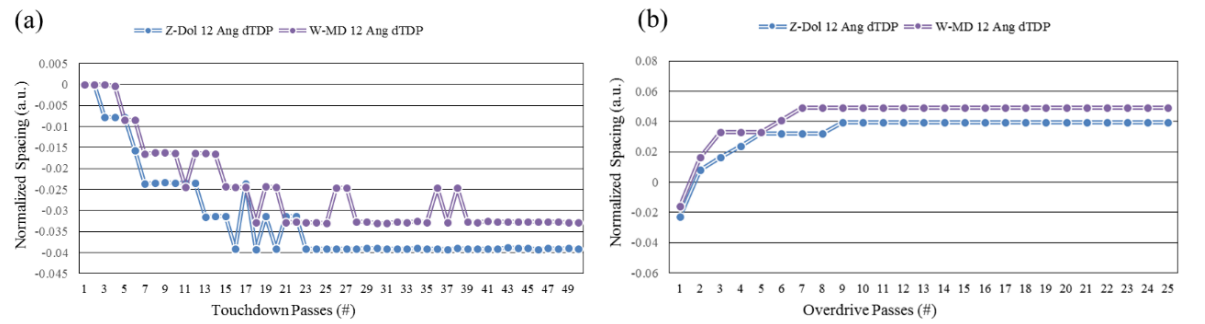

Figure. 5.4.3 dTDP evolution from TD to overdrive

of surface profile. As moguls can form without direct contacts, the formation of moguls under the passive flying condition around the protrusion area may be a hurdle for contact-induced mogul observation.

Nonetheless, when the lubricant surface is relatively clean under the protrusion area, the formation/annihilation of moguls can be observed by the MR. As shown in Figs. 5.4.2-5.4.3, the MR decreases as overdrive progresses. An interesting phenomenon is the increase in the corresponding dTDP. The reverse trends between MR and dTDP over TD and overdrives strengthen the correlation between the two important HDI measures. The combination transition of MR and dTDP, provides another interesting point of view in contact definition. The increase in dTDP can partly result from the removal of moguls and partly from wear in the interface due to friction and impacts.

All the findings suggest a more complete picture: slider modulation can be affected by existing lubricant modulation (Pit's paper [35] showed the passive case, and here we can show the active case), and it can also create moguls on clean surfaces at contact locations. Only light-enough contacts can create moguls, and by the moguls' dimensions the interferences are reasoned to be not more than a few angstroms. Stronger contacts, say 5 mW TFC overdrives, can eliminate these moguls previous created. Together with the trend in TDP variation, it suggests that an increase in MR, and therefore the increase in the mogul's height, could reduce TDP, and vice versa. Since the MR can be related to the mogul development and mogul can inversely effect slider modulation, it is viewed as a reasonable root cause for the reduction of dTDP. The reduction of dTDP is sometimes called "negative burnishing" and was considered as an effect brought by lubricant transfer that reduces the head-disk spacing. However, this study provides another possible explanation for negative burnishing. In fact, lubricant transfer may increase the spacing after a prolonged park time on the ramp with a phenomenon called "lube creeping". When a slider is flying, lubricant transfer often accumulates on the deposit end (same surface for DTD dynamics measurement in chapter 3), which should not affect the flying height *in-situ* [60]. Unless interface contamination is introduced, mogul formation by contact is a more reasonable root cause for it.

5.5 Conclusions

This chapter provides an integrated view of HDI by carefully investigating the slider and lubricant modulations simultaneously, and by using methods developed in chapter 2 and 4.

The slider modulation observed on the LEC, which is a representative measure of the MR, has been shown to be highly correlated with lubricant modulation. Such modulation correlation is not merely a similarity in spectra or a positive correlation in undulation magnitude, but in a location-specific manner. Although the location-specific feature does suggest a slider modulation and induce mogul formation, the causality can only be investigated further by making discreet observations. Figs. 5.5.1-5.5.4 show the raw OSA images indicating contact-induced mogul formation over the four types of lubricant samples studied. There are distributed moguls on the lubricant surface, but only the moguls formed under the thermal protrusion area correspond to the slider modulation. The contact-induced moguls are in general longer than the ones formed under passive flying conditions.

So it is evident that slider modulation is capable of modifying the topography of the contact area, because TFC overdrives can annihilate the moguls. Based on this reasoning, moguls formed after touchdowns may be attributable to repeated touchdowns. This leads to a conclusion that slider modulation can cause the growth of moguls. On the other hand, the slider modulation is also found to be sensitive to existing moguls. This suggests that if a surface is perturbed, slider modulations can occur. In other words, slider and lubricant modulation are reciprocal causations.

Figure. 5.5.1 Raw OSA image showing touchdown induced mogul formation (middle) on a Z-Dol 9 Å sample. (top) Topography of passive flying at 11 minutes, (middle) approximately 30 touchdowns and (bottom) continuous contacts in 900 seconds. Touchdown-induced moguls are circled in read.

The reciprocal causation explains the difficulty in determining either the lubricant's effect or the slider's effect on proximity caused modulation in a HDI experiment. To determine the slider's effect in modulating the lubricant, the targeted surface area needs to be found first, and then the surface needs to be clean prior to having any touchdown. The lubricant's topography depends on the passive flying attitude of the slider, which introduces certain variables into this system. If a lubricant is perturbed too much prior to the touchdowns, the location-specific mogul formation process may not be observable. The effect of lubricant on slider modulation is trickier. It requires very few existing moguls be located on the contact track prior to touchdowns, and it may only be observed with the first slider's touchdown attempt.

It is also worth mentioning that the MR has been shown able to measure the minimum back-off spacing, and the results in section 5.3 suggest it is related to the growth of the mogul heights. The effect of lubricant types therefore can be partly viewed as a result of

the capability to suppress mogul formation. The behavior of the MR during TFC overdrives is also presented.

Figure. 5.5.2 Raw OSA image showing touchdown induced mogul formation on Z-Dol 15 Å sample. (top) Topography of passive flying at 11 minutes, (middle) approximately 30 touchdowns and (bottom) continuous contacts in 900 seconds. Note the sheared mogul formed due to contacts (circled in red) are different from the moguls form outside the thermal protrusion area.

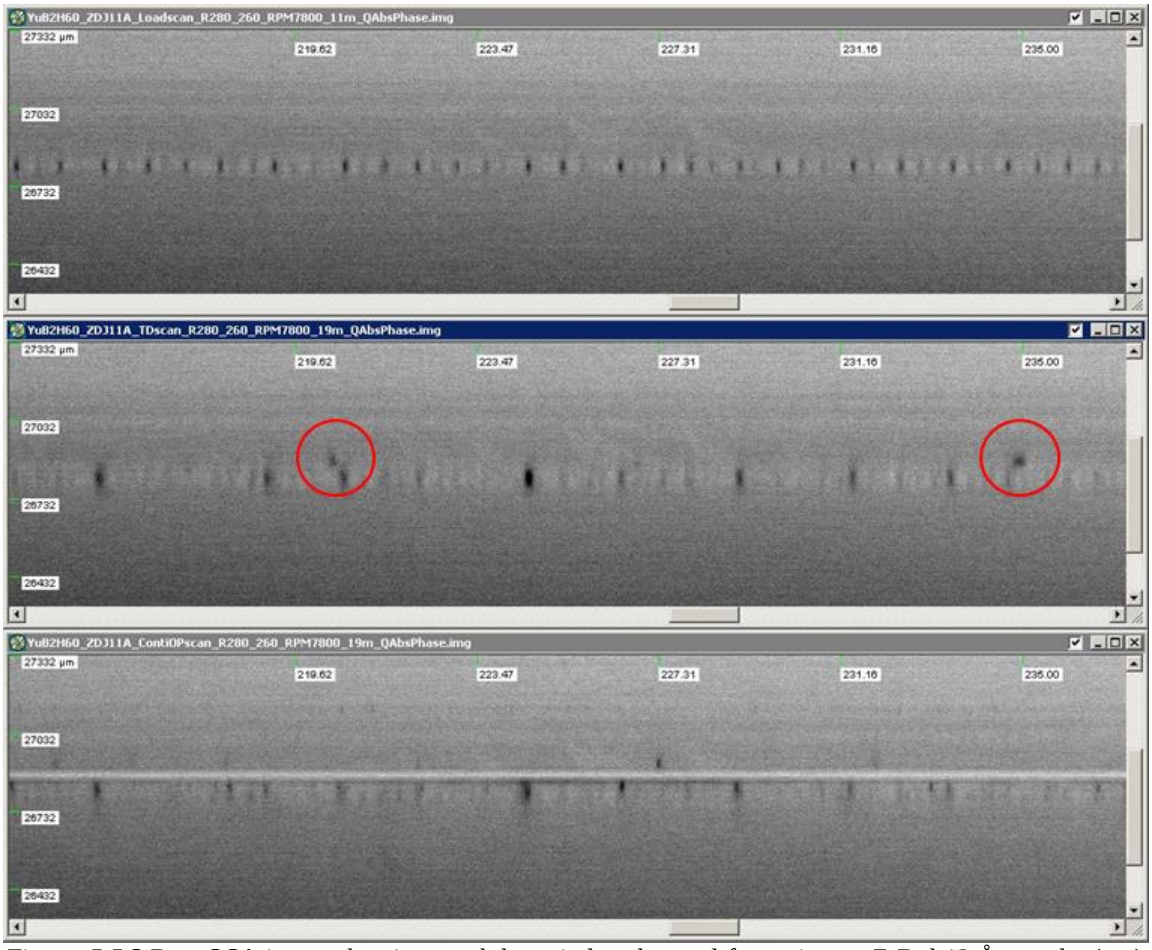

Figure. 5.5.3 Raw OSA image showing touchdown induced mogul formation on Z-Dol 12 Å sample. (top) Topography of passive flying at 11 minutes, (middle) approximately 30 touchdowns and (bottom) continuous contacts in 900 seconds. The contact-induced moguls' (circled in red) dimensions are different form the ones formed in passive flying.

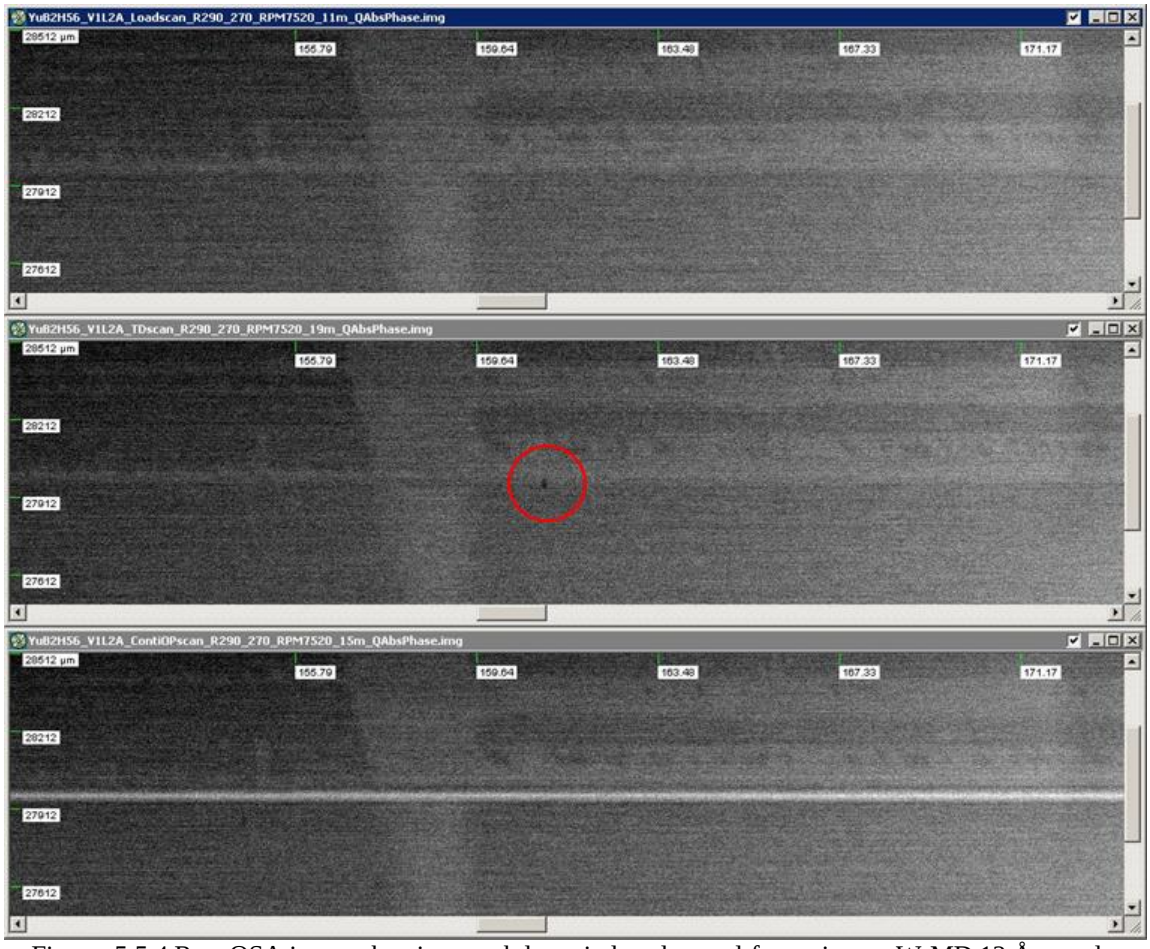

Figure. 5.5.4 Raw OSA image showing touchdown induced mogul formation on W-MD 12 Å sample. (top) Topography of passive flying at 11 minutes, (middle) approximately 30 touchdowns and (bottom) continuous contacts in 900 seconds. Contact-induced mogul (circled in read) is much smaller in area when compared to Z-Dol samples.

Chapter 6

Wear in the head-disk interface

With an accurate touchdown detection scheme and a reliable media design, the HDI should appear as contact-free and therefore wear-free. However, wear still exists in the HDI for various reasons. Statistically the reasons for wear come from the different failure modes, which include poor contact detection, particle contamination and material degradation. Under these unexpected operating conditions, the desired spacing may not be well-controlled and therefore head-disk contacts can be aggressive, and lead to interface material removal from the head or disk or both: i.e., wear. Despite the multiple sources of wear, it is important to understand the formation and evolution of wear and to develop methods for its evaluation. The typical depths of wear of interests are below 2 nm.

6.1 Introduction

In current HDDs, TFC technology has been introduced and applied to magnetic recording heads as a way to locally lower the flying height at the region of the read-write transducers to enhance data recording at the desired areal density. As the thermal protrusion area is brought below a certain flying height, instabilities can occur in the head-disk interface (HDI). In current HDDs the HDI is composed of a carbon coated air bearing surface (~3nm), a thin air gap (~2nm), and a smooth (roughness~0.2nm RMS) disk surface covered by a molecularly-thin (~1nm) PFPE lubricant deposited on an amorphous carbon overcoat. It is the extremely small mechanical spacing (air gap) at the scale of a few nanometers that introduces strong interactions in the HDI causing various undesired effects. The effects on the thin lubricant layers [31], [33], [34] caused by its deformation and transfer to the slider, on the air bearing slider instabilities [39], and on the head-disk contact dynamics [63] have been investigated both experimentally and theoretically. The instabilities that lead to the modulation of the disk lubricant layer, the flying height modulation of sliders, and the head-disk contacts can cause mechanical wear of the sliders. Recent studies used the scanning electron microscope (SEM) at low electron voltage to investigate the wear area [64], and the atomic force microscope (AFM) [40] or Auger Electron Spectroscopy (AES) [65] to quantify the amount of material removed.

However, the above-mentioned methods require specific instrumentations, and the measurements are rather time consuming. As suggested by the component level tribology studies, an in-situ wear measurement technique including the assessment of Angstrom-level wear resistance properties on PFPE lubricants is necessary for the understanding of lubricant performance. Recent publications employed the repeatability of the TDP that indicates the head-disk contact, as a measure of reliability of the HDI under various lubricated surfaces [66]. While several recent papers used the change in TDP as a measure of slider wear to explain the head-disk contact phenomenon, the wear regimes and the amount of wear still needs to be explicitly investigated [66, 67, 69]. In this study, a method based on TFC technology for in-situ monitoring of the carbon overcoat (COC) wear on the head is proposed, experimentally verified, and further applied to evaluate the wear resistance of the molecularly-thin PFPE lubricant layers composed of different molecular structures. The experimental results reveal that the amount of carbon overcoat wear is strongly affected by the lubricant's structure, and it is directly proportional to the change in TDP. The linear relationship holds for the different lubricants considered in this chapter, but the value of the linearity coefficient is lubricant-type dependent. The change in TDP can be used as a measure of carbon overcoat wear after the relationship has been calibrated for the specific head and media.

With the introduction of a recently developed sensor variously named thermal asperity sensor (TAS) [67], touchdown sensor (TDS) [68] or embedded contact sensor (ECS) [79], depending on terminology preferences, the definitions of touchdown may be updated with a consideration of thermal response of this sensor. While the temperature is usually the most direct output from TDS, in this chapter the concept of "thermal resistance (TR)" is used to provide insights in the condition of the HDI. It is suggested that using TR, the flying-height may be statically quantified and it is also sensitive to head wear. It is more advantageous than the firstly developed TDP measure in that the amount of head wear can be read out relatively far away from TDP, which can be a useful identification technology in reliability monitoring.

6.2 Wear development and estimation using TDP

As TDP can be used as a measure for slider-disk clearance, wear is usually suggested by an increase in TDP. However, such reasoning has seldom been documented, and papers related to this topic are rarely found. Sections 6.2.1-6.2.2 represent some research findings obtained as part of the projects done using facilities at Hitachi GST (now HGST, a WD company) during the author's summer Co-op, and section 6.2.3 presents the feasibility of using the same media but with different heads/stages in CML.

6.2.1 Experiments

Fig. 6.2.1.1 shows a schematic diagram of the experimental set-up used in this study. It consists of a spindle with disk mounting hardware, a head load-unload mechanism, an amplifier for AE signals, a TFC circuitry with its power source, and a computer used for spindle and actuator control as well as for data acquisition. The TFC power to the HGA is applied using the TFC power source. The head-disk contact is determined by using an AE sensor mounted on the arm actuator assembly on which the HGA is mounted.

AE sensors have been widely employed in component-level testing for head-disk contact detection. The detection criterion is usually determined by a rise in the RMS value of the AE signal that exceeds a certain threshold. Such AE threshold is used as an indicator of the head-disk contact. However, different AE thresholds are associated with different head-disk contact conditions. A higher AE threshold may result in late touchdown detection. In this chapter we study the wear of carbon overcoat on heads, thus it is essential to calibrate

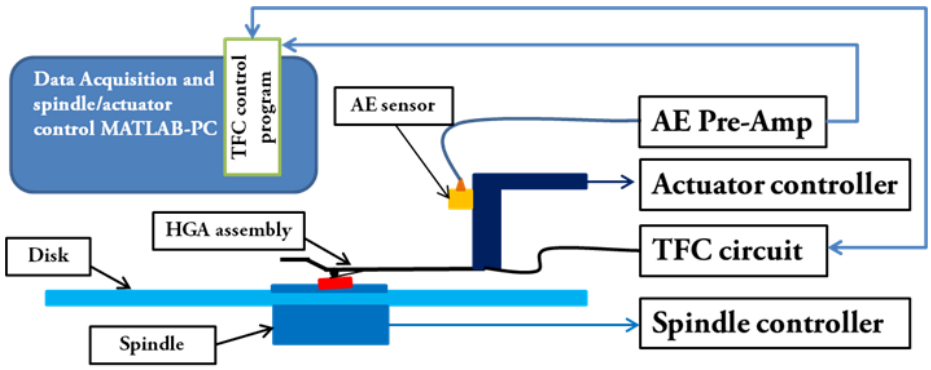

Figure. 6.2.1.1 Experiment set-up diagram

the AE threshold that corresponds to the onset of head wear. In order to calibrate the AE sensor threshold for contact detection, we repeated the TD cycles hundreds of times and the heads were analyzed for physical wear using AES [75]. It was confirmed that no detectable physical wear occurred on the head with zero TFC overdrive for repeated TD cycles at the chosen AE threshold, but head wear started to appear with positive TFC overdrive. Therefore, it was concluded that the TDP at the calibrated AE threshold indicates a slider-disk contact regime somewhere between the top lubricant surface and the disk carbon overcoat (COC). The repeated TFC overdrive experiments were performed at approximately 30% relative humidity and 25 degree Celsius.

After the AE baseline was established, we tested heads with various levels of head-disk interference beyond the TDP using a new head and disk component for each test. Each test involved 100 repeated TD cycles and the chosen overdrive TFC power was applied relative to the TDP of the previous TD cycle for 60 ms with 1 mW increment on each designated track. During each TD cycle, the TDP was updated based on the calibrated AE threshold.

Each slider sample was then examined by optical microscopy for lube pickup and by SEM and AES analysis for wear inspection. The disks were also analyzed using an Optical Surface Analyzer (OSA) for disk lubricant modulation, depletion and COC wear on the test track.

Disks coated with PFPE lubricants of two different molecular structures, used in current HDDs, were investigated for their effect on head wear rate as a function of TFC overdrive. One is ZTMD of 11 Å thickness and the other one is D-4OH of 12 Å thickness, the molecular structures of which that can be found in recent literature [51, 54]The bonding ratio for the ZTMD and D-4OH lubricated samples is approximately 80% and 70% respectively. In terms of their main chain classification, ZTMD is made from Fomblin-Z whereas D-4OH is made of Demnum [55]. However, in view of the polar bonding structures, ZTMD is a multidentate type lubricant whereas D-4OH is of tetraol type. ZTMD can also be viewed as a modified Z-Tetraol, the modification being an insertion of a hydrocarbon sector bearing several pendant (secondary) hydroxyl groups at the center of the molecular chain. The relevant difference between ZTMD and D-4OH is the presence/absence of the central hydrocarbon sector. Both ZTMD and D-4OH lubricants are important in HDD applications. It was explained that both a higher backbone stiffness (Demnum) and a multidentate (ZTMD of Fomblin-Z) main chain structure could achieve lower conformations of lubricants [55], therefore effectively increasing the slider-disk clearance. In this study, the main chain effects were believed to be less significant than the bonding mechanism as contact occurs. The ZTMD and D-4OH lubricants are referred to as lube A and lube B, respectively, in the following discussions.

6.2.2 Wear development and estimations

The degree of head-disk contact depends on the TFC overdrive, i.e., the power beyond touchdown. In the experiments we found that the range of overdrive from zero to 15mW delivers repeatable results on wear. For higher overdrives, the head-disk contacts became too strong for the purpose of wear study and the resulting prolonged contacts with strong vibrations could cause the surface condition to change significantly, and therefore cause the contact criterion set by the AE threshold to be altered. In general, it is inevitable that the lubricated surface condition (moguls, ripples and deformations) will be changed during head-disk contact experiments; however, the surface change can be controlled by restricting the contact durations. The contact durations of each slider in this study were no longer than tens of seconds, and certain non-contact periods between two successive overdrives were applied. It is worth nothing that the measurements revealed that the TFC-induced wear depths under such settings were all less than 10 Å, which is less than half of the typical thicknesses of the slider's COC [67]. The tested track on the disk showed no detectable signs of COC wear under OSA inspections. The same observation was reported in [70, 71], and the amounts of wear are expected to be much larger on non-lubricated disks [66, 69].

Fig. 6.2.2.1 shows the actual progression of change in the TDP on lube A, as a function of TD cycles. The change in TDP (dTDP) is plotted as the difference of TDP from the first

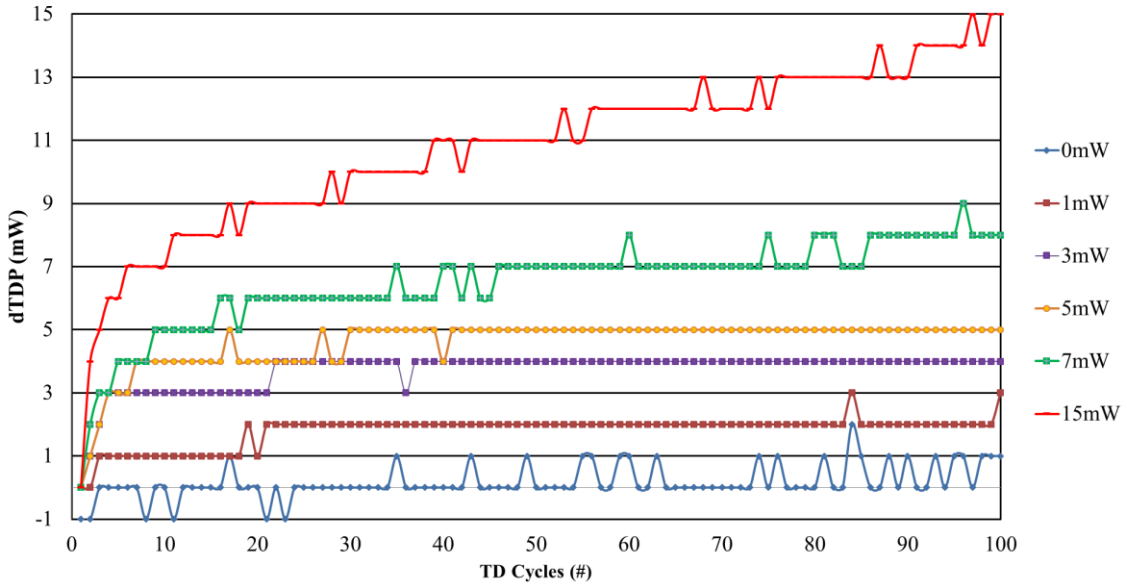

Figure. 6.2.2.1 dTDP as a function of TD cycle under different levels overdrive power.

TD cycle and the last TD cycle. It is observed that the maximum change in TDP at the end of 100 repeated touchdown cycles is least for the 0 mW overdrive case and most for the 15 mW overdrive case. It is also observed from Fig. 6.2.2.1 that for cases where the TFC overdrive was larger than 0 mW, the dTDP grows as the number of contact cycles increases. In all of the overdrive cases, dTDP increases rapidly with the first few TD cycles and then the increase is rather gradual. This is often referred as the "running-in" effect.

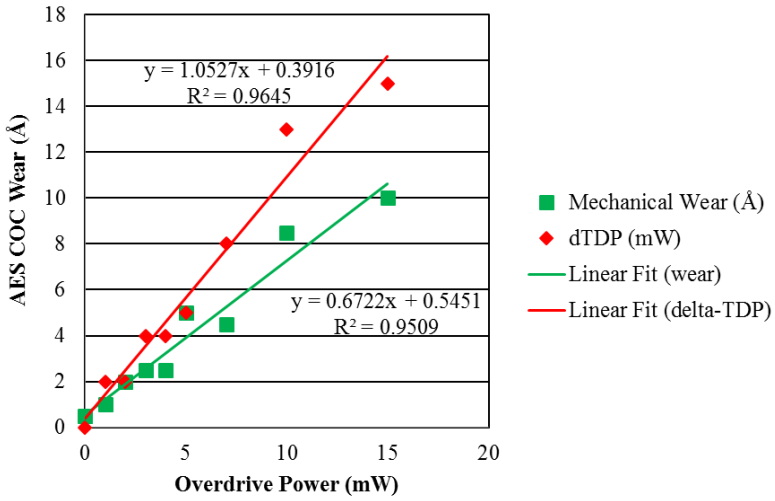

Figure. 6.2.2.2 AES COC wear and dTDP as a function of TFC overdrive.

Fig. 6.2.2.2 shows measured head COC wear using the AES technique, and the dTDP, as functions of the overdrive power from the Fig. 6.2.2.1 samples. From Fig. 6.2.2.2, we observe that almost no wear occurs when the interference level was at the TDP, corresponding to zero overdrive power. This confirms that at the calibrated AE threshold, the AE sensor detects the head-disk contact where there is least interference and no physical wear. It is also observed that both the dTDP and head COC wear are linear functions of the overdrive power, suggesting a linear relationship also holds between slider wear and dTDP. Therefore, the final change in TDP after 100 TD cycles was compared with the resulting AES COC wear measurement, and this relationship is shown in Fig. 6.2.2.3. Multiple such repeated experiments for the lube A showed that the wear-dTDP correlation is repeatable. This result suggests that the use the dTDP from such experiments is an effective predictor for angstrom-level wear, and by using it one can avoid having to carry out the tedious and time-consuming AES analysis. In order to further validate this proposed method, the same experimental procedure was implemented using lube B with the same TFC overdrive range and the same HGA design. The result was a similar linear correlation, as shown in Fig. 6.2.2.4. Since lube A and lube B were chosen to represent quite different lubricant structures, the similar linear relationship is believed to be applicable for head COC wear measurement among interfaces coated with different lubricants.

The linear relationship holds for lubricants with different backbone structures, and therefore we conclude that the dTDP approach can be used for good estimation of head COC wear. The actual progression of TDP in Fig. 6.2.2.1 can now be viewed as a wear evolution history. The head wear takes at least several seconds to reach the angstrom level, and the wear rate is affected by the amount of TFC overdrive. The contact travel distance (proportional to TD cycles) of the head affects the head COC wear depending on the TFC overdrives. For low TFC overdrives, the travel distance appears to affect wear only within the first 25 TD cycles, but it remains in effect for higher TFC overdrives up to 100 TD cycles. We therefore conclude that a combined effect of the increase in contact area due to COC wear tends to reduce contact pressure whereas contact force increases with increasing TFC overdrive.

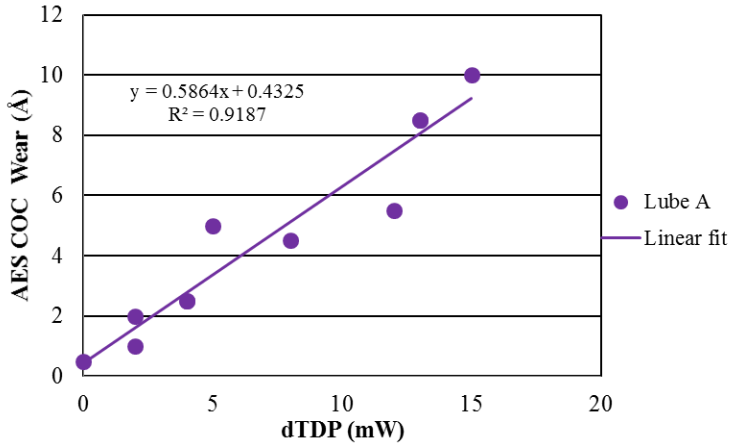

Figure. 6.2.2.3 AES COC wear as a function of dTDP.

The amount of head wear can thus be analyzed using the amount of dTDP as an indicator of the amount of head COC wear under different levels of interference powers, as shown in Fig. 6.2.2.4. From Fig. 6.2.2.4, we observe that the ratio between the amount of wear and interference level reveals the wear resistance performance of the two lubricants studied. The trends show that the ZTMD lubricant produces more carbon wear when the head is brought into contacts, compared with the D-4OH lubricant. The underlying reason could be the different structures that affect the bonding strength between the lubricant molecules and the COC on the disk surface. The ZTMD lubricant is known for having a low tendency to transfer from the disk to the slider, strong lube-disk bonding and higher lube durability in the HDI; however, this study shows that head COC wear can be an issue of reliability with ZTMD lubricated disks. In a recent review of lubricants for HDD applications, the lubricant properties such as viscosity and conformation were discussed together with lubricant stiffness and main chain flexibility [55]. It was demonstrated that the polar bonding-groups enhance the affinity between lubricant molecules and the disk COC, and therefore generate higher viscosity [72]. The ZTMD structure that anchors the main chain down to several confined shorter chains also allows a thinner molecule conformation that increases the effective head-lubricant clearance [54], and such confined main-chain structure provides better surface stability and less flexibility compared with all other non-multidentate type lubricants in the Fomblim-Z family [72]. Higher viscosity, stronger lubricant stiffness and less chain flexibility are desired properties in non-contact conditions. They contribute to a more stable surface that requires more shear force to perturb the lubricant, a less propensity to transfer or deform yet a faster recovery rate [55, 72]. Although more perturbation was observed on the D-4OH lubricant, which has less viscosity and stiffness in general, it showed a better head wear performance. Since in our

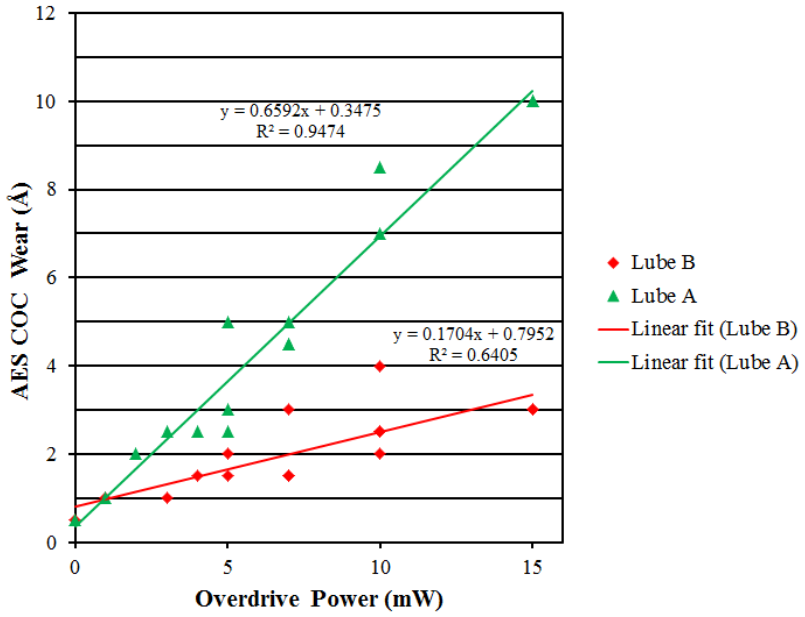

Figure. 6.2.2.4 Wear resistant performance of ZTMD lubricant (lube A) and D-4OH (lube B) lubricant under TFC overdrives. Multidentate lubricant induced more wear during slider-disk contacts

experiments the only significant difference is in lubricant samples, we surmise that the main reason for the differences in wear performance lies in the lubricant's structure, especially in the number and position of the polar bonding-groups. Another possible reason for D-4OH providing a better head wear performance may be its slightly higher propensity to transfer to the slider's surface reducing the head-disk contact strength. However, the protection mechanism by lubricant transfer requires more investigations [66], and in our study, the lubricant transfer after head-disk contacts shows no essential differences between the two lubricant types by the use of the optical microscope. When the head-disk spacing during read/write operations is lowered to less than 2 nm, intermittent contacts may occur either due to disk defects sticking out of the lubricant surface or head-disk spacing modulation due to slider dynamics. This in turn results in physical wear of the head COC during long term HDD operation making it a reliability concern. The choice of lubricant thus becomes critical from the HDI reliability standpoint.

The difference between lube A and lube B can be inferred using the AES COC wear and dTDP correlation, as shown in Fig. 6.2.2.5, where we observe that each dTDP step corresponds to approximately 0.53 Å carbon wear for lube A, but only 0.33 Å for lube B. For dTDP around 10 mW, the estimated difference between the two lubricants is approximately 2Å. We speculate that this difference comes from a slight difference in lubricant main chain flexibility. A more flexible main chain structure may allow the lubricant to locally deform more under the same air-bearing effects, which in turn provides more clearance for the TFC slider to compensate under the same amount of head COC wear. In this regard, lube B has higher main chain flexibility than lube A. The wear/dTDP ratio or wear rate can be used to estimate the expected COC loss for a given interference

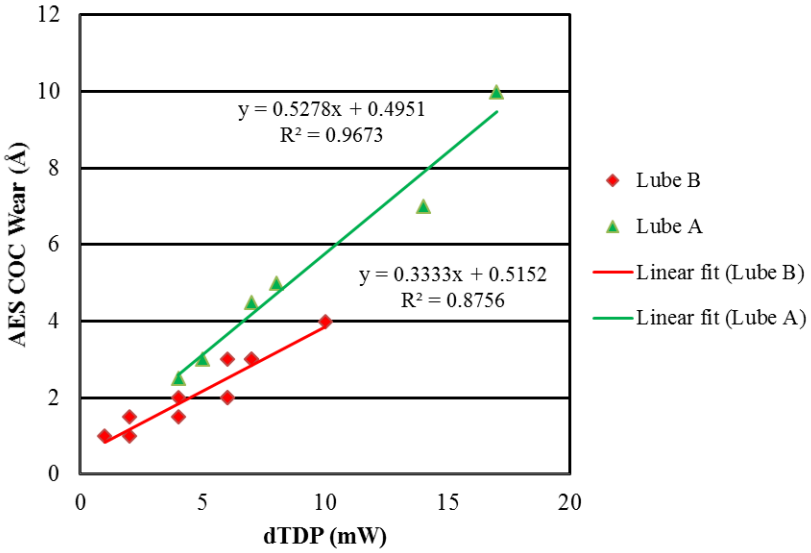

Figure. 6.2.2.5 Lubricant dependence on AES COC wear as a function of dTDP.

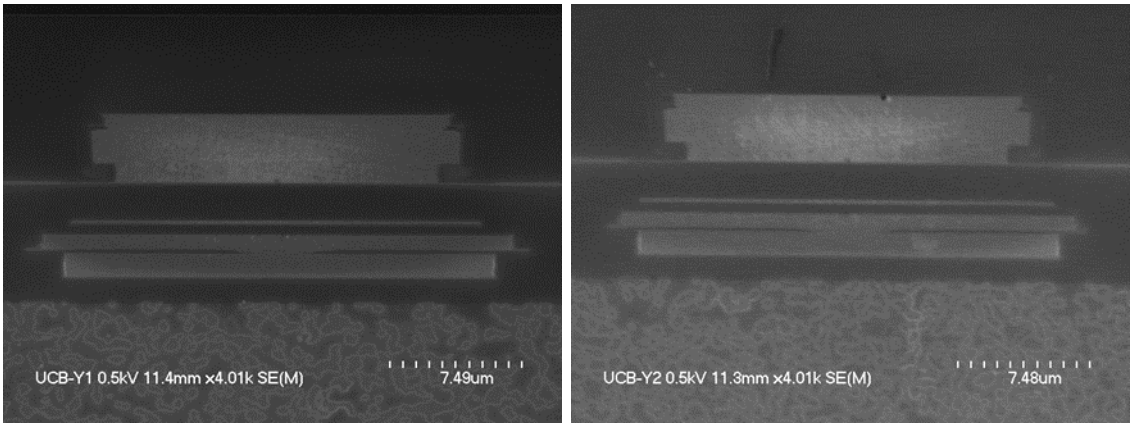

Figure. 6.2.3.1 HGA#1 wear under SEM inspections: (left) showing 10 mW TFC overdrives and (right) 20 mW TFC overdrives against Z-Tetraol lubricated surfaces. SEM images were credited to Kaynam Chun at WDC.

contact power for a particular lubricant type, which indicates that the lubricant structure affects both the HDI durability and the wear measurements using dTDP.

6.2.3 Comparative study at CML

A similar TFC overdrive scheme was adopted in CML on Z-Tetraol lubricated surfaces using both HGA#1 and HGA#2 for wear area inspections. It is shown that for different heater designs the geometry of writer pole and reader shields vary. However, the wear pattern is similar regardless of designs. As shown in Figs. 6.2.3.1 and 6.2.3.2, the worn area is mostly concentrated around the writer return pole. In the SEM images, the worn area appears to be lighter than its neighborhoods. In general a higher TFC overdrive level causes a larger wear zone. The wear zone provides a conservative estimation of contact area during slider-disk interactions. It is also worth noting that the SEM images were taken at a very low accelerating voltage of 0.5 kV to inspect surface contrasts that resulted from COC wear. COC wear is usually very shallow in depth and therefore a typical accelerating voltage level at 5 kV or higher will not work as it does for structural imaging in typical MEMS structures.

From the verification of using dTDP for wear measurement, and its dependency on lubricant types, it is reasonable to assume that as long as the media-lube combination is similar to ZTMD disks used here, the phenomenon should be transferrable to a different stage and different HGAs. In CML, a similar batch of ZTMD disks are used, and a similar wear development in terms of TDP evolution can be observed. The TDP-based wear measurement is assumed to be valid in CML results presented in section 6.3 by using the same type of media without a post verification using AES.

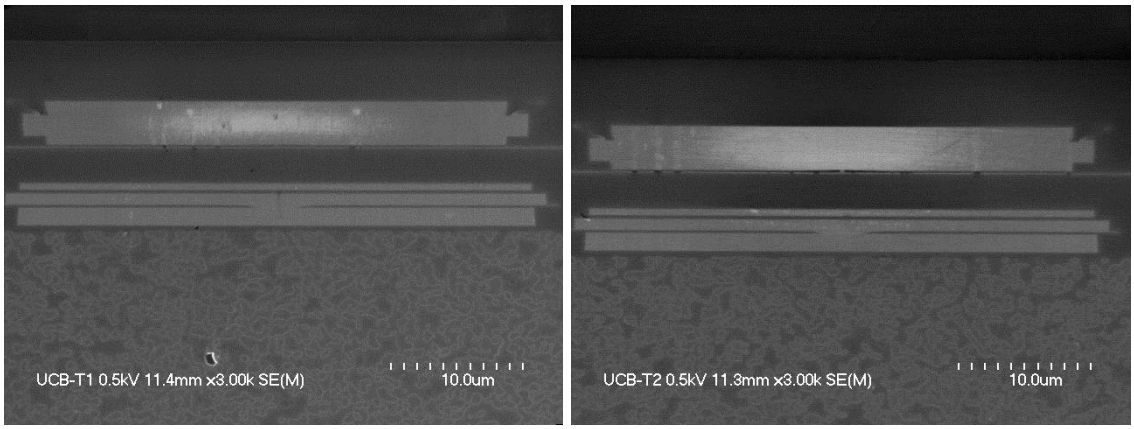

Figure. 6.2.3.2 HGA#2 wear under SEM inspections: (left) showing 10 mW TFC overdrives and (right) 20 mW TFC overdrives against Z-Tetraol lubricated surfaces. SEM images were credited to Kaynam Chun at WDC.

6.3 Wear estimations using Temperature Response

Although a wear estimation method has been established and validated using TDP, it is noted that a TD is required to estimate the amount of wear or spacing variation in drives. The necessity to gauge the wear or spacing increase in the HDI inevitably introduces a reliability concern, and in this section a new method is proposed to detect the spacing variation from the temperature distribution on the read-write region of the head. Approximately 5-6 years after TFC technology had been widely implemented in commercial HDDs, TDS started to appear for contact detection based on frictional heating. Most studies discussed how TDS detects contact and its correlation to AE sensor contact detection and defect type and size [78, 79, 80]. However, in this section it is discovered that TDS possesses the capability to estimate wear without repeating a contact event. This is achieved by not only studying the temperature data as a function of TFC power but also the interfacial resistance in HDI, or more precisely the "thermal resistance (TR)" between the head and fast rotating disk surface. The concept of thermal resistance [82, 84, 85, 87] is often used in characterizing thermal conductivity of thin-film materials by comparing the ratio between the amount of heat flux injected to the target and its resulting temperature distribution, which in turn reads the material's property in resisting heat flow. The heat transfer model was investigated for HDI in CML in 1997 [88], and it indicated the dominance of air conduction. Later studies advanced this concept with a more dedicated parametric modeling [90] for heat flux estimation. All the developed theoretical models suggest a dependence between heat flux and slider-disk spacing.

In the HDI, the thin-film material is the air gap, and the air gap is a function of TFC power. As the TFC power ramps up prior to reaching disk proximity, the temperature distribution

around the heater area rises due to the increasing heat flux. The TDS is located on the recessed surface between the writer poles, and is closer to the return pole. When the heater is energized, the disk contact first occurs on the most protruded area and is highly design dependent [75]. In this dissertation the wear being estimated should occur on the writer's return pole. The idea is illustrated as follows: when a portion of COC is worn by contacts, the mechanical spacing in the HDI increases from material loss. This material loss results in a higher flying height and therefore affects the temperature on the writer return pole. The writer return pole experiences a higher temperature due to an increase in thermal resistance by a thicker air gap. Because TDS is not on the worn surface, its flying height will not be directly affected but its temperature will be affected by that of the neighboring return pole. Therefore, the temperature of the TDS can be sensitive to the COC wear on the return pole.

Nonetheless, the temperature itself is a function of TFC power regardless of the existence of the air gap. Merely observing the temperature data may not be the best approach for wear estimation. The temperature of the TDS ultimately results from the competition between the amounts of transferrable heat flux and the supplied TFC power. The use of TR can potentially normalize the heating effect by TFC power and deliver the intrinsic heat conductivity as a function of air gap width. This idea will be validated via experiments on ZTMD lubricated surfaces.

6.3.1 Experiments

Experiments were performed on the same stage as that introduced in chapter 5 with proper instrumentation to accommodate the TDS measurement. TDS measurements are performed in two ways. One method is to provide the TDS with a constant current source at a current of 2.5 mA and monitor the voltage drop across the TDS for resistance measurement, which is proportional to the its temperature [80]. The other method is to customize a constant voltage source using a voltage regulator circuit and integrate the TDS into a Wheatstone bridge circuit. The output of the Wheatstone bridge is then amplified, and wired to the differential analog voltage inputs of the NI-6110. Both methods yield the same result but the latter presents a better noise control, so in this section the results obtained from the customized voltage source and bridge circuitry are presented. The increase in the resistance of the TDS with respect to the reading with zero TFC power, and TR is the ratio between the rise in resistance and TFC power. Disks lubricated with 10 Å and 80% bonded ZTMD were used in this experiment.

The TR curve as a function of TFC power is measured and averaged for 5-10 repeated TDs. Wear is introduced to the head by intentionally applying TFC overdrives at 10 mW for 25 cycles and a continuous contact at TFC overdrive of 50 mW for 120 seconds sequentially. Therefore, a total of three TR curves representing no wear, wear after 10 mW TFC overdrive cycles and 50 mW continuous TFC overdrives are obtained respectively. These TR curves are then compared with reference to the amount of wear as suggested from the TDP variation.

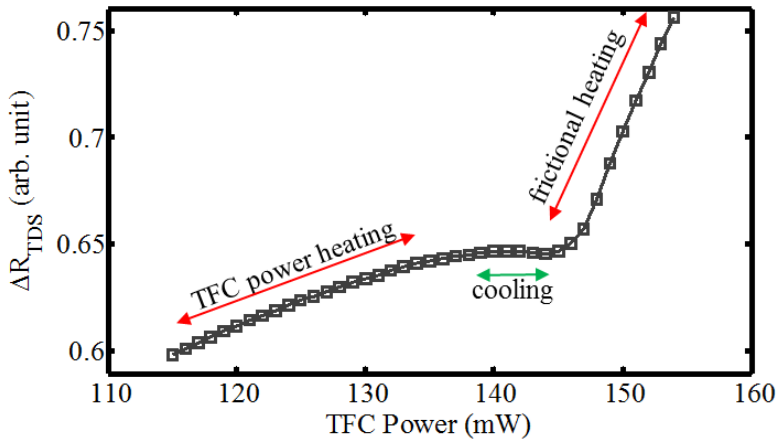

Figure. 6.3.2.1 Typical temperature response of TDS from flying to contact.

6.3.2 Wear estimation using the touchdown sensor

A typical TDS response is presented in Fig. 6.3.2.1. The temperature of the TDS keeps increasing as the TFC power ramps up, and the rate of temperature increase per mW slows down at contact proximity. The temperature of TDS rises again when the TFC power further increases. The temperature increase before TD is considered as the dominant effect of TFC power heating. The regime with a slowdown in temperature rise (some cases with a decrease in temperature [79]) is considered to be a strong air cooling that dominants over the TFC power heating [79, 80]. The rapid rise in temperature after the cooling regime is mostly attributed to frictional heating from engaged contact conditions.

While the transitions of the TDS as a function of TFC power seem to be a suitable characterization of HDI, its functionality is very similar to the method of AE for contact detection [67]. The TDS provides in-situ contact detection primarily based on heat that requires no external instrumentation, and it is very practical in drive-level integration.

In addition to just being an alternative to AE-based or LDV-based contact detection method, the TDS can estimate wear using TR. As shown in Fig. 6.3.2.2, when the TDS response is processed in terms of TR, TR monotonically decreases in the range from approximately below 50% TDP to TDP. Since TR is the ability to resist heat flow, a monotonically decrease in TR means the increase in heat conductivity. This trend is consistent with previously established models which suggest a heat flux increase with decreasing flying-height. The use of TR quantifies the heat transfer condition, which cannot be directly observed from temperature. It is worth noting that TR, which is calculated by dividing the temperature rise by the supplied TFC power, includes the heat dissipations in all directions. However, the use of TR can still give a good estimation for the “cooling” effect from HDI by reasoning that the heat transfer is mainly channeled through the air gap [91].

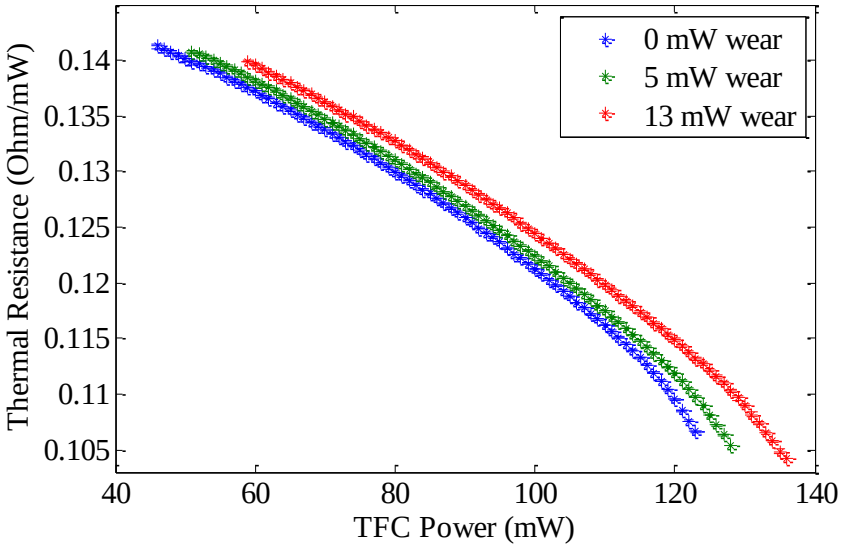

Figure. 6.3.2.2 Representative TR curves as functions of TFC powers up to TDP with different amounts of wear

Further, from Fig. 6.3.2.2, it is seen that TR curves evaluated at different amounts of wear levels are separated from each other. At the same TFC power, the same head with 13 mW wear has a higher TR than with 5 mW wear, which has higher TR than with zero wear. It simply reflects the temperature increase as a result of decrease in thermal conductivity from head-disk spacing increase by mechanical wear. In addition to the vertical separation in TR

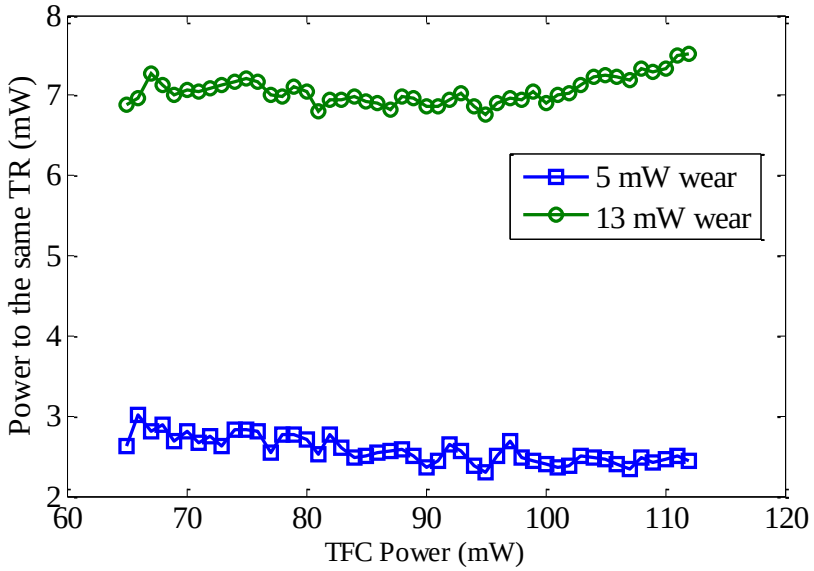

Figure. 6.3.2.3 PtTR and wear readings from dTDP

at the same TFC power, a separation in TFC power at the same TR could also be observed. In Fig. 6.3.2.3, the horizontal separation is designated as “power to the same TR (PtTR)” from approximately 60% TDP to 90% TDP. Literally, PtTR measures the additional TFC power required to reach the same TR on the worn head with reference to the zero wear TR curve at each power step. The separations are therefore measured in PtTR in the units of mW and are found to be almost constants over the power steps being analyzed. A constant horizontal separation means a mechanical wear on the head COC is equivalent to a right shift in the TR curve. A total of seven HGAs were used to examine this method and the results are shown in Fig. 6.3.2.4. In Fig. 6.3.2.4 the mean, minimum and maximum value of PtTR from approximately 60% TDP to 90% TDP of each HGA are plotted as a function of each corresponding wear level. Good linear correlations are obtained from all the mean, minimum and maximum PtTR values with respect to dTDP. It is worth noting that the similarity in linear coefficients among the mean, minimum and maximum values represents the consistency of PtTR over the 60%TDP to 90%TDP range. From section 6.2 and the linear correlation between PtTR and dTDP here, it is concluded that PtTR can provide an effective wear estimation. The results imply that an estimation at 60% TDP will be sufficient and no contact is required for wear evaluation.

The use of PtTR provides an efficient methodology for wear estimation without going into contacts, and is fundamentally different from the AE-based and LDV-based methods. The methods associated with oscillations cannot be used to tell flying height variation from a large TFC power back off. However, TR, can distinguish heat transfer condition variations from one power step to another. This is particularly useful for contact proximity sensing prior to the lightest perturbation that could be captured by AE or LDV. Both AE and LDV are blind to spacing variations before the TFC power reaches the MR, and MR is expected to be small on a thin and multidentate lubricated surface. The use of TR, considering its in-situ capability and its sensitivity to spacing variations, may be important to the reliability for next generation HDI.

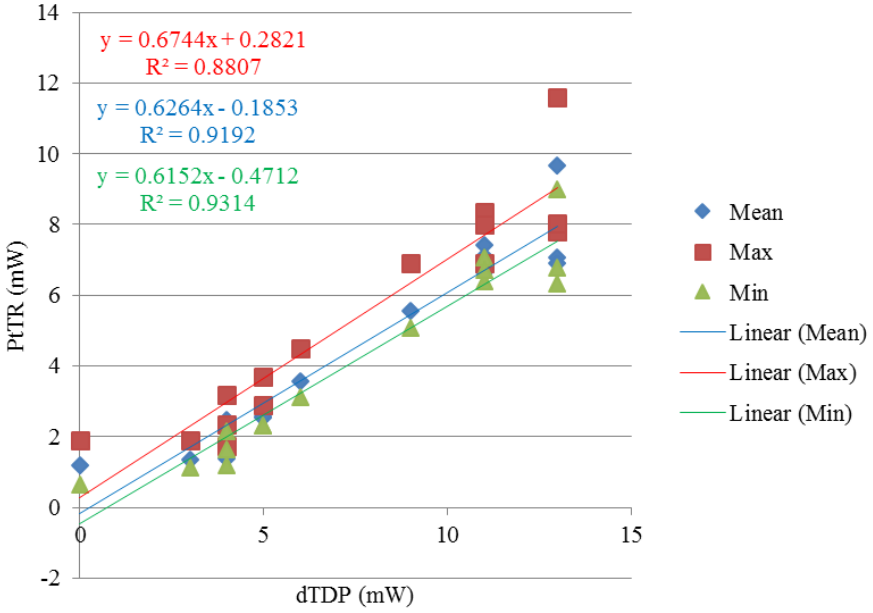

Figure. 6.3.2.4 PtTR and dTDP correlation

6.4 Limiations on the use of TR and dTDP for wear estimation

The use of dTDP for wear measurement is basically achieved by gauging the additional mechanical spacing required to reach contact. The method of dTDP for wear estimation thus requires a very stable lubricant surface. The good dTDP-wear correlations are obtained on ZTMD and D-4OH, and both the multidentate and Demnum types of lubricants are known for superior surface stability under air bearing pressure fields.

For a less stable surface with a thicker lubricant layer or less polar-end groups, the surface topography is more prone to change when contact occurs. As suggested in chapter 5, moguls can form under both passive flying conditions and repetitive contacts, and the formation of moguls can affect the contact characteristics and therefore the TDP. When a TDP is altered by lubricant topography modification, dTDP inevitably includes the mogul's effect. In chapters 4 and 5, the physical meaning and evolution of MR and dTDP has shown a dependency on mogul formation, which is itself highly lubricant dependent. The method of dTDP is limited to calibrated and modulation-resistant lubricant surfaces. It is expected that dTDP will be less accurate on lubricants with more mobility.

TR, however, represents a complement for the use of dTDP. TR requires no oscillation and is sensitive to spacing variation as TFC power ramps up. The use of PtTR quantifies the TR curves separated by wear but requires an assumption: that the TR in the HDI depends

only on head-disk spacing but due to material loss. The dependency on head-disk spacing, which is equivalent to the thickness of the air gap, can be reasoned by assuming that the heat transfer mechanism is mostly affected by air conduction at disk proximity; however the loss of COC could potentially reduce the amount of TR. In general the thermal conductivity is of orders higher for DLC than air [92], so the TR contributed by COC could be negligible when the air gap is on the order of a few nm, which is comparable to the thickness of COC. However, when the TR is evaluated at disk proximity, the contribution of COC may play a role. When wear thins the COC, at the same flying height, the TR should be slightly smaller due to a better conduction condition from the view of TDS. Therefore, TR may be subjected to changes due to wear when the head is at disk proximity. This may be one of the possible reasons why the separations between TR curves "spread out" towards TDP as shown in Fig. 6.3.2.2. However, the region 60% TDP-90% TDP works well for this assumption.

As a recapitulation, TR is derived from TDS whose neighborhood may not directly contact the surface neither worn by contacts. The effectiveness of TDS for sensing wear in the HDI is most likely due to internal head conduction through the worn area as an updated heat transfer boundary condition. Therefore, the location and size of the TDS and the internal structure of heads are all design variables that can seriously affect the use of TR from one design to another. Nevertheless, this section demonstrated the possibility of utilizing the concept of TR for sensing wear without the necessity of performing contacts.

Chapter 7

Conclusions and Future Research Directions

This dissertation investigates slider-disk interactions with focus on proximity detection, lubricant modulation and wear. While the three topics seem quite independent, the connection between the methods used in each subject are intertwined and highly cross-referenced. Proximity detection is surface dependent and therefore highly affected by lubricant topography. Not surprisingly lubricant modulation is also sensitive to the slider's behavior. Head wear highlights the proper use of contact reference and temperature response. From all the information regarding slider dynamics, lubricant modulation and wear the understanding of contact mechanisms in the HDI advances.

7.1 Summary

In this dissertation, several definitions of contacts in the HDI can be readily derived, and they possess distinct perspectives. Focusing on the characterization and dynamical behavior of the HDI at contact proximity is of both academic interest and industrial need.

The slider-disk interaction is elucidated at contact proximity using AE, LDV and OSA simultaneously. The close inspection using LDV discloses the subtle transition in slider dynamics from flying to the onset of contact. The head-disk contact is observed to be initiated by in-plane excitations and the conventional measurement preference on the TEC sacrifices the sensitivity to it. However, from the HGA's configuration, the in-plane excitation can also be observed vertically on the LEC, and the use of the LEC instead of DTD greatly increased the accessibility to proximity oscillations in component-level testing. It is further found that the in-plane excitation evolves within a range of a few TFC power steps towards touchdown, after which the trend of the LEC and TEC modulation becomes altered. The distinct switch from the LEC dominant mode to the TEC dominance is a unique way to view touchdown. The TFC power regime where the LEC dominates the slider's modulation is defined as the MR and is proved to be important in contact characterization.

The MR is the mechanical spacing range between contact and the initiation of the slider's LEC/DTD modulation, and it is lubricant dependent. It depends on the lubricant thickness and effective bonding end-groups. The MR also represents the minimum stable back-off spacing, which is a measure that differs from the overall clearance when the slider flies passively. However, the genesis of the MR was not clear until the detailed study on the lubricant surface was conducted.

Lubricant modulations under slider-disk contacts are investigated followed by TFC overdrive schemes that allow an in-situ positioning of the thermal protrusion area against the disk surface. While moguls do form and were reported to be a cause for slider modulation, their behavior at contact proximity was unclear and were poorly understood. In this dissertation, for the first time, a direct evidence of reciprocal causality between the slider's modulation and mogul formation at contact proximity is found. The slider modulation at contact proximity matches the location of mogul formation under the thermal protrusion area. This finding is important in that it implies the DTD/LEC modulation is associated with the moguls' formation that is caused by a certain shear. The MR turns out to be self-explanatory after the mogul-modulation correlation is established. Lubricant and slider modulation correlation is further enhanced by repetitive TFC overdrives among lubricant designs. The behavior of the MR and the lubricant surface, becomes another way to look at slider-disk contact.

Two techniques in head wear estimation are proposed and verified. The method of TDP requires head-disk contacts and a stable lubricant surface under light contacts, and the method of TR has the potential to gauge wear at a large back-off power, and it can be less sensitive to lubricant modulation at a higher flying heights. However, the use of TR is not directly a measure of mechanical spacing but it is inferred through the associated heat transfer condition and temperature field. Therefore the use of TR is sensitive to the design parameters such as location, geometry and material.

In summary, this dissertation explores the physics of HDI contact proximity, and it advances the knowledge of the subtle head-disk contact phenomena from both slider dynamics, lubricant modulation and wear prior to fully engaged contacts being established.

7.2 Future Research Directions

The successful implementation of the TDS is now at a similar development phase as TFC technology 10 years ago. The research related to TFC technology is reaching a more mature stage and the application and understanding of TDS is burgeoning. TDS involves many thermal aspects of nanoscale heat transfer and could be highly relevant to the success of a reliable HAMR HDI. The perturbation-based contact detection technology is restricted to establishing contacts as *a priori* and could be controversial in the ultimate detection scheme, requiring an extremely sensitive contact detection method with an extremely stable HDI.

The desire for stability rules out the tolerance for modulation and the only way to reach this goal is to utilize DC-based methods. TR is one of the pioneering ways of looking at the property of HDI, and it is believed that TDS can proceed further towards a better understanding of heat transfer between two fast rotating surfaces.

7.2.1 Heat transfer modeling in the HDI with TDS support

The theoretical modeling for heat transfer in the HDI has been well developed in CML [89, 90.]. The thermomechanical analysis established in CML has been successfully applied to the prediction of thermal protrusion and flying height [76]. However, the validation of the predicted temperature field has always been challenging. The temperature field can be quantified by the resistance change of the reader [84, 85, 86] but it is not very practical in most component-level studies. In addition, the readers are not typically designed to be the lowest flying area, and so its sensitivity could be affected.

With the introduction of TDS which is solely designed for temperature sensing, the temperature field can be at least verified for the neighborhood of the TDS. A direct temperature reading from resistance change can be used to verify the existing heat transfer models at spacing below 5 nm together with TFC technology. If a slider can position the head stability below 5 nm, TDS can be used as an excellent probe for heat transfer studies over fast rotating substrates. This can provide a unique system and tool for heat transfer study that a typical AFM cannot replace. The near-field heat transfer under well controlled spacing over a fast rotating substrate can potentially be a good research topic.

7.2.2 Wear resistant HDI

Although wear is not expected to occur during normal HDD operations, it is nevertheless one of the major reasons for failure. To prevent wear, certain methods have been strategically adopted in commercial HDDs. For example, the COC is applied to both the head and disk surface for collision and corrosion protection, and PFPE lubricants are coated on the disk COC layer to mitigate contacts and lower the surface energy [93]. However, when contact occurs wear is still inevitable. The Head COC is more vulnerable to wear than the disk COC, and interestingly multidentate lubricants are more prone to cause wear than other types of lubricants. The coexistence of wear and lubricant is not uncommon in a sub-boundary lubricated interface like the HDI, but the mechanism that allows wear to develop is still not well understood. Compared to the rather well studied molecularly-thin lubricants' kinetics at slow shear/scanning rates [94, 95, 96], the behavior under high-speed impacts may be an unknown key to the wear formation with lubricant coatings [97]. This suggests that further efforts should be made for wear reduction such as reducing the shearing force that a lubricant layer can exert on the head [98]. In fact, the mechanism of wear is still under development, and it is found to involve not only mechanics but also chemical reactions [99]. The thickness of any coating layer in the HDI is only a few nanometers and the atomic-level amount of material removal is critical for HDI reliability as well as understanding the tribology fundamentals.

7.2.3 Contact-stable HDI design

Until now the slider-disk contacts are detected using perturbations. On sliders the AE, LDV, friction force and TDS are used and the counterpart on the disk is the lubricant modulation. However, as suggested in chapters 4 and 5 the more stable the lubricant, the less the perturbation can be detected on both the head and disk surface. This leads to a stringent contact detection tolerance if the detection scheme is still perturbation-based. Ultimately both the sensitivity and stability at contacts are to be maximized, and this idea rules out the perturbation-based detection scheme. In fact, the TDS may be able to provide good sensitivity to proximity by the use of TR without perturbations. However, even with TR a good reference is required for contact. How to define a good contact reference without mechanical oscillation is the key to the next generation HDI.

It is important to point out that, in a HAMR HDI, the laser-induced protrusion is much smaller than the TFC thermal bulge [100]. The mechanical vibration may not be picked up for current contact detection schemes prior to the sacrifice of the miniature laser-induced contact area.

Bibliography

1. H. Jost, “Tribology—origin and future,” *Wear* 136, pp. 1–17 (1990).
2. Marchon, B., Pitchford, T., Hsia, Y.-T. and Gangopadhyay, S.,”The head-disk interface roadmap to an areal density of 4 Tbit/in^2,” *Adv. Tribol*. vol. 2013, pp. 521086-1–521086-8, Feb. 2013.
3. IBM Archives, “IBM 350 disk storage unit,” Online: http://www-03.ibm.com/ibm/history/exhibits/storage/storage_350.html.
4. IBM Archives, “IBM 3340 direct access storage facility,” Online: http://www-03.ibm.com/ibm/history/exhibits/storage/storage_3340.html.
5. M. N. Baibich, J. M. Broto, A. Fert, F. Nguyen Van Dau, F. Petroff, P. Etienne, G. Creuzet, A. Friederich, and J. Chazelas, “Giant magnetoresistance of (001)Fe/(001)Cr magnetic superlattices,” *Phys. Rev. Lett*., vol. 61, 2472, 1988.
6. A. Chiu, I. Croll, D. E. Heim, R. E. Jones, P. Kasiraj, K. B. Klaassen, C. D. Mee, R. and G. Simmons, “Thin-film inductive heads,” *IBM. J. Research and Development*, vol 40, pp. 283-300, 1996.
7. C. Tsang, T. Lin, S. MacDonald, M. Pinarbasi, N. Robertson, H. Santini, M. Doerner, T. Reith, L. Vo, T. Diola and P. Arnett, “5 Gb/in^2 recording demonstration with conventional AMR dual element heads and thin film disks,”*IEEE Trans. Magn*., vol. 33, no. 5, pp. 2866–2871, Sept. 1997.
8. T. Albrecht, D. Bedau, E. Dobisz, H. Gao, M. Grobis, O. Hellwig, D. Kercher, J. Lille, E. Marinero, K. Patel, R. Ruiz, M. Schabes, L. Wan, D. Weller and T.-W. Wu, “Bit Patterned Media at 1 Tdot/in^2 and beyond,” *IEEE Trans. Magn.*, vol. 49, no. 2, pp. 773–778, Feb. 2013
9. R. Wood et al., “The feasibility of magnetic recording at 10 terabits per square inch on conventional media,” *IEEE Trans. Magn.*, vol. 45, no. 2, pp. 917–923, Feb. 2009.
10. R. Rottmeyer et al., “Heat-assisted magnetic recording,” *IEEE Trans. Magn.*, vol. 42, no. 10, pp. 2417–2421, Oct. 2006.
11. HGST, a WD company, “Perpendicular magnetic recording technology,” HGST White Paper, Nov. (2007).
12. Qinghua Zeng, Brian H. Thornton, David B. Bogy, and C. Singh Bhatia, “Flyability and flying height modulation measurement of sliders with sub-10 nm flying heights,” IEEE Trans. Magn., 37, 894 (2001).
13. M. R. Kazemi, “Suspension assembly for hard disk drive,”, *Encyclopedia of Tribology, Springer*, pp. 3514-3519, 2013.

14. D. Meyer, Z.-E. Boutaghou and B. Wei, "Proximity recording-The concept of self-adjusting fly heights", *IEEE Trans. Magn.*, 33, 912 (1997).

15. DW Meyer, PE Kupinski, and JC Liu. "Slider with temperature responsive transducer positioning", *United States Patent 5991113*, 1999

16. J. Zheng and D. B. Bogy, "Dynamic instability of thermal-flying-height-control sliders at touchdown", *Microsyst. Technol.*, vol. 18, 9-10, pp.1319-1322, Sept. 2012.

17. R.P. Ambekar, V.Gupta and D.B. Bogy, "Experimental and numerical investigation of the dynamic instability in the head-disk interface at proximity," *ASME J. Tribol*., vol. 127, no. 3, pp. 530-36, July 2005

18. Steven W. Meeks, Walter E. Weresin and Hai J. Rosen. "Optical Surface Analysis of the Head-Disk-Interface of Thin Film Disks", *Journal of Tribology*, 117, 112-118, 1995.

19. T. Cheng, B. Zhao, J. Chao, S. Meeks and V. Velidandea, "The lubricant migration rate on the head disk surface", *Tribol. Lett*., vol. 9, no.3-4, pp. 181-185, 2000.

20. Sripathi Vangipuram Canchi, *Thermal Fly-height Control Slider Dynamics and Slider-Lubricant Interactions in Hard Disk Drives*, Ph. D. dissertation, Department of Mechanical Engineering, University of California, Berkeley, California, USA, 2011

21. B. Knigge, T. Suthar and P. Baumgart, "Friction, heat and slider dynamics during thermal protrusion touchdown", *IEEE Trans. Magn*., 42, pp. 2510-2512 (2006).

22. Rohit Pradeep Ambekar, *Dynamic Stability and Slider-Lubricant Interactions In Hard- Disk Drives*, Ph. D. dissertation, Department of Mechanical Engineering, University of California, Berkeley, California, USA, 2007

23. A. Vakis, S. Lee and A. Polycarpou, "Dynamic head-disk interface instabilities with friction for light contact (surfing) recording", *IEEE Trans. Magn.*, 45, 4966–4971, 2009

24. D. Chen and D. B. Bogy, "Numerical Investigation of bouncing vibrations of an air bearing slider in near or partial contact", *J. Tribol.*, 132, 011901, 2009

25. Wei Hua, Bo Liu, Shengkai Yu and Weidong Zhou, "Nanoscale roughness contact in a slider–disk interface", *Nanotechnology* **20**, 285710 (2009)

26. A. Vakis and A. Polycarpou, "Head-disk interface nanotribology for Tbit/inch^2 recording densities: near contact and contact recording", *J. Phys. D: Appl. Phys*. **43** , 225301 (2010)

27. B Liu, MS Zhang, SK Yu, WHua, YS Ma, WD Zhou, L Gonzaga, and YJ Man. Lube-surfing recording and its feasibility. *IEEE Trans. Magn.*, 45, 899–904, 2009

28. L. V. Gonzaga, B. Liu, S. Yu, W. Hua and W. Zhou, "Slider design optimization for lube-surfing head-disk interface scheme", *IEEE Trans. Magn.*, 46, 1922–1924, 2010

29. H. Tani, T. Yamaguchi and N. Tagawa "Experimental study of head-disk interface instability on light contact recording using dynamic flying height control", *IEEE Trans. Magn.*, vol. 47, no. 1, pp.117 -123 2011

30. Qinghua Zeng, Chao-hui Yang, Soramany Ka, and Ellis Cha, "An experimental and simulation study of touchdown dynamics", *IEEE Trans. on Magn.*, 47, 3433-3436, 2011.

31. N. Li, Y. Meng and D. B. Bogy, "Experimental study of the slider-lube/disk contact state and its effect on head-disk interface stability", *IEEE Trans. on Magn.*, 48, 2385-2391, 2012.

32. G. W. Tyndall and R. J. Waltman, "Strucure of molecularly-thin perfluoropolyether films on amorphous carbon surfaces", MRS Proc., vol. 517, pp.403-414. 1998

33. R. Ambekar, D. B. Bogy, Q. Dai, and B. Marchon, "Critical clearance and lubricant instability at the head-disk interface of a disk drive," *Appl. Phys. Lett.*, vol. 92, 033104, 2008.

34. R. Pit, B. Marchon, S. Meeks, and V. Velidandla, "Formation of lubricant "moguls" at the head/disk interface," *Tribol. Lett.*, vol. 10, no. 3, pp. 133-142, Mar. 2001

35. R. Pit, Q. Zeng, Q. Dai, and B. Marchon, "Experimental study of lubricant-slider interactions," *IEEE Trans. Magn.*, vol. 39, no. 2, pp. 740-742, Mar. 2003.

36. B. J. Cox and D. B. Bogy, "The CML Air Bearing Design program (CMLAir), Version 7 User Manual," University of California at Berkeley, 2007.

37. Q. Zeng and D. B. Bogy, "The CML slider-air bearing parameter identification program," *CML Blue Report*, University of California at Berkeley, 1997.

38. S. Canchi and D.B. Bogy, "Slider dynamics in the lubricant-contact regime," *IEEE Trans. Magn.*, vol. 46, no.3, pp.764 –769, Mar. 2010.

39. Y. Chen, J. Zheng, and D. B. Bogy, "Light contact and surfing state dynamics of air bearing sliders in hard disk drives," *Appl. Phys. Lett.*, vol. 100, 243104, 2012.

40. L. Su, Y. Hu, E. Lam, P. Li, R. Ng, D. Liang, O. Zheng, H. Liu, Z. Deng and J. Zhang, "Tribological and dynamic study of head disk interface at sub-1-nm clearance," *IEEE Trans. Magn.*, vol. 47, no. 1, pp. 111-116, Mar. 2011.

41. Y. Shimizu, J. Xu, H. Kohira, M. Kurita, T. Shiramatsu, and M. Furukawa, "Nano-scale defect mapping on a magnetic disk surface using a contact sensor," *IEEE Trans. Magn.*, vol. 47, no. 10, pp. 3426-3432, Oct. 2011.

42. W. Song, L. Matthes, A. Ovcharenko, B. Knigge, F. E. Talke, "Experimental study of slider dynamics induced by contacts with disk asperities", *Microsyst. Technol.*, June 2013.

43. Q. H. Zeng and D. B. Bogy, "Dynamics of suspension–slider–air-bearing systems: experimental study", *IEEE Trans. Magn.*, vol.3, no. 3, pp. 210-217, Sept. 1998.

44. Q. H. Zeng and D. B. Bogy, "Experimental evaluation of stiffness and damping of the slider-air bearing in hard disk drives", *ASME J Tribol.*, vol.121, pp. 102-107, 1999.

45. Q. H. Zeng, L. S. Chen and D. B. Bogy, "A model analysis for slider air bearing in hard disk drives", *IEEE Trans. Magn.*, vol.33, pp. 102-107, 1997

46. Y. Wang, X. Jin, S. Chen, X. Wei and K. Tsui, "Effect of low-frequency vibration in Z-direction (Out-of-plane) on slider dynamics," *IEEE Trans. Magn.,* 2013 doi:10.1109/TMAG.2013.2252359

47. R. Ambekar, L. Zheng, J. Lee and D. B. Bogy, "Effects of radial and circumferential disk features on slider dynamics," *IEEE Trans. Magn*., vol. 45, no. 1, pp. 206-211, Jan. 2009.

48. J. Zheng and D. B. Bogy, "A numerical investigation of different touchdown patterns of thermal-flying-height-control sliders," *Microsyst. Technol.,* June 2013. doi 00542-013-1823-y

49. J. Zheng and D. B. Bogy, "Numerical Simulation of Touchdown Dynamics of Thermal Flying-Height Control Sliders," *IEEE Trans. Magn.,* vol. 48, no. 9, pp. 2415-2420, Sept. 2012.

50. K. Ono, "Replenishment speed of depleted scar in submonolayer lubricant", *Tribol. Lett.,* vol. 52, no. 2, pp. 195-203, Nov. 2013

51. Li, N., Meng, Y., Bogy, D. B. "Effects of PFPE lubricant properties on the critical clearance and rate of the lubricant transfer from disk surface to slider," Tribol. Lett. 43, 275–286 (2011).

52. B. Marchon, Q. Dai, V. Nayak and R. Pit, "The physics of disk lubricant in the continuum picture", *IEEE Trans. Magn.,* vol. 41, no. 2, pp. 616-620, Feb. 2005.

53. B. Marchon, Q. Dai, B. Knigge and R. Pit, "Lubricant dynamics in the sub-nanometer clearance regime", *IEEE Trans. Magn.*, vol. 43, no. 9, pp. 3694-3698, Sept. 2007.

54. Guo, X. C., Knigge, B., Marchon, B., Waltman, R.J., Carter, M. and Burns, J. "Multidentate functionalized lubricant for ultralow head/disk spacing in a disk drive," *J. Appl. Phys.* 100, 044306 (2006)

55. Marchon, B. "Lubricant design attributes for subnanometer head-disk clearance," *IEEE Trans. Magn.* 45, (2009) doi: 10.1109/TMAG.2008.2010661

56. R. J. Waltman, H. Deng, G. J. Wang, H. Zhu and G. W. Tyndall, "The effect of PFPE film thickness and molecular polarity on the pick-up of disk lubricant by low-flying slider", *Tribol. Lett*., vol. 39, no.2, pp. 211-219, 2010

57. X.-C. Guo and R. J. Waltman, "Mechanism of ultraviolet bonding of perfluopolyethers revisited", *Langmuir,* 23 (8), pp-4293-4295, 2007.

58. R. J. Waltman and X.-C. Guo, "AFM force-distance curves for perfluoropolyether boundary lubricant films as a function of molecular polarity", *Tribol. Lett.,* vol. 45, no.2, pp. 275-289, 2012.

59. S. Canchi and D. B. Bogy, "Slider-lubricant interactions and lubricant distribution for contact and near contact recording conditions", *IEEE Trans. Magn.*, vol. 47, pp. 1842-1848, 2011

60. C. Mathew Mate, B. Marchon, A. N. Murthy and S.-H. Kim, "Lubricant-induced spacing increases at slider-disk interfaces in disk drives", *Tribol. Lett*., vol. 37, pp. 581-590, 2010

61. R. J. Waltman, B. K. Yen and R. L. White, "The adhesion of monomolecular hydroxyl-terminated perfluoropolyether liquid films on the sputtered silicon nitride surface as a function of end group acidity and mobility", *Tribol. Lett.*, vol. 20, no.1, pp. 69-81, 2005.

62. R. J. Waltman, V. Raman and J. Burns, "The contribution of thin PFPE lubricants to slider-disk spacing. 3. Effect of main chain flexibility", Tribol. Lett., vol. 17, no.2, pp. 239-244, 2004.

63. Zheng, J. and Bogy, D. B.:"Investigation of flying-height stability of thermal fly-height control sliders in lubricant or solid contact with roughness," *Tribol. Lett.* 38, 283-289 (2010)

64. Li, N., Zheng, L., Bogy, D.B., Meng, Y. "Flyability and durability test of dynamic fly-height sliders at 1-nm clearance," *Tribol. Trans*. 53, 212-218 (2010)

65. Wu, T. W.,Deline, V.,Scharf, T. W., Yen, B. K. and Barnard, J. A."Wear of ultra-thin carbon overcoat characterized by micro-wear scan and auger electron spectroscopy," *J. Vac. Sci. Technol*. A 19, 986 (2001).

66. Kim, S. H., Guo,X., Waltman,R. J., Tu, H., Shatz, T., and Pocker,D. J. "Durability against contact wear of nonlubricated disks in the head–disk interface of disk drives," *IEEE Trans. Magn.* 47, 239–243 (2011)

67. Wang, Yu., Wei, X., Tsui, K.-L. and Chow, T. W.S. "Tribological degradation of head-disk interface in hard disk drives under accelerated wear condition," *IEEE Trans. Magn.* (2013) doi: 10.1109/TMAG.2013.2286579.

68. Y. Ma, S. Xue, J. Peng and D. B. Bogy, "Study of hard disk interface characterization using touchdown sensor and electro-magnetic signal in hard disk drives", *IEEE Trans. Magn.*, 10.1109/TMAG.2015.2434371 (2015)

69. Canchi, S. V., Bogy D. B., Wang, R.-H. and Murthy, A. N. "Parametric Investigations at the head-disk interface of thermal fly-height control sliders in contact," *Adv. Tribol*. (2012) doi: 10.1155/2012/303071

70. Karis, T. E. and Guo, X.-C. "Molecular adhesion model for the bridged state of a magnetic recording slider," *IEEE Trans. Magn*. 45, 2232-2234 (2007)

71. Karis, T. E., Guo, X.-C. and Juang J.-Y. "Dynamics in the bridged state of a magnetic recording slider," *Tribol. Lett.* 30, 123-140 (2008)

72. Marchon, B., Guo, X.-C., Karis, T., Deng, H., Dai, Q., Burns, J., and Waltman, R. "Fomblimmultidentate lubricants for ultra-low magnetic spacing," *IEEE Trans. Magn.* 42, 2504-2506 (2006).

73. S. K. Sinha, M. Kawaguchi, T. Kato, F. E. Kennedy, "Wear durability studies of ultra-thin perflouropolyether lubricant on magnetic hard disks", *Tribol. Intl.* vol. 36, pp. 217-225, 2001.

74. T. E. Karis, G. W. Tyndall and R. J. Waltman, “Lubricant bonding effects on thin film disk tribology”, *Tribol. Trans.*, vol. 44, pp. 249-255, 2001.

75. Jia-Yang Juang, Joel Forest and F.-Y. Huang, ”Magnetic head protrusion profiles and wear pattern of thermal flying-height control sliders with different heater designs," *IEEE Trans. Magn.*, vol.47, no.10, pp.3437-3440, Oct. 2011.

76. Jia-Yang Juang, T. Nakamura, B. Knigge, Y. Luo, W.C. Hsiao, K. Kuroki, F.Y. Huang and P. Baumgart, “Numerical and experimental analyses of nanometer-scale flying height control of magnetic head with heating element,” *IEEE Trans. Magn.*, vol.44, no.11, part 2, pp.3679-3682, Nov. 2008.

77. T.E. Karis, X.-C. Guo and Jia-Yang Juang, “Dynamics in the bridged state of a magnetic recording slider,” *Tribol. Lett.*, vol.30, no.2, pp.123-140, 2008.

78. Y. Shimizu, J. Xu, H. Kohira, T. Shiramatsu and M. Furukawa, “Nano-Scale Defect Mapping on a Magnetic Disk Surface Using a Contact Sensor”, *IEEE Trans. Magn.*, vol. 47, pp. 3426–3432, Oct. 2011.

79. J. Xu, Y. Shimizu, M. Furukawa, J. Li, Y. Sano, T. Shiramatsu, Y. Aoki, H. Matsumoto, K. Kuroki and H. Kohira, “Contact/Clearance sensor for HDI subnanometer regime”, *IEEE Trans. Magn.*, vol. 50, 3300205, Mar. 2014.

80. L. Matthes, B. Knigge and F. Talke, “Head-disk proximity sensing using contact sensors in hard disk drives”, *IEEE Trans. Magn.*, vol. 50, 3303404, Nov. 2014.

81. J. Xu, M. Tokuyama, M. Kurita, and Y. Maruyama, “High resolution measurement of temperature distribution of head coil and air-bearing surface,” *IEEE Trans. Magn.*, vol. 39, no. 5, pp. 2411–2413, 2003.

82. T. Imamura, M. Yamagishi, and S. Nishida, “In-situ measurement of temperature distribution of air bearing surface using thermography,” *IEEE Trans. Magn.*, vol. 38, pp. 2147–2149, Sept. 2002.

83. J. Xu, M. Kurita, and M. Tokuyama, “Thermal analysis of a magnetic head,” *IEEE Trans. Magn.*, vol. 40, no. 7, pp. 3142–3144, Jul. 2004.

84. Ju, Y. S., 2005, “Self-Heating in Thin-Film Magnetic Recording Heads Due to Write Currents,” *IEEE Trans. Magn.*, vol. 41, no.12, pp. 4443–4448

85. R. H. Wang, X. Z. Wu, W. Weresin, and Y. S. Ju, “Head protrusion and its implications on head-disk interface reliability,” *IEEE Trans. Magn.*, vol. 37, no. 4, pp. 1842–1844, Jul. 2001.

86. Y. S. Ju, R. Xu, X. Wu, N. Smith, R. Fontana, W. Lee, K. Carey, M. Ho, D. Hsiao, and B. Gurney, “A combined experimental and numerical study of temperature rise in GMR sensors due to self-heating,” *IEEE Trans. Magn.*, vol. 37, no. 4, pp. 1701–1703, Jul. 2001.

87. B. Gotsmann, M. A. Lantz, “Quantized thermal transport across contacts of rough surfaces”, Nat.Matr., 12, 59-65, 2013

88. Shuyu Zhang, Numerical Investigations of Particle Contamination and Thermal Effects in a Slider Disk Interface, Ph. D. dissertation, Department of Mechanical Engineering, University of California, Berkeley, California, USA, 1997

89. D. Chen, N. Liu and D. Bogy, "A phenomenological heat transfer model for the molecular gas lubrication system in hard disk drives", *J. Appl. Phys.*, 105, 084303, 2009

90. N. Liu, J. Zheng and D. B. Bogy, "Predicting the flying performance of thermal flying-height control sliders in hard disk drives", *J. Appl. Phys.*, 108, 016102, 2010.

91. Jia-Yang Juang, "Transient characteristics of nanoscale air bearings subjected to Joule heating", *Tribol. Lett.*, vol.53, no.1, pp.255-260, Jan. 2014.

92. M. Shamsa, W. Liu, A. Balandin, C. Casiraghi, W. Milne and A. Ferrari, "Thermal conductivity of diamond-like carbon films", *Appl. Phys. Lett.*, 89, 161921, 2006.

93. C. Mathew Mate, *Tribology on the small scale*, Oxford University Press, 2008.

94. C. Mathew Mate, "Anomalous diffusion kinetics of the precursor film that spreads from polymer droplets", *Langmuir*, 28, pp. 16821-16827, 2012.

95. J. Wu, C. Mathew. Mate, "Contact angle measurements of lubricated silicon wafers and hydrogenated carbon overcoats", Langmuir,

96. C. Mathew Mate, "Atomic-force-microscope study of polymer lubricants on silicon surfaces", *Phys. Rev. Lett.*, vol. 68, pp. 3323-3326, 1992.

97. X. Ma, H. Tang, M. Stirniman and J. Gui, "Lubricant thickness modulation induced by head-disk dynamic interactions," *IEEE Trans. Magn.*, vol. 38, pp. 112-117, 2002

98. C. Mathew. Mate, "Shear response of molecularly thin liquid films to an applied air stress", *Phys. Rev. Lett.*, vol. 85, pp. 3902-3905, 2000.

99. T. DB Jacobs, R. Carpick, "Nanoscale wear as a stress-assisted chemical reaction", Nat Nanotechnology, vol. 8, pp. 108-112, 2013

100. E. Schreck, D. Li, S. Canchi, L. Huang, G. P. Singh, B. Marchon, H. J. Richter, B. Stipe, and M. Staffaroni, "Thermal aspects and static/dynamic protrusion behaviors in Heat-Assisted Magnetic Recording," *IEEE Trans. Magn.*, vol. 50, pp. 126-131, 2014